UNIVERSITÉ DU QUÉBEC EN OUTAOUAIS

Conception de nouvelles topologies de métasurfaces pour refaçonner l'environnement du canal de propagation sans fil

Yassine Zouaoui

Département d'informatique et d'ingénierie

Thèse

Présenté en vue de l'obtention du diplôme de

Philosophiae Doctor

en Sciences et technologies de l'information

UNIVERSITÉ DU QUÉBEC EN OUTAOUAIS

Design of new metasurface topologies to reshape the wireless propagation channel environment

par

Yassine Zouaoui

Thèse présentée au

Département d'informatique et d'ingénierie

Pour l'obtention du grade de

Philosophiae Doctor (Ph.D.)

en Sciences et technologies de l'information

Membres du jury :

Président	*Prof. Luigi Logrippo, UQO*
Examinateur externe	*Dr. Jafar Shaker, Carleton University, Ottawa*
Examinateur interne	*Prof. Halim Boutayeb, UQO*
Directeur de thèse	*Prof. Larbi Talbi, UQO*
Co-directeur	*Dr. Khelifa Hettak, CRC, Ottawa*

DEDICATION

To my dear parents Ahmed Zouaoui and Samia Mansour. Without their endless love, tireless efforts, and encouragement, I would never have been able to complete my graduate studies. I love you both and I appreciate everything that you have done for me.

To my lovely wife Azza Ferchichi, who always encourage me with passion and endless support.

To my sisters, Imen, Chaima, Sirine and Amira.

To Achref Ferchichi, Hanen belhadj and Leila belhadj.

To my family.

To all my friends and acquaintances.

To the memory of my uncle Bachir, my grandmother Wassila, my father in law Med Ali and my aunt Radhia.

To those who contributed from near or far to the completion of this research work.

To my son, may Allah bless you.

ACKNOWLEDGEMENTS

First and foremost, I would like to praise Allah the Almighty, the Most Gracious, and the Most Merciful for His blessing given to me during my study and in completing this thesis. May Allah's blessing goes to His final Prophet Muhammad (peace be up on him), his family and his companions.

I would like to express my deepest gratitude to my advisors Pr Larbi Talbi and Dr Khelifa Hettak for their continuous support during my PhD research, for their patience, motivation, enthusiasm, insightful comments, and immense knowledge. Their guidance has helped me throughout the research and writing up this thesis.

I would like to thank my research lab colleagues and my friends: Abdelwadoud Stambouli, Khaled Kedjar, Vincent Fono, Betty Savitri, Youssef Karmous, Karim Idoudi, Aymen Talbi and Temim Samah. I have enjoyed working with you all and I appreciate sharing with you ideas, help and good humour.

My ultimate thanks are dedicated to my parents Ahmed Zouaoui and Samia Mansour for their support, encouragement and help. I am eternally grateful for everything they have done; your prayers have been answered. I also would like to thank my sisters Imen, Chaima, Sirine and Amira. Also, I would like to express my thanks to all my family members.

Last but not the least; I would also like to express my gratitude to my lovely wife Azza Ferchichi, your love, patient, and encouragement helped me to be succeeded.

RÉSUMÉ

La technologie de communication sans fil a énormément évolué au cours des dernières années. Cette évolution, fortement croissante, a également eu comme conséquence l'apparition des nouvelles technologies ainsi que l'innovation de plusieurs applications à haut débit telles que les applications mobiles, la téléphonie sur voix IP (VoIP) et l'internet des objets (IOT). Cependant, la technologie sans fil traditionnelle ne peut pas répondre aux contraintes des services émergents, qui exigent souvent l'utilisation de bande de fréquences de plus en plus grande pour être opérationnels. Face à cette demande de plus en plus forte de transmission de données, un nouveau concept basé sur l'intégration des surfaces électromagnétiques dans un milieu de propagation se présente comme une technologie clé qu'il faut étudier et identifier tous ses défis technologiques.

Le déploiement de ces surfaces dans un tel environnement offre plusieurs avantages. Ces avantages sont entre autres la possibilité de fournir des communications fiables et efficaces en établissant des canaux en visibilité directe ce qui permet d'offrir des débits beaucoup plus importants tout en économisant de l'énergie. De plus, ces surfaces ont l'avantage de rendre l'environnement plus sécuritaire grâce à ses caractéristiques de filtrage.

En conséquence, de nouveaux travaux s'orientent vers l'utilisation des surfaces électromagnétiques dans des environnements complexes afin de permettre une utilisation plus efficace du spectre radiofréquence.

Le déploiement des surfaces électromagnétiques dans un milieu de propagation est une idée prometteuse pour les futures générations de systèmes de communication sans fil. En effet, la conception de ces surfaces nécessite la prise en considération de certains défis techniques, à savoir, la stabilité de la fréquence de résonance avec l'angle d'incidence, la bande passante, le contrôle des harmoniques et la sensibilité par rapport à la polarisation de l'onde d'incidence. Bien que la réduction des éléments constituant la surface électromagnétique présente une solution adéquate pour ces défis. Il reste que la procédure de miniaturisation est en soi un très grand défi. Ainsi, un grand intérêt est apparent pour développer de nouvelles structures capables de surmonter tous ces défis.

La conception de nouvelles topologies métasurfaces exige un progrès technologique et une méthodologie dans l'exploitation des connaissances de dispositifs micro-ondes. En premier lieu, une méthode de synthèse sera établie dans le troisième chapitre en utilisant des circuits équivalents

dans le but de déterminer les paramètres géométriques d'une métasurface flexible conçue par des dipôles croisés. La synthèse des paramètres géométriques constitue la méthode qui sera utilisée pour contrôler la bande passante. Par la suite, le concept des résonateurs à saut d'impédance (RIS) utilisé pour la miniaturisation et la fabrication de nouvelles topologies, sera présenté. D'autre part, le concept de résonateurs pliés sera étudié pour les structures périodiques dans le but de concevoir des structures à large bande. Finalement, les prototypes obtenus seront réalisés et analysés et de nouvelles avenues de recherche seront aussi dressées.

ABSTRACT

In this thesis we present the design, analysis, and experimental verification of a new type of metasurface (MS). The theory of the MS is introduced in Chapter 2. Chapter 3 presents a simple synthesis method for designing a flexible metasurface (MS). The proposed design, when operating at 10 GHz, has extensive shielding properties against Electromagnetic Interference (EMI). In addition, a parametric study of the proposed MS aiming to optimize the bandwidth has been presented. The proposed MS holds similar responses for TE (Transverse Electric) and TM (Transverse Magnetic) modes of polarization at normal incidence. Further, the conformal behavior of the proposed MS in comparison with a planar MS is presented and evaluated. The size of the proposed unit cell is $0.4\lambda_0 \times 0.4\lambda_0$, where λ_0 is the free space wavelength at the desired resonant frequency. The measured results of the proposed MS agree well with the simulations. Chapter 4 explores the potential of using stepped impedance resonators (SIR) to design a dual orthogonal polarization MS with low sensitivity to the incident angles of plane wave excitation. The proposed MS consists of crossed stepped impedance resonators printed on the two interfaces of a single dielectric substrate. A significant size reduction of the cell element size can be achieved to the extent that $p = \lambda_0/16$, where λ_0 is the free-space wavelength of resonant frequency and p is the periodicity of the element. In addition, harmonic frequencies can be controlled by simply changing the SIR impedance to design a multiband MS which resembles a similar development for stepped impedance resonators in microwave filter theory. A simple design procedure is developed based on transmission line theory. The structure is fabricated and tested subsequently in a free space measurement facility which demonstrated a stable angular response up to 60^o of the incident angles for both the TE and TM plane wave excitations. Finally, Chapter 5 introduces a novel methodology to design dual pole spatial filters by using folded stubs. The proposed methodology is used to design a band-stop MS for X band applications. The fabrication of the dual pole filters is significantly simplified by using a single layer of a dielectric substrate. Two structures are designed, fabricated, and measured to verify the proposed methodology. The first structure is polarization dependent, while the second structure is polarization independent. The measurement solution verifies the simulation software procedure, and the qualitative analytical algorithm. This study can be used for many applications in electromagnetic engineering, such as designing secure buildings and shielded structures.

TABLE OF CONTENTS

LIST OF TABLES

LIST OF FIGURES

LIST OF SYMBOLS AND ABBREVIATIONS

MSs	Metasurfaces
MS	Metasurface
EMI	Electromagnetic Interference
EC	Equivalent Circuit
λ_0	free space wavelength
TE	Transverse Electric
TM	Transverse Magnetic
VoIP	IP telephony
IoT	Internet of Things
RF	Radio Frequency
FSS	Frequency Selective Surfaces
EBG	Electromagnetic Bandgap Structures
HISs	high impedance surfaces
θ	Angle of incidence
ε	Dielectric constant
P	Unit cell periodicity
L	Equivalent inductance
C	Equivalent capacitance
l	Strip length
w	Strip width
g	Gap between the adjacent strips
h	Substrate thickness
E	Electric field

H	Magnetic field
K	Wave vector
f_0	Operating frequency
Q	Quality factor
Z_0	Free-space wave impedance
Y_0	Free-space wave admittance
ε_{eff}	Effective permittivity
R	Equivalent resistance
PEC	Perfect Electric Conductor
PMC	Perfect Magnetic Conductor
TX	Transceiver antenna
RX	Receiver antenna
PNA	Performance Network Analyzer
Z_{TE}	TE mode impedance
Z_{TM}	TM mode impedance
SE	Shielding effectiveness
SIR	Step Impedance Resonator
K	Impedance ratio
w	Strip width
w_1	Strip width
w_2	Strip width
l_1	Strip length
l_2	Strip length
Z_1	Strip impedance

Z_2	Strip impedance
Z_{0o}	Strip impedance for odd mode
Z_{0e}	Strip impedance for even mode
θ_o	Electrical length for odd mode
θ_e	Electrical length for even mode
ε_{eff}	Effective permittivity
Z_{0o}	Strip impedance for odd mode
L_{Odd}	Strip length for odd mode
λ_{g_Odd}	Guided wavelength for odd mode
L_{Even}	Strip length for even mode
λ_{g_Even}	Guided wavelength for even mode
I	Electric current
L_T	Total length of the stepped resonator
L_C	Central strip length
L_S	Stub length

CHAPTER 1 INTRODUCTION

1.1 Motivation

In recent years, the field of wireless communication has seen significant growth. Its rapid development led to the introduction of new technologies and to many new high-speed applications. Among these include, IP telephony (VoIP), and the Internet of Things (IoT). These technologies and many others require communication channels capable of transporting greater and greater amounts of information.

However, in term of frequency bands and data transmission, traditional wireless technology cannot meet the demands of these emerging services. As a result, the radio frequency (RF) spectrum is becoming crowded. Recently, a new concept of electromagnetic surfaces has been used to meet the rapid development of communication technology in terms of high data rates and system capacity. The idea revolves around the deployment of periodic structures into the walls of buildings to make the propagation environment more favorable [1-4]. Electromagnetic surfaces have widely been used to control the propagation environment [5-8], reduce interference at specific frequency bands [9], enhance the directivity of wireless transmissions [10], optimize the communication efficiency [11], and save energy. They are classified into metamaterials, frequency selective surfaces (FSS), reflectarrays, electromagnetic bandgap structures (EBG), and metasurfaces (MSs). Among these structures, MSs are prominent structures used to control electromagnetic waves. They have a wide range of applications in electromagnetics, including absorbers [12-13], high impedance surfaces (HISs) [14], and spatial filters [15-16]. However, these structures suffer from many technical difficulties. In this thesis, we intent to resole some of these technical issues in order to make these MSs more adaptable to a wider range of applications.

1.2 Research problems and objectives

The idea of employing electromagnetic surfaces within the propagation environment opens a window for new and interesting applications. However, as mentioned previously, the fabrication of these surfaces are fraught with many technical difficulties, namely, the bandwidth, size of MS's unit cell, sensitivity to the incident angle and sensitivity to the polarisation. Indeed, the design of

these surfaces requires the consideration of these technical challenges, which can restrict the use of MS in many applications.

The main objective of this thesis is to design a new class of spatial filters for wireless communication systems in order to improve the propagation channel performance. This is achieved by designing MSs with desired features, such as: insensitivity to polarization and incident angles wave excitation, flexibility, and wider bandwidth.

1.3 Thesis Contribution

The first contribution is a simple synthesis method for ultra-thin double-sided cross-dipole-based FSS. The presented technique is used to design a flexible band-stop FSS for Electromagnetic Interference (EMI) (shielding) applications operating at 10 GHz. In addition, this method can be used to control the bandwidth of the FSS. The second contribution is the design of stable FSS that is insensitive to polarization and incident angles of plane wave excitation. This is achieved by using stepped impedance resonators in order to reduce the size of MS's unit cell. A simple design procedure based on transmission line theory is developed, as well, to synthesize a step impedance unit cell. The proposed technique is used to design a band stop MS for X band applications. Finally, the third contribution is the design of a dual pole MS through the use of folded stubs to enhance the broadband characteristics of the designed MS. This new MS has a bandstop behaviour at the central frequency of 10 GHz.

This research overcomes the problems associated with the design of MSs with ideas inspired from microwave theory.

1.4 Thesis Structure

The thesis is organized as follows: Chapter 2 presents a literature review of previous work on the characteristics of FSS & metasurface structures and their applications. A substantial portion of the text is devoted to describing electromagnetic frequency selective surfaces and metasurfaces, and it provides a comprehensive overview of FSS and metasurface structures. It concluded with a very useful comparison of the various techniques for reducing the unity cell, increasing bandwidth, and improving angular stability in these types of spatial filters. The chapter is very didactic and follows a logical progression. It provided a broad overview of this field, and the references provided are numerous and beneficial to the reader.

Chapter 3 described a general approach to synthesis of a typical band reject spatial filter. A generalised equivalent circuit model is used to provide physical insights into the proposed design, and a synthesis technique is used to provide a versatile implementation capability of FSS filters using unit cell period (p), metal length (l), metal width, and the gap between adjacent strips (g). To demonstrate the significance of the proposed synthesis technique, its concept is used to synthesise double-sided parallel cross-dipoles-based FSS for a specific frequency band, as well as the required size for the double-sided parallel cross-dipoles topology. It generates a specific bandwidth, which is an additional degree of freedom relevant to the proposed synthesis technique, which differs from techniques reported in the open literature. The proof of concept is accomplished through the design and implementation of a flexible band-stop MS for Electromagnetic Interference (EMI) (shielding) applications operating at 10 GHz. This technique allows the realisation of variable-size spatial filters while maintaining the desired filter response.

Chapter 4 addressed research questions concerning the development of a miniature single band metasurface with more design degrees of freedom and high stability over incident angle. Translation and application of analogue stepped impedance resonator concept for standardised and algorithmic synthesis of frequency selective metasurface are the steps taken to arrive at the answers. It used FSS cell elements of canonical shape in conjunction with stepped impedance techniques to generate and control higher frequency selective metasurface resonances. The specific areas of innovation that was planned include, the validation of high frequency (10 GHz) single layer FSS designs with stable angular and polarization response that are amenable to PCB fabrication techniques, development of rigorous single order frequency selective metasurface design approaches, and new capability to tailor canonical shape of frequency selective metasurface cell elements to control higher order resonances. Finally, the ultimate goal was to demonstrate the advantage of combining the approximate stepped impedance resonator dimensioning (based on network synthesis) and optimization (based on EM modeling), to achieve a fast and accurate design.

Chapter 5 addressed the design of a multi-pole FSS on a PCB substrate using analogue bandstop filter techniques (f_0=10.0GHz). The stopband spatial filter was generated using analogue cross-coupling stubs. It combined an approximate pair of quarter wavelength open circuited stubs separated by a quarter wavelength (based on network synthesis) and optimization (based on EM modelling), resulting in a fast and accurate design. The simplest way to implement a bandstop

spatial filter is to use an open circuit shunt stub with an electrical length of 90. The roll-off of the filter can be improved by increasing the number of shunt stubs; however, the circuit size will be increased as well. Cross coupling is introduced into the design via two shunt stubs while maintaining roll-off performance. The ability to morph the shunt open-circuited stub is now required in the synthesis of multilayer multi-pole FSS structures. An experimental characterization of dual pole FSS was demonstrated, with the aim of validating a novel topology with polarization independent capability for 5G application. The tests performed appear to be well-selected with respect to the application. This experimentation leads to the observation of unique properties, such as the possibility of designing spatial filter with multipole capability. Clarity of thought with respect to the design of broadband bandwidth is demonstrated and designs for optimal performance are proposed. The chapter ends with a description of the performance of the final prototype designed at 10 GHz for 5G applications, that a maximum measured bandwidth around 50% with the possibility of guaranteeing a mechanical angular stability range of ±30º, allowing the comparison of measurements and simulations and validating this novel concept.

Chapter 6 concludes the work and highlights the key points of this work and the prospects that may follow.

1.5 Publications

1. Zouaoui, Yassine, Larbi Talbi, Khelifa Hettak, and Naresh K. Darimireddy. "Synthesis of Planar and Conformal Single-Layered Double-Sided Parallel-Cross Dipole FSS Based on Closed-Form Expression." IEEE Access 9 (2021): 104051-104058.

https://doi.org/10.1109/ACCESS.2021.3096419 **(published)**.

2. Zouaoui, Yassine, Larbi Talbi, and Khelifa Hettak. "Cross dipole FSS bandwidth enhancement." In 2019 IEEE International Symposium on Antennas and Propagation and USNC-URSI Radio Science Meeting, pp. 947-948. IEEE, 2019.

https://doi.org/10.1109/APUSNCURSINRSM.2019.8889365 **(Conference)**.

3. Zouaoui, Yassine, Larbi Talbi, and Khelifa Hettak. "A novel ultra-miniature 90° metamaterial phase shifter for beamforming applications." Microwave and Optical Technology Letters 61, no. 6 (2019): 1505-1508. https://doi.org/10.1002/mop.31767 **(published)**.

CHAPTER 2 METASURFACES

2.1 Introduction

This chapter is dedicated to the theoretical background of MSs. It also provides a comprehensive view of their operational mechanism, and suggested applications in electromagnetic engineering.

2.2 A brief Metasurfaces history

MSs have been the subject of much research in the field of microwave and optical engineering due to their capacity to control electromagnetic waves. Historically, they can be traced back to the 20th century, when the American physicist Robert W. Wood discovered that the reflection spectra of subwavelength metallic gratings had dark areas. This phenomenon was called Wood's anomaly [17]. These structures are often composed of a periodic arrangement of metallic or aperture sub-wavelength cells of arbitrary shape, generally supported by or embedded in a dielectric substrate [18]. The sub-wavelength cells differentiate the metasurfaces from conventional frequency selective surfaces (FSSs). The main difference between MSs and FSSs is the size of the unit cell. Typically, the unit cell size (periodicity) of the FSS corresponds to the operating wavelength. MSs have the advantage of taking up less physical space compared to FSSs and are low-sensitivity structures to incident angles of plane wave excitations. Additionally, they are easy to fabricate, flexible, lightweight, and reliable [19, 20].

As previously mentioned, MSs are two-dimensional structures that consist of extremely thin sheets, much smaller in comparison to bulky volume structures. Based on this definition, these structures are classified into two classes. The first class is called metafilm, where the structure follows the cermet topology (an array of identical isolated scatters) [21] as shown in Figure 2.1(a). The second class is called metascreen, where the structure follows the fishnet topology (an array of identical apertures in a planar conducting screen) [22] as shown in Figure 2.1(b). Besides these structures, other kinds of MSs can be defined based on a combination of these two classes [23,-24].

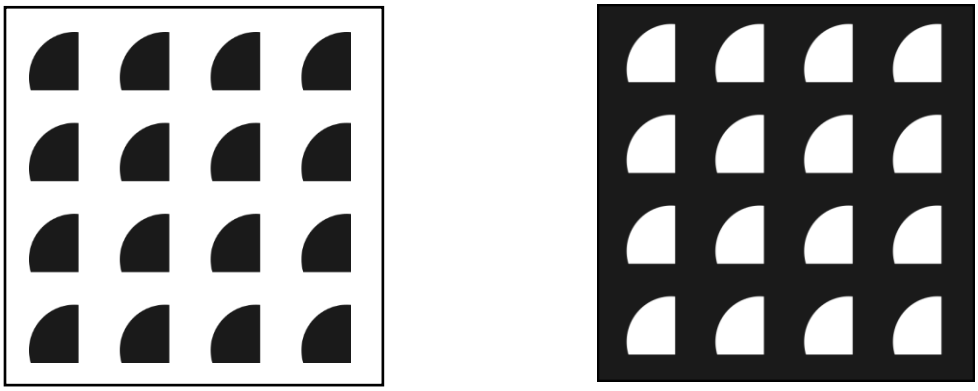

(a) (b)

Figure 2.1 The Metasurfaces classes. (a) metafilm, and (b) metascreen.

2.3 Classification of Metasurfaces

Metasurfaces can be broadly classified based on their functionality, or element geometry type. Several functionalities can be realized by MSs. Figure 2.2 shows some of the functionalities that can be realized by metasurfaces:

1. Frequency selective surfaces: These structures were used as a spatial filter for incoming electromagnetic waves (bandpass or bandstop frequency response);

2. Absorbers: These structures were used to absorb the incident waves in such applications;

3. Polarization transformers: These structures were used to manipulate the polarization of incident waves;

4. Wavefront shaping surfaces: These structures were used to manipulate the wavefront of incident waves.

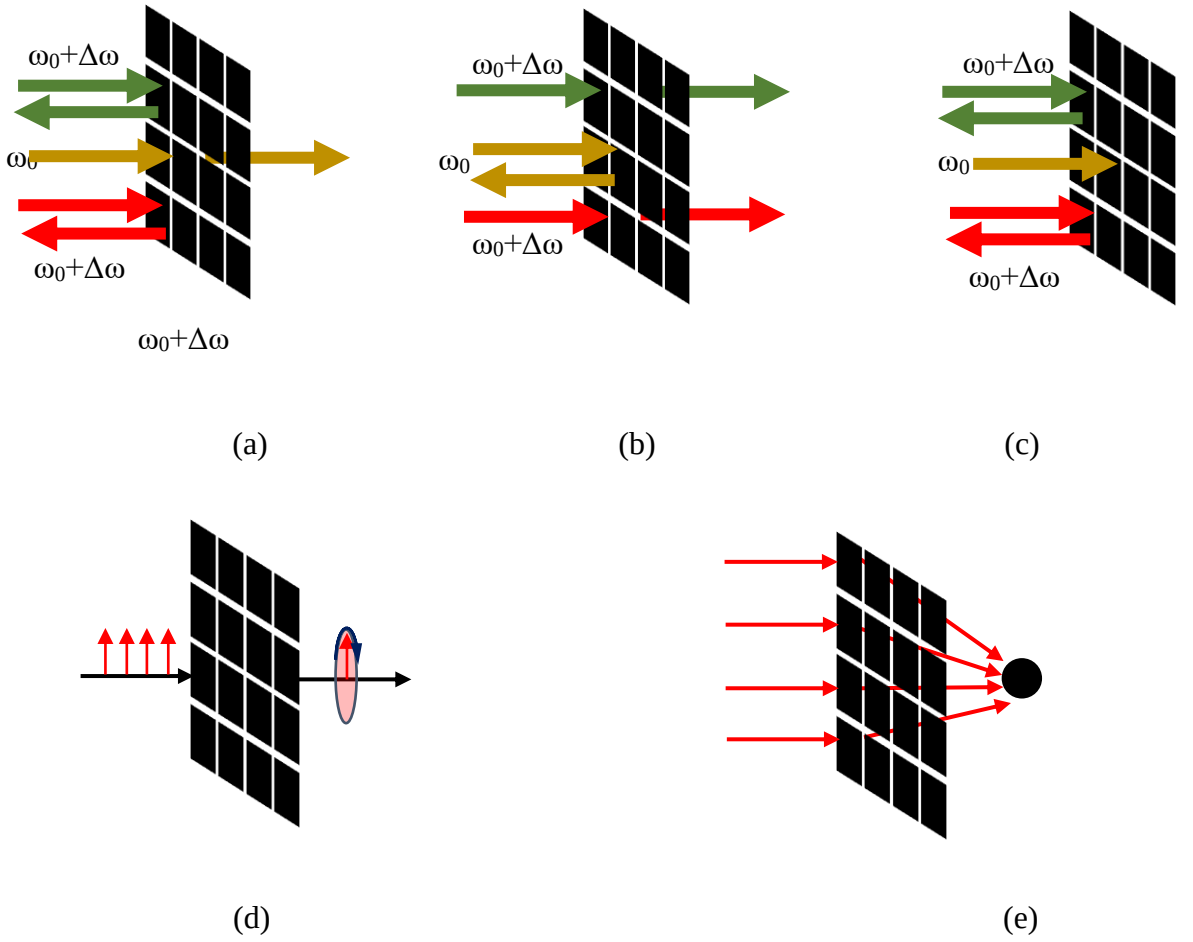

Figure 2.2 Metasurface functionalities. (a) bandpass frequency selective surface [25]; (b) bandstop frequency selective surface [26]; (c) absorber [27]; (d) linear-to-circular polarization converter [28]; (e) focusing transmitarray [29].

In addition to their functionalities, MSs can be classified based on their element geometry as shown in figure 2.3. According to Munk [30], MSs can be arranged into four groups as follows: the first group is the center-connected elements, including dipoles [31], tripoles and other multipolar elements [32-33]. The second group includes any shape formed by a loop, such as the hexagonal loop [30], the square loop [34-35] and the circular loop [36]. The third group is the patch elements, such as the hexagonal patch, the square patch and the circular patch [37-39]. The fourth group is a combination of elements [40-42], which can be used to design a structure with specific frequency responses.

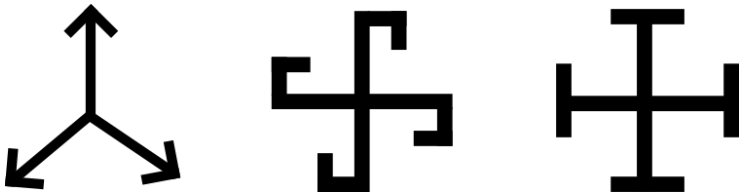

(a) Center-connected

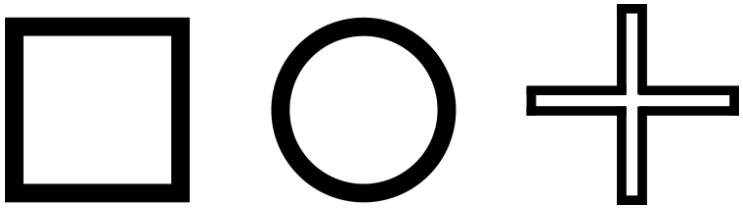

(b) Loops

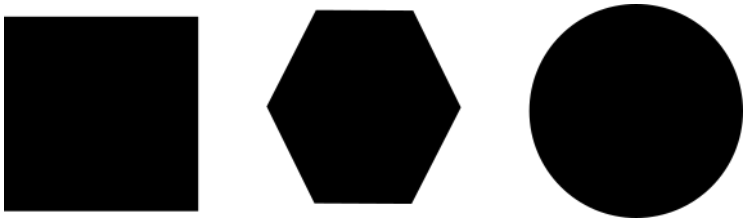

(c) Patch

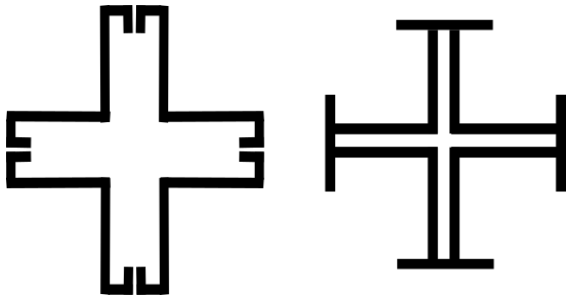

(d) Combinations

Figure 2.3 Metasurfaces elements.

2.4 Design problem

In general, to design MSs, some technical points must be carefully addressed. The electromagnetic response of a MS can be affected by many factors, including the incident angles, the polarization of the wave, the properties of the substrate, the periodicity of the unit cell, the bandwidth and the flexibility of the structure.

2.4.1 Angle of incidence

In practice, electromagnetic waves illuminate MSs at any angle of incidence. As a result, the effective length of the element changes in function of the angle of the incident wave. Figure 2.4 shows an array of metallic strips excited by an incident wave at an angle of incidence θ. The variation of the incident angle of electromagnetic waves cause a variation of the effective length [43]. Since the electromagnetic response of the MS depends on the geometry of the unit cell, the variation of the incident angle causes the electromagnetic response to change. For this reason, the variation of the incident angle must be considered by the designer of MS.

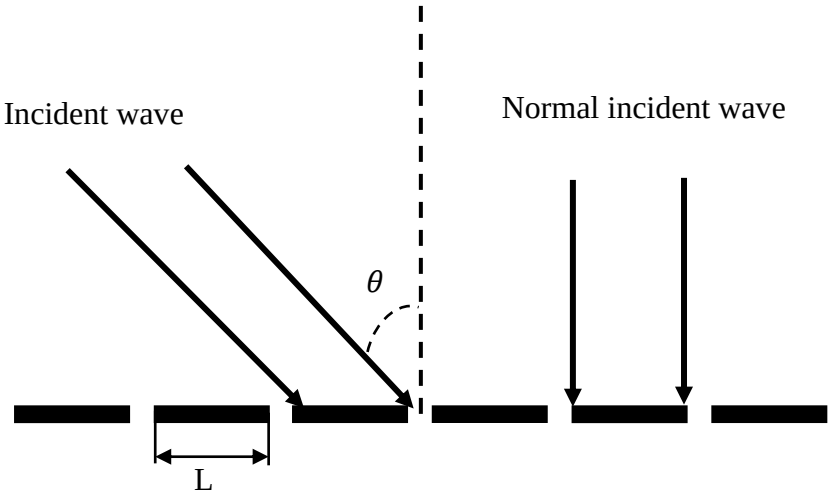

Figure 2.4 The effect of incident angle of the wave on the effective length of the strip.

2.4.2 Angle of polarization

In addition to the incident angles of the electromagnetic wave, the electromagnetic behaviour of MSs can be affected by the orientation of the electric and magnetic field (meaning

the polarization of the electromagnetic wave). Figure 2.5 shows an array of metallic strips excited by an electromagnetic wave. When the electric field is perpendicular to the strips, the strips can be modeled as a capacitive element. The value of the capacitance can be calculated by the equation [44],

$$C = \varepsilon \frac{2l}{\pi} \cos\theta \left[ln \operatorname{cosec}\left(\frac{\pi g}{2l}\right)\right] \tag{2.1}$$

where l is the length of strips, θ is the incident angle of the electromagnetic wave, ε is the dielectric permittivity of the substrate, and g is the gap between the adjacent strips.

On the other hand, when electric field is parallel to the strips, the strips can be modeled as an inductive element. The value of the inductance can be calculated by the equation [44],

$$L = \mu \frac{P}{2\pi} \cos\theta \left[ln \operatorname{cosec}\left(\frac{\pi w}{2P}\right)\right] \tag{2.2}$$

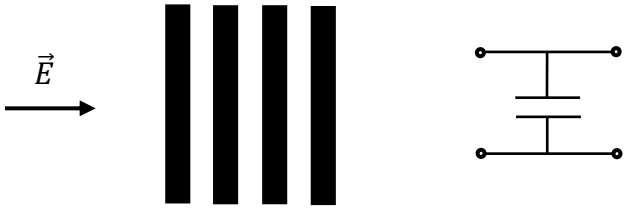

a) Capacitive strips

b) Inductive strips

Figure 2.5 Capacitive and inductive strips.

2.4.3 The dielectric substrate proprieties

In practical design, an MS is surrounded by a dielectric substrate, which is used as a mechanical support. According to Munk [30], the dielectric substrate has an effect on the resonance

frequency of the MS. The dielectric substrate reduces the resonance frequency by a factor of $\sqrt{\varepsilon_r}$, where ε_r is the dielectric constant. Usually, the periodic structure has a single layer of a dielectric substrate on one side. In this case, the resonance frequency would be reduced by a factor of $\sqrt{(\varepsilon_r + 1)/2}$.

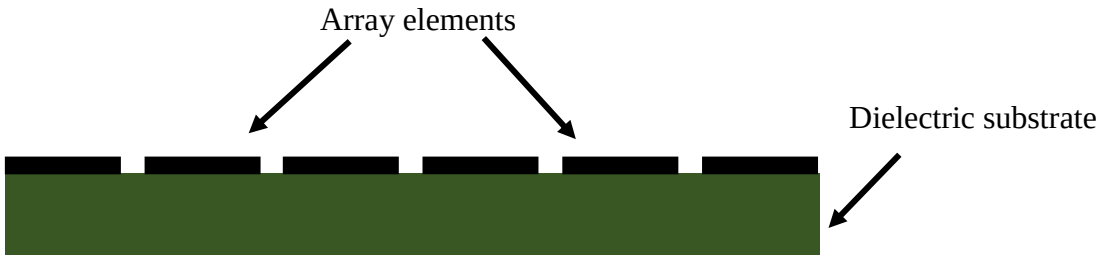

Figure 2.6 MS on the top side of a dielectric substrate.

2.4.4 Periodicity

The periodicity of the unit cell also has an important effect on the frequency response. The apparition of the gratings lobes is related directly to the periodicity. These lobes are usually seen as a bad thing as they reduce the efficiency of the periodic structure due to the dispersion of energy [45]. These unwanted lobes occur when the periodicity of the unit cells become comparable to the incident electromagnetic waves.

The appearance of grating lobes can be predicted by the following equation

$$P(\sin\theta_i + \sin\theta_m) = m\lambda,$$

where P is the periodicity of the periodic structure, θ_i is the incident angle of the electromagnetic wave, θ_m is the direction of propagation of the m^{th} mode, and m is the mode number.

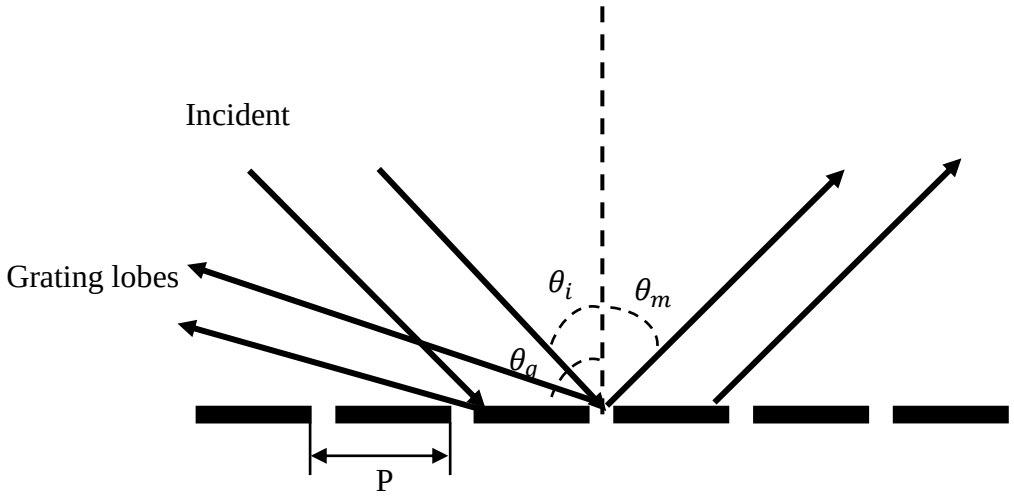

Figure 2.7 Gratings lobes.

To prevent the appearance of grating lobes, the unit cell size must be much smaller than $\lambda/2$. Hence by reducing the size of the unit cell, the appearance of grating lobes can be successfully avoided.

2.4.5 Conformal Behaviour

In many applications, a MS needs to be mounted to the surface, such as the surface of an aircraft or radome [46-47], which means that the structure has to be curved. For this reason, the conformal behaviour of a MS also has an important effect on the electromagnetic response. Specifically, the frequency response depends on the nature of the curvature. This is due to the fact that the curvature can cause changes in coupling between the elements of the MS compared to planar structures [48]. This property needs to be taken into consideration in some applications.

2.5 Applications

MSs are widely used in electromagnetic applications ranging from low microwave to optical frequencies. These applications include, stealth technology [49-51], absorbers [52-53], harvesters [54-55], dichroic sub-reflectors [56], and electromagnetic shielding [57]. MSs have also been used to improve the radiated power and reduce loss of antennas [58]. In wireless indoor environments, they were used to reduce the interference level and multipath fading [59-60]. Figure 2.8 presents some examples of these applications. In figure 2.8(a), a MS was used as an antenna radome [61], while figure 2.8(b) shows a MS used in modern military platforms [62].

(a)

(b)

Figure 2.8 MSs in different applications.

2.6 Conclusion

This chapter discussed the history, theory, and operation of MSs. Several issues related to the design of the MSs were considered, including the effects of incident angles, polarizations, the MS's curvature, and grating lobes. The potential applications of MS in the electromagnetic engineering have been reviewed.

CHAPTER 3 SYNTHESIS OF PLANAR AND CONFORMAL SINGLE-LAYERED DOUBLE-SIDED PARALLEL-CROSS DIPOLE FSS BASED ON CLOSED-FORM EXPRESSION

3.1 Introduction

Several numerical techniques have been proposed to analyze periodic structures. These techniques include full-wave analysis [63-64], iterative approach [65], and an equivalent circuit model [66–69]. As the electromagnetic performance of the MS can be expressed by the inductive and capacitive behavior, the equivalent circuit model is the most widely used technique due to its simplicity. The analysis of FSS is essentially a method based on geometric parameters like the period of the unit cell (p), metal length (l), metal width, and the gap between the adjacent strips (g). In these techniques, the knowledge of the physical parameters is vital for accurate design.

On the other hand, to find these parameters for given filtering properties, a few synthesis methods have been presented in the literature, especially for double-sided parallel-cross-dipoles-based FSSs. In this regard, this chapter proposes a straightforward technique for synthesizing a flexible double-sided parallel cross-dipoles-based FSS for a particular frequency band and provides the required size for the double-sided parallel cross-dipoles topology. Besides, producing a specific bandwidth is another degree of freedom relevant to the proposed synthesis technique and is different from the techniques reported in the open literature. The double-sided parallel cross-dipoles-based FSS in the article is a deformation of the Jerusalem cross-slot [70]. However, the proposed closed-form equations in this chapter deal with FSS synthesis. The proposed synthesis method in this chapter allowing the prediction of the physical parameters of the unit cell for Double-Sided Parallel-Cross Dipole FSS operating at 10 GHz and for an arbitrary value of quality factor $\boldsymbol{Q}$=$\mathbf{7.5}$. The proposed FSS has the same frequency response for TE and TM polarizations with a fractional bandwidth of 10.42% at normal incidence. In addition, the structure presents a high level of shielding performance for both polarizations.

The Section 3.2 of the chapter explains the theory of operation of double-sided parallel cross dipoles-based FSS. In Section 3.3, the result obtained by the analytical solution is compared with the numerical simulation. Section 3.4 explores the bandwidth control technique of double-sided

parallel cross-dipoles. In Section 3.5, the band-stop principle of double-sided parallel cross-dipoles FSS design at 10 GHz has been explored. Finally, the work is concluded in Section 3.6.

3.2 Theoretical approach

According to Marcuvitz [45], the electromagnetic behavior of the metal strip lines is represented by the polarization of the wave. The parallel strips to the electric field are equivalent to an inductive element, and the perpendicular strips to the electric field correspond to a capacitive element, as presented in Figure 3.1(a). The proposed double-sided parallel cross-dipoles-based FSS can be described by the equivalent circuit model shown in Figure 3.1(b).

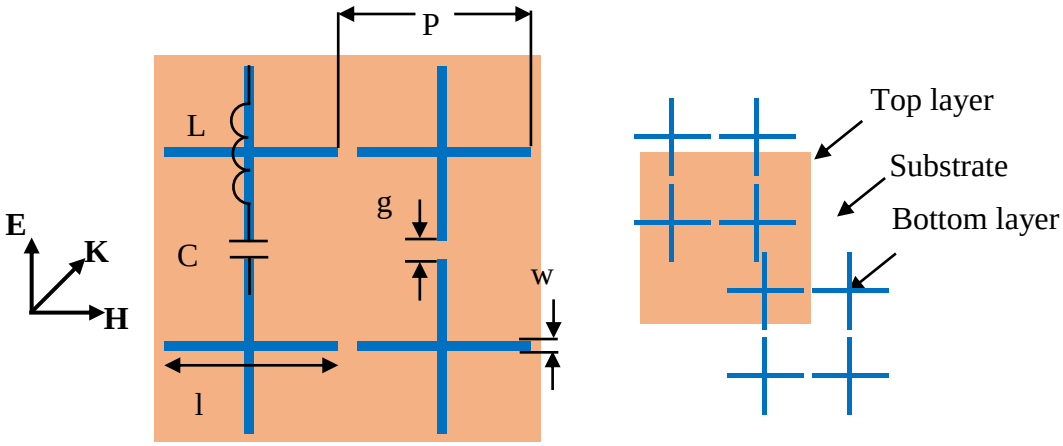

(a)

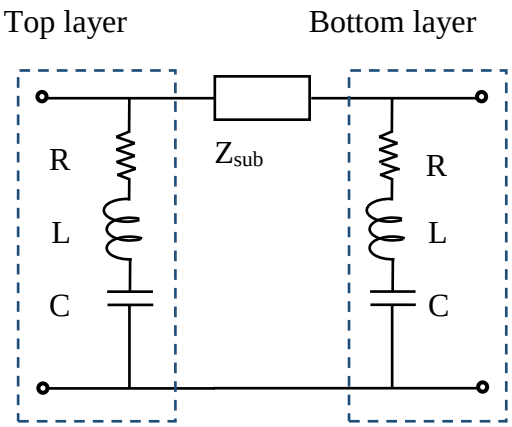

(b)

Figure 3.1 Double-sided parallel cross dipoles FSS structure and its equivalent circuit model.

The equivalent circuit model of the proposed FSS is shown in Figure 3.1(b), represents a band-stop filter. With this circuit, a double-sided parallel cross dipoles FSS can be synthesized to control the reflection level of the signal and the bandwidth enhancement. Therefore, by specifying the operating frequency $\left(f_0 = 1/2\pi\sqrt{LC}\right)$ [71] and the approximate quality factor of the overall circuit $(Q_1 + Q_2)/2$, where $\left(Q_1 = Q_2 = \sqrt{L}/R\sqrt{C}\right)$ [72], all the circuit parameters can be determined.

The first step in the proposed synthesis procedure is to obtain the parameters of the equivalent circuit model presented in Figure 3.1(b). The series RLC resonator is implemented with the periodic arrangement of the metal strips, where 'L' is an equivalent inductance of the vertical dipoles, 'C' is the capacitance between the vertical ends of the two double-sided parallel crossed dipoles. And, the equivalent resistance 'R' corresponds to the ohmic losses of the metallic strips. The lumped element values of the equivalent circuit are commonly calculated using (3.1), (3.6), and (3.8), where 'P', '*l*', '*w*', and 'g' are the dimensions of the unit cell of a double-sided parallel crossed-dipole respectively. The 'θ' is the incidence angle with the normal incidence.

The equivalent inductance 'L' is given by [26], and Marcuvitz [70] as

$$\omega L = Z_0 \frac{l}{P} \cos\theta \, F(P, w, \lambda_0, \theta) \tag{3.1}$$

where 'ω' is an angular frequency, Z_0 and λ_0 are free-space wave impedance, and wavelength respectively.

$$F(P, s, \lambda_0, \theta) = \frac{P}{\lambda_0}\left[\ln\left\{\frac{\csc \pi s}{2P}\right\}\right] + G(P, s, \lambda_0, \theta) \tag{3.2}$$

$$G(P, s, \lambda_0, \theta) = \frac{(1-\beta)^2[(1-\beta^2/4)(A_+ + A_-) + 4\beta^2 A_+ A_-]}{2 \times (1-\beta^2/4) + \beta^2(1+\beta^2/4-\beta^2/4)(A_+ + A_-) + 2\beta^6 A_+ A_-} \tag{3.3}$$

where,

$$A_\pm = \frac{1}{\sqrt{\left[1 \pm \frac{2P\sin\theta}{\lambda_0}\right] - \left(\frac{P\cos\theta}{\lambda_0}\right)^2}} - 1 \tag{3.4}$$

$$\beta = \sin\left(\frac{\pi s}{2P}\right), \text{with } s = w \text{ or } g \tag{3.5}$$

The equivalent capacitance 'C' is given by Langley and Drinkwater [73] as

$$\omega C = 4Y_0 \frac{(2 \times w + g)}{P} \cos\theta \, F(P, g, \lambda_0, \theta)\varepsilon_{eff} \tag{3.6}$$

where "ω' is the angular frequency, Y_0 and λ_0 are free-space wave admittance and wavelength, respectively.

The factor ε_{eff} in (3.6) represents an effective permittivity [72] and is calculated by

$$\epsilon_{eff} = \epsilon_{rh} + (\epsilon_{rh} - 1)\left[\frac{-1}{exp^N(x)}\right] \tag{3.7}$$

with *x = (10*h/P)*; where '*h'* is the thickness of the substrate, '*P'* is the size of the unit-cell, $\varepsilon_{rh} = \varepsilon_r$ (if dielectric presents on both sides of the FSS) and $\varepsilon_{rh} = (\varepsilon_r+1)/2$ (if dielectric presents only on one side), and *N* is an exponential factor that varies from 1.3 to 1.8 for different cell shapes in terms of the unit-cell filling factor. For double-sided parallel cross-dipole-based MS, the optimal value of 'N' is 1.3.

The equivalent resistance 'R' can be calculated from [74] as

$$R \approx R_s \frac{S}{A} \tag{3.8}$$

where '*Rs*' is the surface resistance, $S = P^2$ is the area of one-unit-cell, and $'A'$ is the surface area of the lossy element within a single unit cell. Using Equations (3.1) to (3.8), the equivalent circuit parameters in Figure 3.1(b) can be readily determined.

Finally, the quality factor Q of the proposed FSS can be derived by substituting (3.1), (3.2) and (3.8) in the quality factor expression ($Q = \sqrt{L}/R\sqrt{C}$) as

$$Q = \frac{Z_0 A}{2R_s S}\sqrt{\frac{l \times F(P, w, \lambda_0, \theta)}{(2 \times w + g) \times F(P, g, \lambda_0, \theta)\varepsilon_{eff}}} \tag{3.9}$$

From these formulas, it can be concluded that the Q factor is a function of the different geometric parameters of the unit cell. However, the values of the strip length and periodicity can not be chosen freely. The dipole length is approximately equal to $\lambda/2$ at the resonance frequency, while the periodicity of the structure must be much smaller than the wavelength. Subsequently, the quality factor can be controlled freely by the strip width.

In summary, the methodology and synthesis procedure of the proposed FSS are outlined as follows:

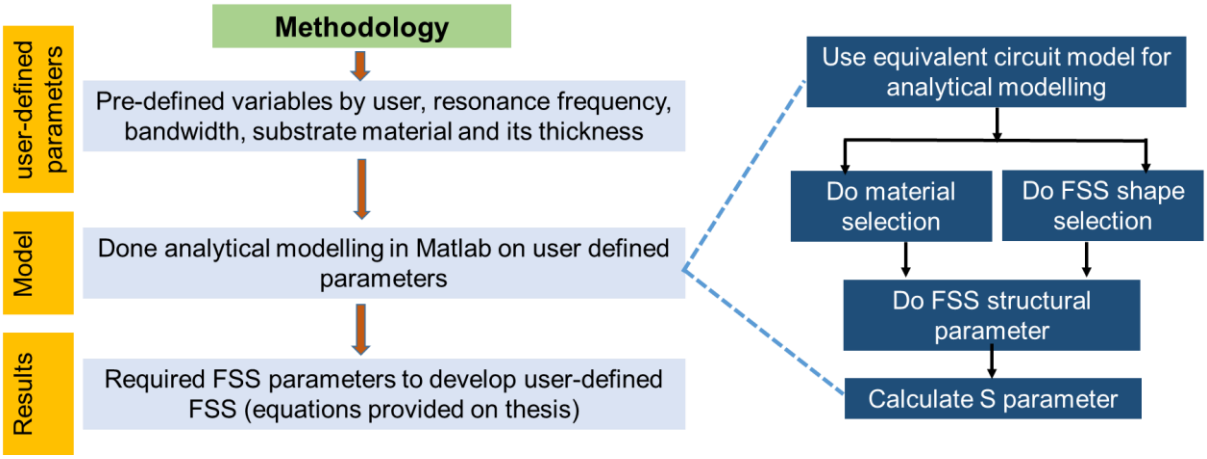

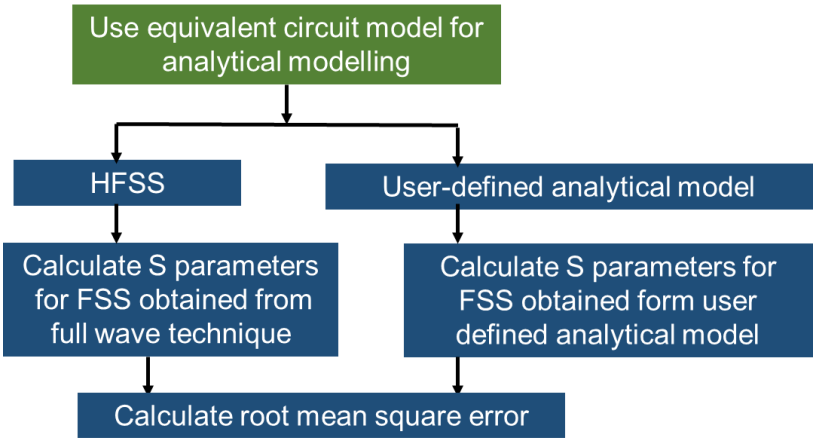

A. First, with the given values of the center frequency (f_0) and quality factor (Q), the parameters of the equivalent circuit elements can be obtained.

B. The dipole length 'l' is approximately equal to $\lambda/2$ at the resonance frequency.

C. Based on this calculated dipole length 'l' and with a starting value of the metal width 'w', estimate the value of the FSS's periodicity using the relation of equivalent resistance i.e., Eq. (3.8).

D. By enforcing the angle of incidence at normal incidence and for a given substrate, determine the value of the metal width 'w' using Eq. (3.6).

The above method allows the equivalent circuit shown in Figure 3.1(b) to synthesize the desired filtering response. It demonstrates the relationship between the equivalent circuit elements and the physical dimensions of the proposed FSS.

3.3 Numerical results

The synthesis steps described in Section 3.2 are followed to design a stop-band FSS having a resonant frequency at 10 GHz for an arbitrary value of quality factor $\boldsymbol{Q}$=**7.5**. Hence, the values of EC parameters are calculated as R = 0.05 Ω, C = 0.031 pF, and L = 8 nH. After acquiring the equivalent circuit parameters and choosing the dielectric substrate (εr = 2.94, h = 0.13 mm, tan δ = 0.02), the initial values of the unit-cell dimensions are obtained. Hence, the dipole length '*l*' = 11.1 mm, the element size (or the period of the unit cell) 'P' = 11.6 mm, and the dipole strip width '*w*' = 0.2 mm. It should mention that these physical parameters are obtained for the normal incidence. Based on these values, the proposed FSS is designed, and verified with the full-wave simulation. The obtained geometrical parameters of the unit-cell are tuned by using Ansys HFSS [75] to reach the desired frequency response. The transmission coefficient predicted by the equivalent circuit model is compared with the simulated results obtained by the initial geometry parameters and the tuned parameters are shown in Figure 3.2. It is observed that the optimized HFSS simulated results are in close agreement with the obtained theoretical results. The surface current distribution of the proposed FSS for TE and TM modes is depicted in Figure 3.3. From this figure, it is evident that the proposed model has the same frequency response for both modes.

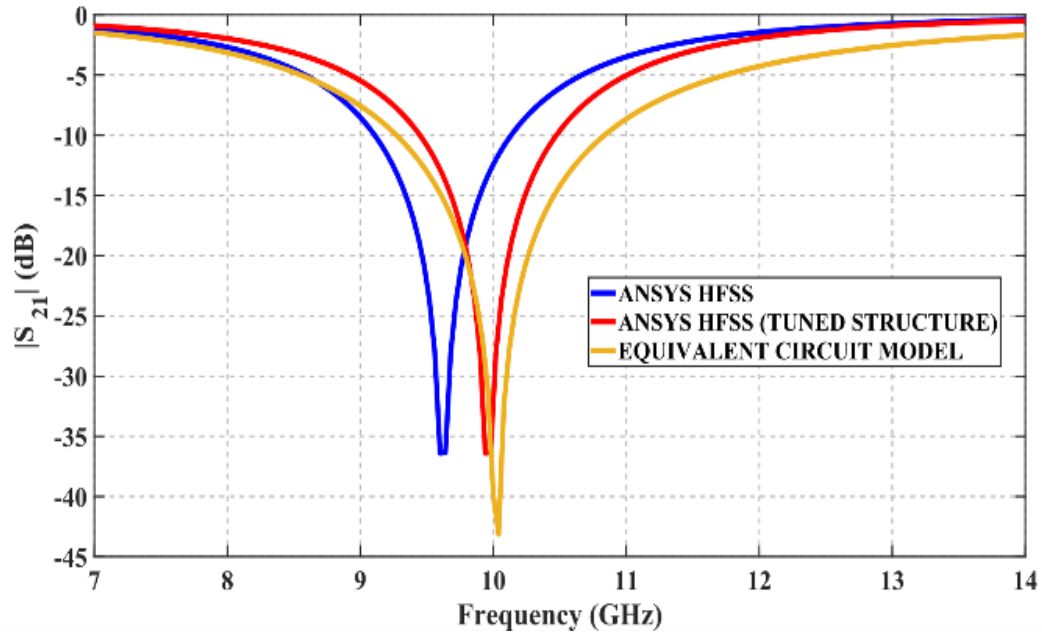

Figure 3.2 Transmission coefficient obtained by different methods for normal incidence.

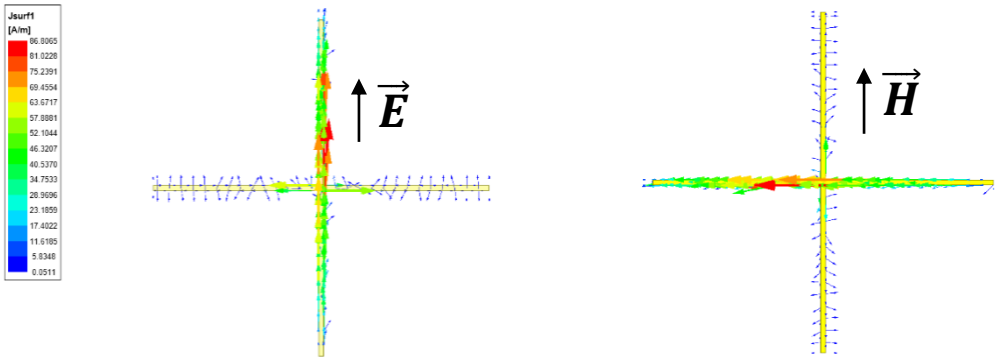

(a) (b)

Figure 3.3 Surface current distribution of the proposed FSS at 10 GHz. (a) TE, and (b) TM mode of polarization.

3.4 Bandwidth enhancement

To obtain a wide stopband, the quality factor (Q) has to be decreased. Based on the filter theory [71], Q can be reduced by reducing the equivalent inductance and increasing the equivalent capacitance at the same time. From Eq. (3.1) described in section 3.2, it is evident that using a large value of inductive element implies a gradual shift of the resonance frequency and generates poor

stability under oblique incidence. Therefore, it is necessary to keep the inductance constant and, at the same time, increase the capacitance of the FSS to obtain a larger bandwidth. From Eq. (3.6) described in section 3.2, it is necessary to choose a wider element to increase the capacitance of the FSS. For this reason, the metal width of the unit-cell is predicted as a function of the quality factor Q. Based on Eq. (3.9), the value of the metal width can be estimated for various values of Q. By using this synthesis method, the dipole width of the unit-cell is estimated for given frequency response and dielectric substrate at normal incidence. The data used for this case is as follows: the resonant frequency is 10 GHz, and the FSS is designed on a 0.13 mm thick RT/Duroid 6002 substrate with a relative dielectric constant of 2.94. The illustrated Figure 3.4 represents the strip width '*w*' of the unit-cell under the quality factor variation. It can be observed that, for a wider bandwidth performance, should use a wider metal strip.

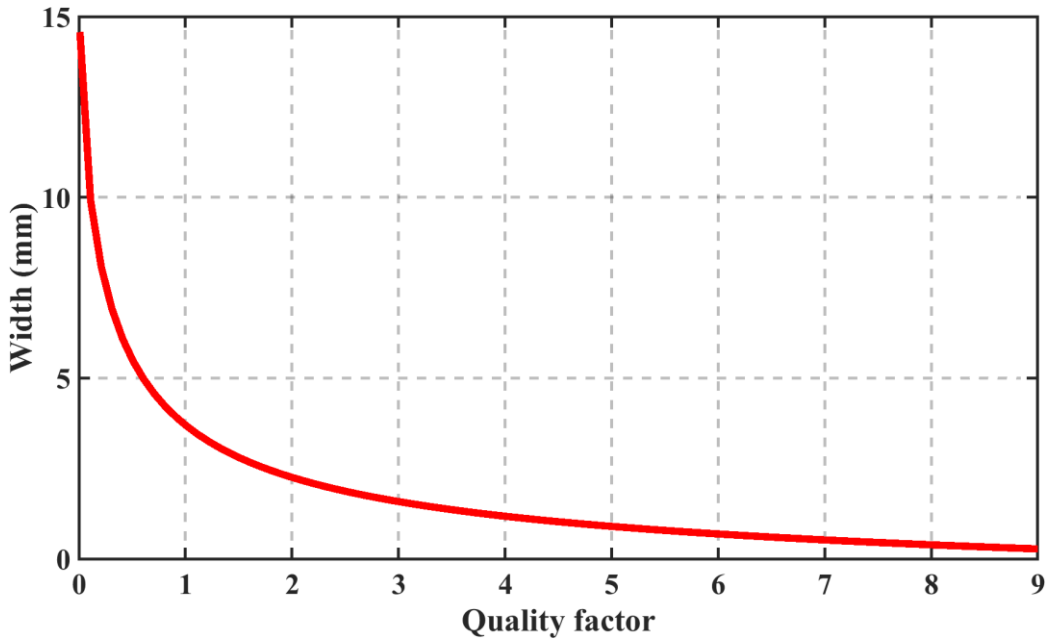

Figure 3.4 Plot for strip-width (*w*) as a function of the Quality factor.

3.5 Conformal behaviour

In real-time applications, such as aerospace fuselage, parabolic reflectors, radome antennas, and many others, the conformal FSS is a significance factor, which is flesh mounted to the surface. Hence, the conformal behavior of the proposed FSS is analyzed using the bending option in Ansys HFSS. Based on a semi-infinite model described in [76], the conformal FSS is evaluated, and the same is simulated, as shown in Figure 3.5. A finite array of FSS with 1×25 is simulated using wave

ports. The top and bottom walls of the waveguide are assigned as PEC or PMC boundaries, whereas the side walls are assigned as open boundaries. This technique helps to evaluate the conformal structure at normal incidence. Figure 3.6 shows the simulated transmission coefficient for planar and conformal FSS. It should also mention that the frequency response of the planar geometry is obtained by using periodic boundary conditions.

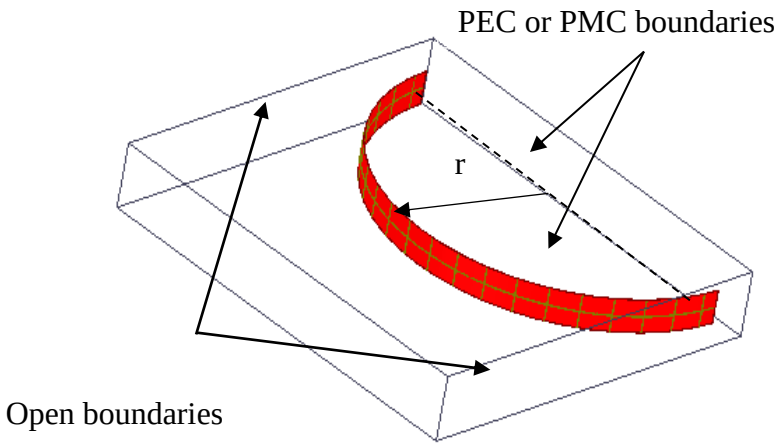

Figure 3.5 Simulation setup of the conformal FSS.

Figure 3.6 presents the comparison of the simulated transmission coefficient of the conformal FSS and the planar FSS at the normal angle of incidence for both polarizations. It is observed that the resonant frequency for the FSS shifts from 10 GHz when the structures are bent. Figure 3.6(a) shows that for the TE mode of polarization at the normal incidence, when the FSS is bent with a radius (r) of 83 mm, the simulated resonance frequency is shifted from 10 GHz to 10.19 GHz. On the other hand, for the TM mode of polarization, as shown in Figure 3.6(b), the resonance frequency is shifted from 10 GHz to 10.2 GHz. This slight variation in the resonance frequency for both the polarization is attributed to the variation of the impedance proprieties and the interelement coupling of the FSS when it is bent [77].

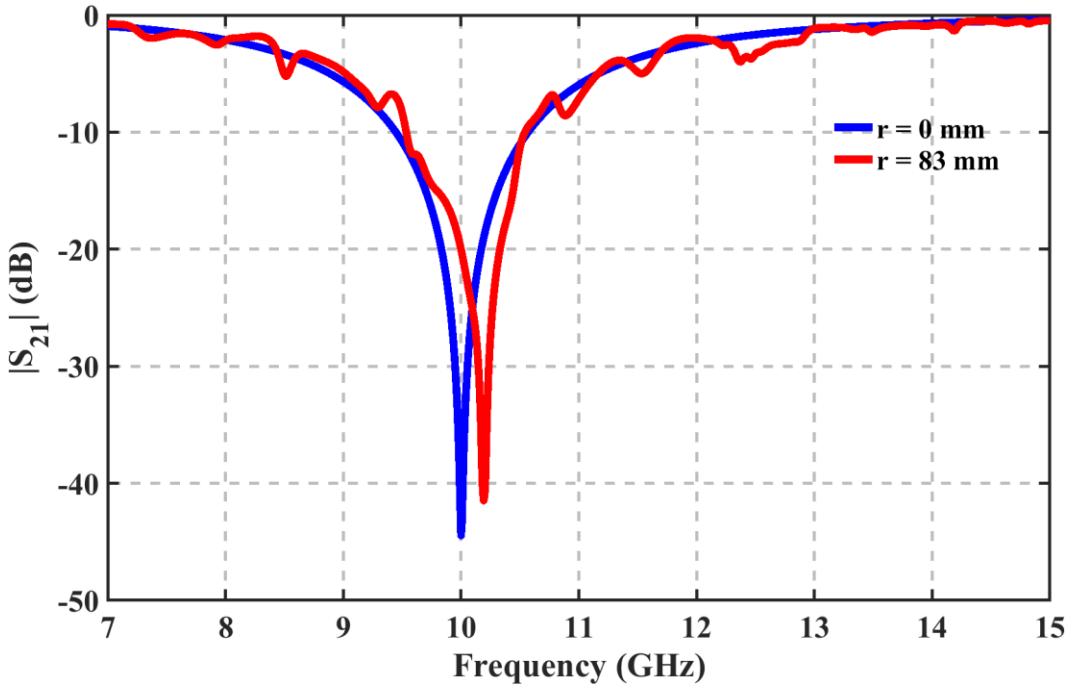

(a)

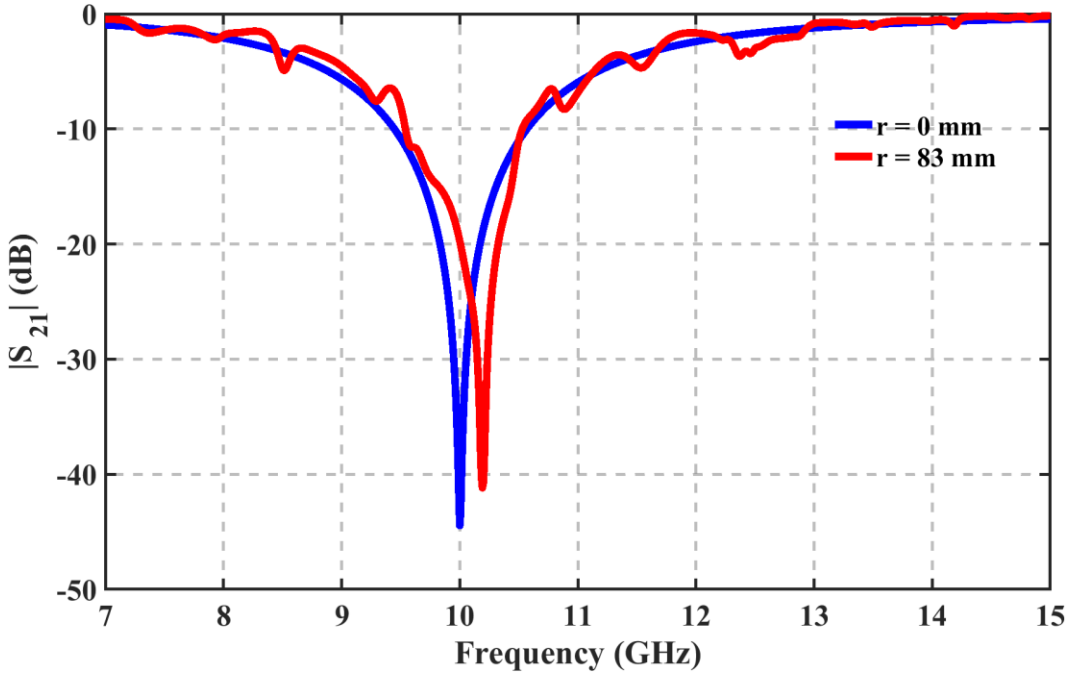

(b)

Figure 3.6 Simulated transmission coefficient for conformal (r=83 mm) and planar (r=0) FSS at normal incidence (a) TE, and (TM) modes respectively.

3.6 Experimental results

3.6.1 Planar FSS

To experimentally validate the synthesis method described in section 3.2, a prototype of the double-sided parallel cross-dipoles FSS, as shown in Figure 3.7, is fabricated and measured. The dimensions of the FSS prototype are 304 mm × 304 mm, containing 25 × 25 elements for a metal width of 0.2 mm, a dipole length of 11.91 mm, and a periodicity of 12.16 mm, respectively. The measurement is performed in an enclosed room, where two wideband horns (1 GHz to 18 GHz) are used in the experimental setup. As shown in Figure. 3.8, the FSS prototype is placed between horn antennas, and the measurements are taken using an Agilent (PNA-X N5242A) network analyzer. As a reference, the transmission coefficient without FSS structure is measured. After that, the subsequent measurements of the transmission coefficients, for various angles of incidence and polarization, are obtained using a rotating mechanical system. The TE and TM modes were measured by using the method described in Figure 3.9.

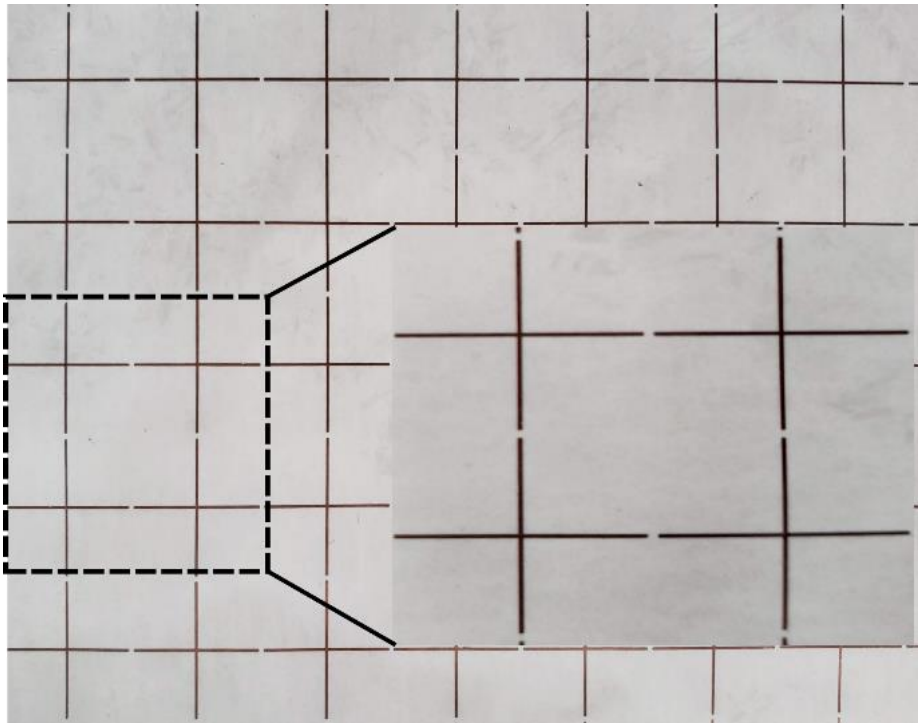

Figure 3.7 Photograph of the fabricated FSS prototype.

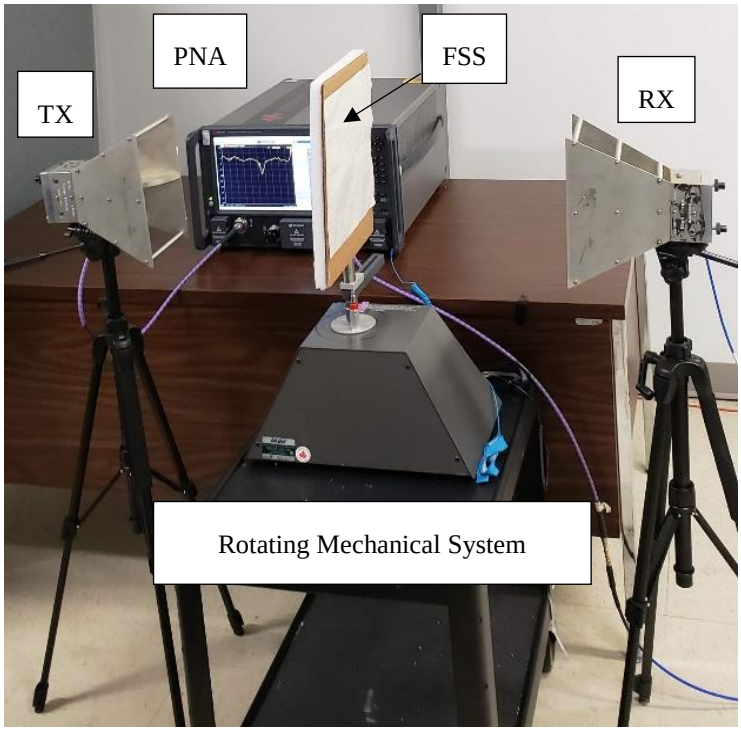

(a)

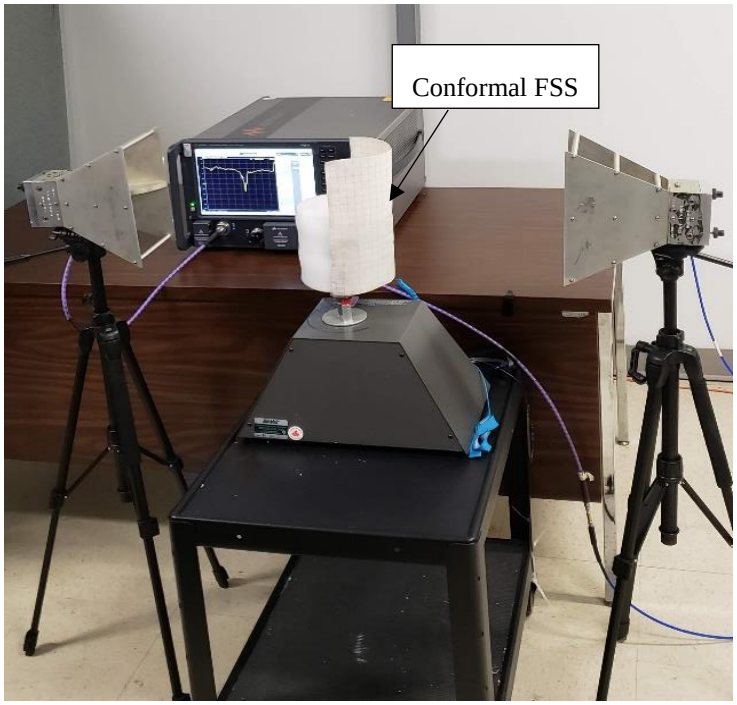

(b)

Figure 3.8 Experimental setup for measuring transmission coefficient for (a) Planar and (b) Conformal FSS.

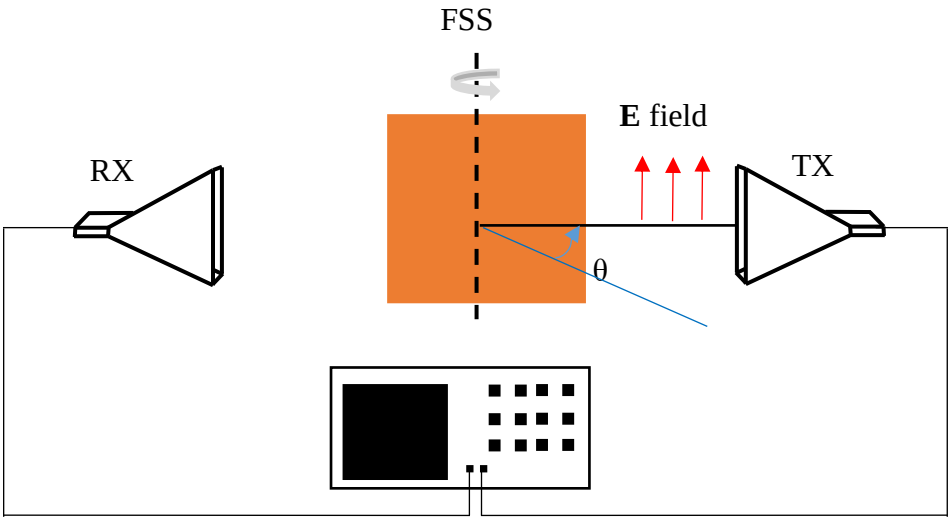

(a)

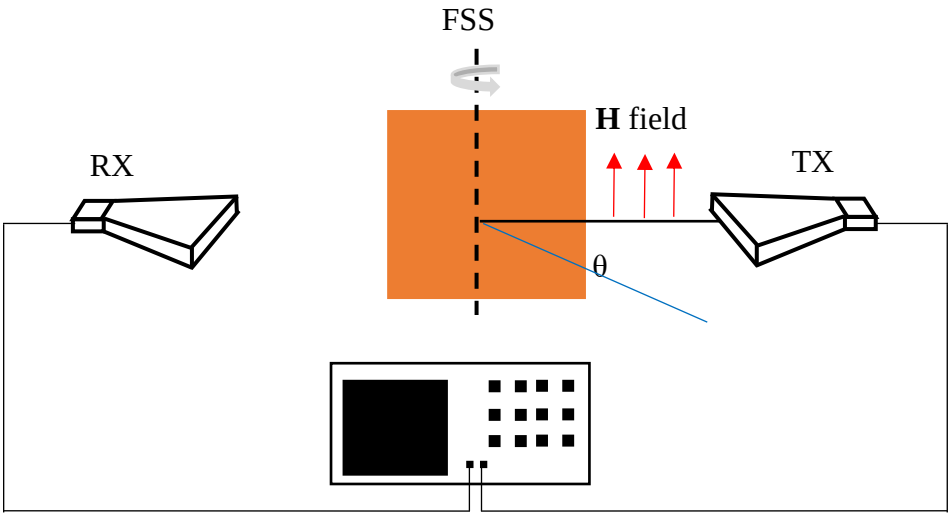

(b)

Figure 3.9 Measurement method for (a) TE, and (b) TM mode of polarization.

The measured transmission coefficient for both TE and TM mode of polarizations for various angles of incidence are plotted in Figure 3.10. The measured FSS response for the TE polarization with different angles of incidence is plotted in Figure 3.10(a). For the TE mode of polarization, it is observed that, as the angle of incidence increases, the bandwidth increases. Different behavior is observed for TM mode of polarization as shown in Figure 3.10(b). When the angle of incidence increases from 0° to 60°, the bandwidth decreases. The resonant frequency shift is observed for both polarizations when the incident wave angle varies from 0° to 60°. This occurs due to the impedance on the angle of incidence as given by the relation ($\boldsymbol{Z_{TE} = Z_0/\cos\theta}$, $\boldsymbol{Z_{TM} = Z_0 * \cos\theta}$).

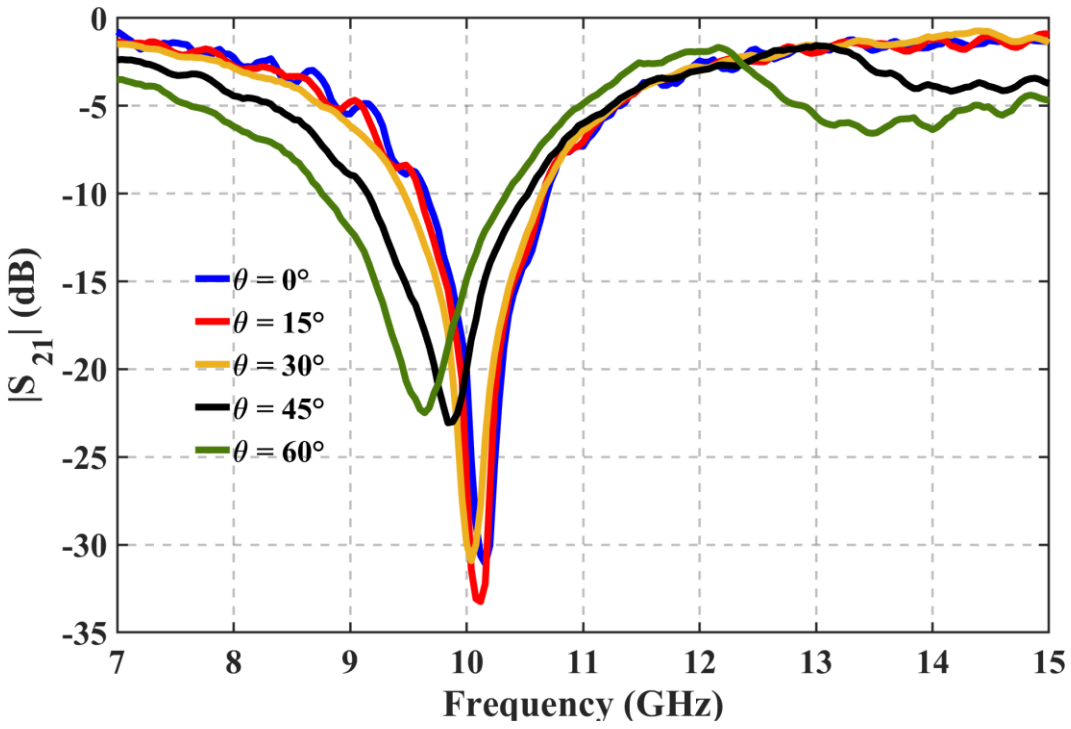

(a)

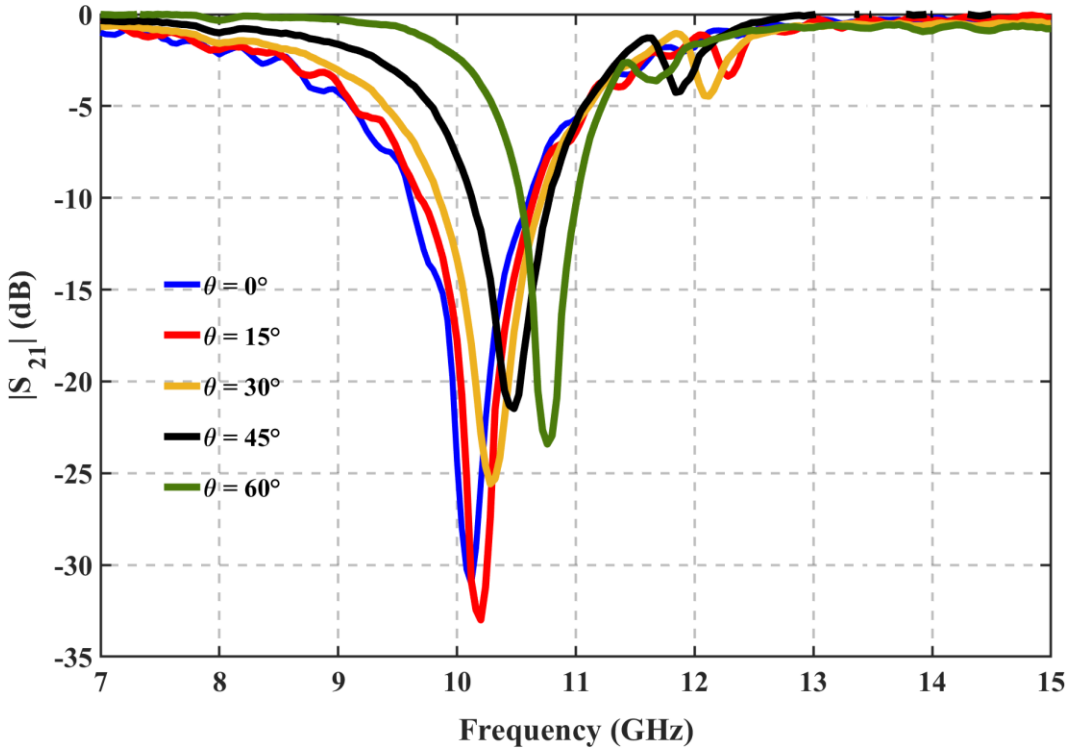

(b)

Figure 3.10 Measured transmittance for (a) TE, and (b) TM mode of polarization.

3.6.2 Conformal FSS

The transmission coefficient of the conformal FSS is obtained with a setup shown in Figure 3.8(b) at normal incidence for both TE and TM modes. The planar FSS is bent on an arc of radius 'r' of 83 mm. The structure is attached to semi-circular cylinder foam that has similar dielectric properties with the free space (ε_r = 1). Figure 3.11 shows the comparison of the measured transmission coefficient for both configurations. The conformal FSS exhibits a stable frequency response compared to the planar FSS at normal incidence for both polarizations.

To understand the shielding performance of the proposed FSS, shielding effectiveness (SE) is obtained using the following equation [78]:

$$SE(dB) = -20 \times \log\left|\frac{E_t}{E_i}\right| \tag{3.10}$$

Figure 3.12 presents the shielding performance (SE) of the proposed FSS for both polarizations at normal incidence. It is evident that the proposed FSS provides a high SE level around 10 GHz for both TE and TM modes. Hence, the proposed FSS is suitable for EMI shielding applications.

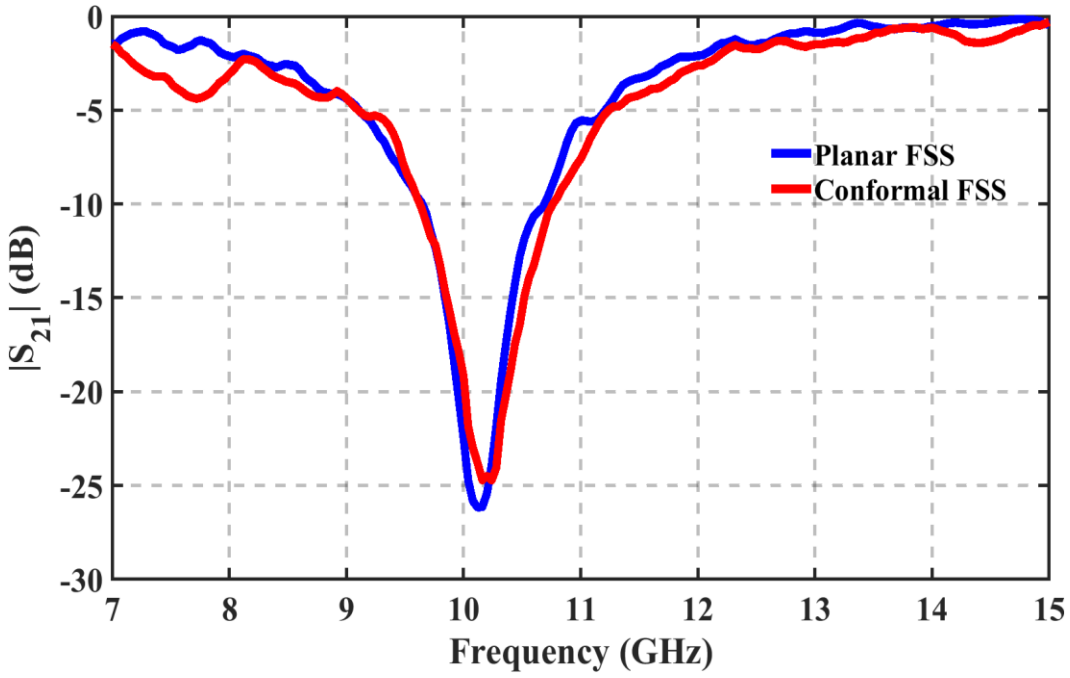

(a)

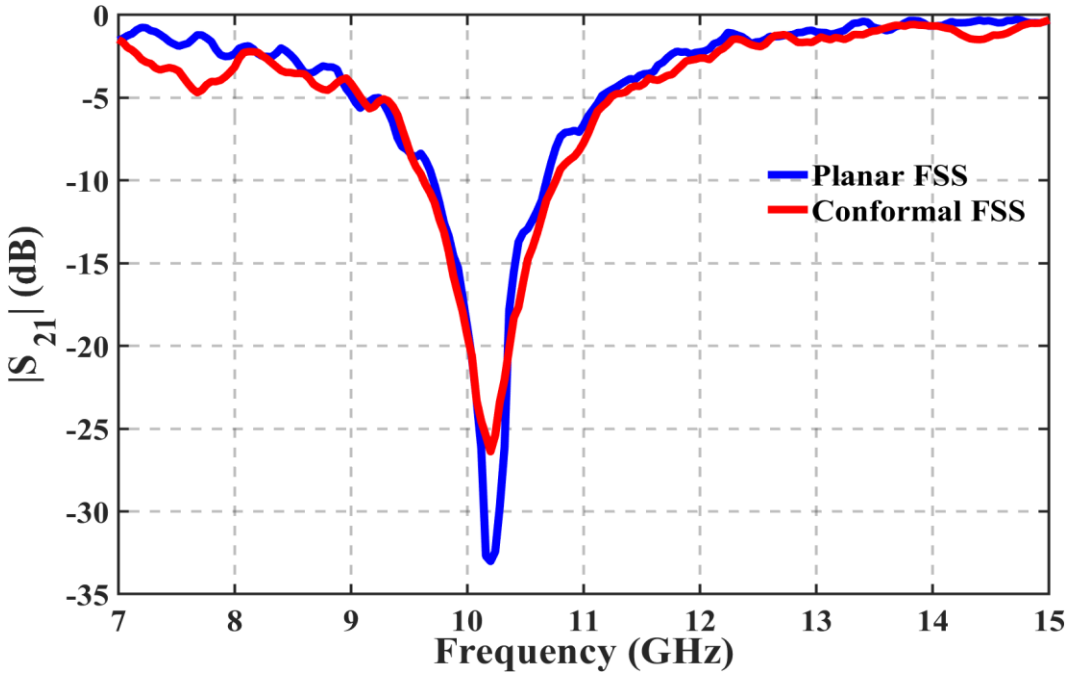

(b)

Figure 3.11 Measured transmission coefficient for conformal and planar FSS at normal incidence (a) TE, and (TM) modes respectively.

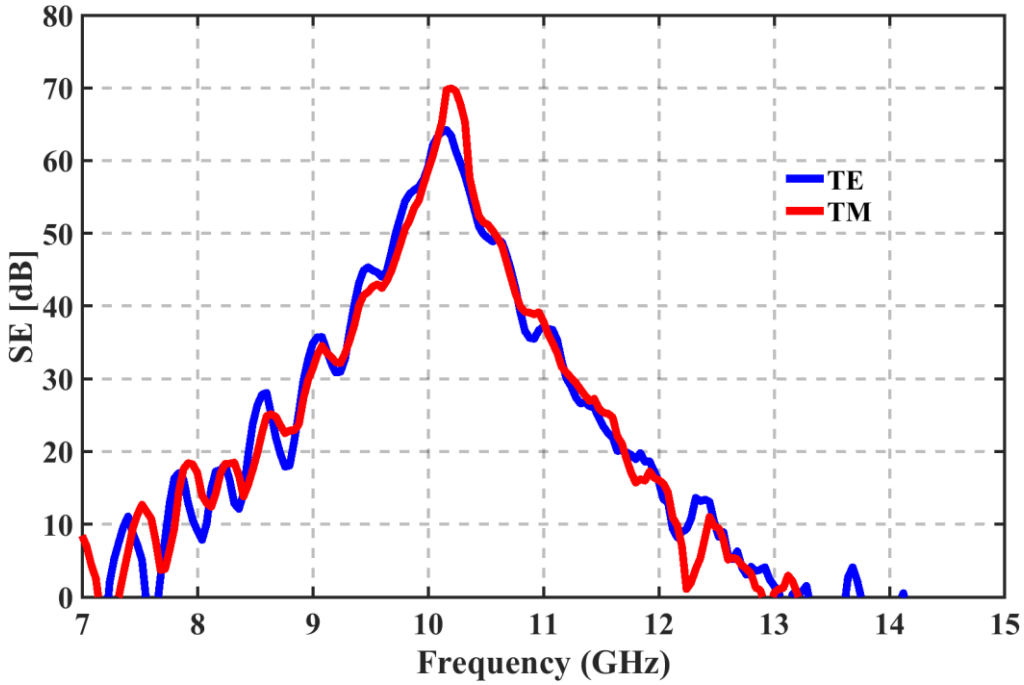

Figure 3.12 Measured shielding effectiveness of the proposed FSS for both polarizations at normal incidence.

Further, the comparison of the proposed work with the related works is shown in Table 3.1. It is evident from Table 3.1 that the proposed design method solves the synthesis problem, which is rarely described in the literature especially for double-sided crossed dipoles. The proposed synthesis method is based on the equivalent circuit model provides a simple way for designing conformal FSS, which can be applied in electromagnetic interference shielding applications. In addition, this method provides a formula for the Q factor as a function of the geometric parameters of the unit cell, which can be used to improve the bandwidth.

Table 3.1 Comparison with related works

Ref	**Element used**	**Center frequency (GHz)**	**Method**	**Flexibility**	**Number of layers**
[69]	Complementary JC element	10	Analysis method	Yes	Single
[79]	Square loop	13.5	Synthesis method	No	Double
[80]	Crossed dipoles	8	Synthesis method	No	Single
[81]	Patch	10	Analysis	No	Single
Proposed work	Double-sided Crossed dipoles	10	Synthesis	Yes	Single

3.7 Conclusion

In this chapter, a simple method for synthesizing band-stop FSS and control of bandwidth is presented. The band-stop FSS consists of double-sided parallel cross-dipoles. The proposed conformal FSS is analyzed based on the equivalent circuit model at the desired frequency response, which allows acquiring the optimized physical parameters. The proposed work is verified by

designing an ultra-thin FSS prototype having a band-stop response with a quality factor of 7.5 at 10 GHz. Full-wave simulations and experimental verifications have demonstrated the performance of the proposed FSS. The fabricated FSS is tested under different incident wave angles for both TE and TM modes of polarization.

CHAPTER 4 SYNTHESIS OF BANDSTOP METASURFACE BASED ON STEPPED-IMPEDANCE CROSS DIPOLE RESONATORS

4.1 Introduction

MSs are extensively used in modern wireless communications, such as radar systems, aircraft radomes, broadband communication, and antenna engineering [82-87]. It is considered as a spatial filter for incoming electromagnetic waves due to their great frequency filtering property. MS is often composed of a periodic arrangement of metallic or apertures cells with arbitrarily shape, generally supported by or embedded in a dielectric substrate [44]. Similar to analog filters, frequency selective surfaces can demonstrate low-pass, high-pass, band-pass, or band-stop frequency responses. In contrast to their circuit counterparts, the electromagnetic response of the MSs depends not only on frequency, but also on the geometry of the unit cell, as well as the angle and polarization of the incident wave. Moreover, the periodicity of the unit cell should be smaller than $0.4\lambda_0$ ($\lambda_0$is the free- space wavelength of the resonant frequency) to achieve a stable resonant frequency under various angles of incidence [30]. This particular constraint puts the search for a miniaturized unit cell into perspective.

Generally, the resonance frequency and the size of the MS element are inversely related to the inductance and capacitance of its equivalent circuit for series or parallel resonance. Therefore, increasing both of these parameters leads to a reduction of the size of the MS unit cell. Consequently, different techniques have been proposed in the past to miniaturize the size of the MS unit cell. The simplest approach to achieve size reduction is to embed lumped elements into the MS [88-90]. Another approach to achieve the size reduction is the use of multilayer substrates [91-92]. In [91], ultrathin dielectrics were used to increase the capacitance across different layers of a substrate. Metallic patches and wire grids have also been used to construct a compact MS [92]. Moreover, complex geometries were used to design a miniaturized MS. Using metallic meander lines, space-filling curves and fractal structures increases the inductance by increasing the electrical length of the MS element while the decreasing of the separation between the adjacent conductors increases the equivalent capacitance of the MS [93-100]. Recently, 2.5- and 3-dimensional MS have gained more attention [101-104]. For the 2.5-D MS, the vias are used to increase the capacitive coupling between adjacent elements by connecting adjacent substrate layers within the element to increase the inductance [101].

However, using these techniques to avoid sensitivity to polarisation or incident angle can increase the complexity of the MS structure. This complexity can restrict the use of MSs in many applications.

In this chapter, we propose a new technique for designing miniaturized metasurfaces using stepped-impedance resonators [105]. This technique is already used and verified for analog RF filters. The proposed MS unit cell has a dimension of $0.065\lambda_0 \times 0.065\lambda_0$. This MS exhibits highly stable frequency selective characteristics when the incident angles range from 0° to 60° for both TE and TM polarizations. Besides the ability to control the spurious frequencies by changing the impedance ratio *k* of the stepped impedance, there is another degree of freedom relevant to the proposed technique which can be used to synthesize and achieve dual-band response. Conventional design procedures focus on the first resonance of the MS and no mechanism is introduced to control the second (and higher) resonances in isolation of the first resonance. Such capability has become more relevant and important. As a notable example is the recent 5G developments which call for a multiband operation of the MS. For instance, both 28GHz and 60GHz have been allocated for 5G operations and their near multiple integer relationship cannot be ignored in the MS design for 5G applications.

In Section 4.2, the design evolution and process of the unit cell is described, the MS geometry and the numerical results are presented in section 4.3, and the experimental results of the conventional stop band MS are discussed in section 4.4, followed by the conclusion in section 4.5.

4.2 Evolution and synthesis of the proposed MS unit cell

In the first subsection, the concept of stepped impedance in the context of analog microwave filter design is introduced and a detailed presentation of the structure is provided in the subsequent section.

4.2.1 General overview of stepped impedance resonator

Figure 4.1 shows the steps in the evolution and synthesis of the proposed unit cell of the MS. The design methodology was inspired by traditional microwave filter theory. The first step of unit cell design was the selection of a conventional topology. The design requirements of the MS governed the selection of the topology. The objective of the synthesis was to obtain a unit cell that renders the resulting MS with low sensitivity to the polarization and incident angle of plane wave excitations. Considering these requirements, a cross dipole element was selected as the starting point of the synthesis process to maintain insensitivity to orthogonal linear polarizations. On the other hand, it is well known this structure is sensitive to the variation of the incident angle of the incoming plane wave [82]. To overcome this shortcoming, a new design was proposed based on conventional the step impedance resonator (SIR) approach. Thus far, SIRs [105] have been used extensively in the design of analog microwave filters. These resonators have many advantages compared to uniform resonators including size reduction and control of spurious frequencies. These features offer flexibility for the design of MSs. Figure. 4.1 shows the general process of the evolution of the basic structure of the stepped impedance resonator.

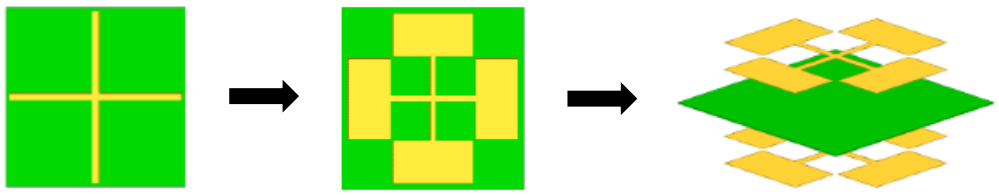

(a) (b) (c)

Figure 4.1 Design flowchart. (a) Conventional crossed element. (b) Stepped impedance (SI) crossed element. (c) Proposed Double Sided SI element.

4.2.2 Detailed presentation of the synthesis of stepped impedance resonators

The first step in the design process aims to figure out the link between analog and spatial filter design. Figure 4.2 shows the double sided parallel crossed elements unit cell, which consists of crossed dipoles printed on both sides of a dielectric substrate. Due to the symmetric geometry, the unit cell can be analyzed for single polarization of normal incidence as shown in Figure 4.3. Since the proposed unit cell is based on parallel resonators, the even- and odd- mode analysis should be performed. According to the transmission line theory, the characteristic propagation of parallel resonators can be expressed by the characteristic impedance and the propagation constant. In order to investigate them, a commercial simulator was used. The propagation characteristics of the parallel strips can be extracted by using the terminal mode of ANSYS HFSS [75]. Wave ports voltage were used in this process. To investigate the propagation characteristic of the proposed structure, the structure was designed on RT/Duroid 6002 dielectric substrate with $\varepsilon_r = 2.94$ and thickness of 0.13 mm.

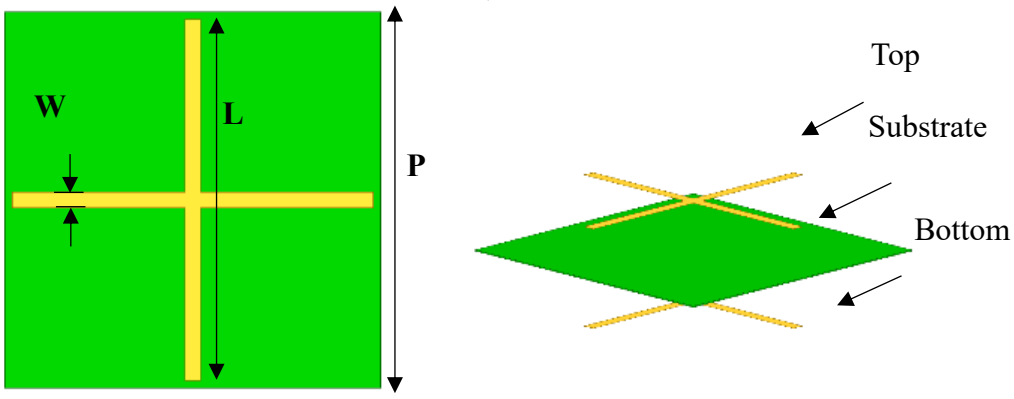

Figure 4.2 Double sided parallel cross dipole unit cell.

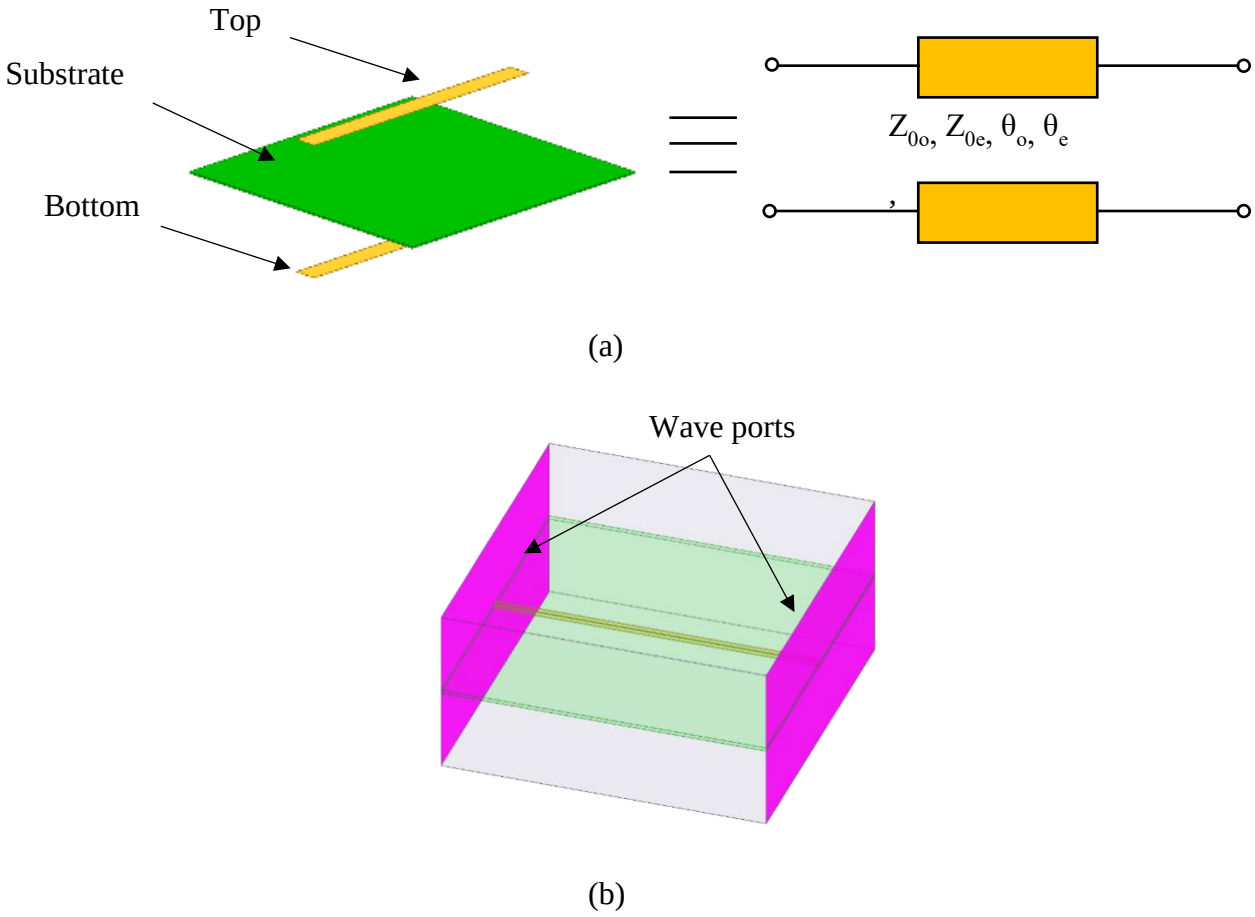

Figure 4.3 Parallel strips. (a) Propagation characteristic. (b) Wave ports excitation.

The illustrated Figures 4.4 and 4.5 represent effective permittivity and characteristic impedance under the frequency and strip width variation for even-odd modes. It can be observed from Figure. 4.4, that, the effective permittivity remains constant when the frequency varies for both modes. The effective permittivity for even and odd modes were influenced by the strip width variation. It can be seen from the presented results that the effective permittivity decreases when the metal strip increases for odd mode, whereas it increases for even mode. As for the characteristic impedance,

it can be concluded from Figure 4.5, that, for both modes, it was influenced by the metal width variation.

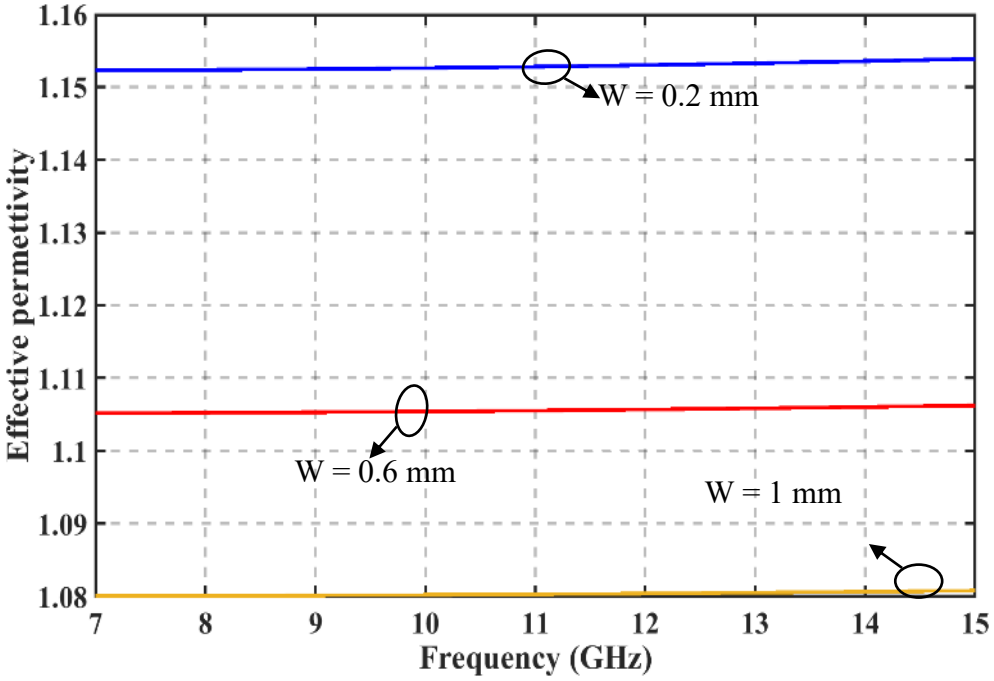

(a)

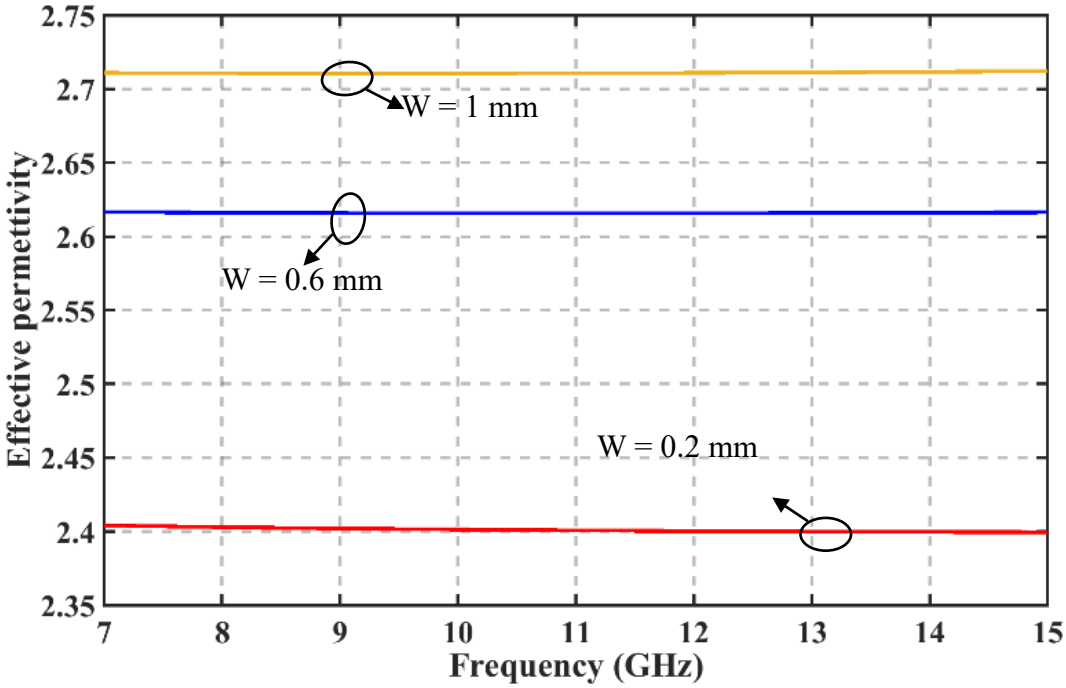

(b)

Figure 4.4 Effective permittivity. (a) Even mode. (b) Odd mode.

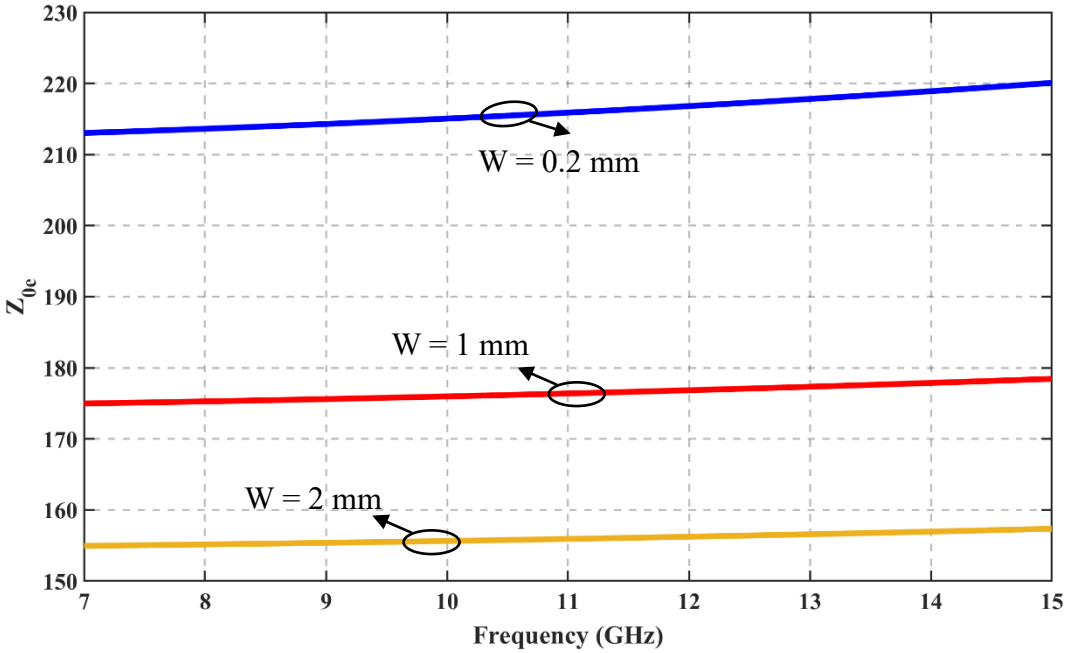

(a)

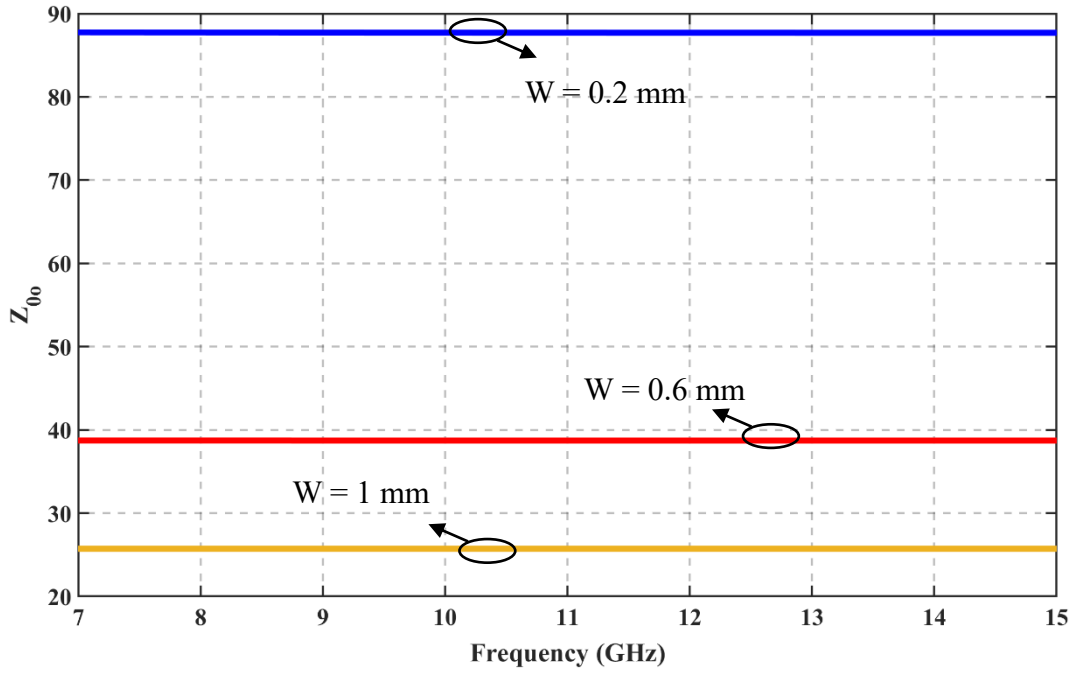

(b)

Figure 4.5 Characteristic impedance. (a) Even mode. (b) Odd mode.

Table 4.1 Electrical parameters of the parallel dipoles

	Symbol	Analog filter	
		Odd MODE	Even MODE
$W_1 = 0.2$ mm	Z_0	87.71	215.06
	ε_{eff}	2.75	1.15
$W_2 = 0.6$ mm	Z_0	38.72	175.98
	ε_{eff}	2.62	1.10
$W_3 = 1$ mm	Z_0	25.72	155.64
	ε_{eff}	2.40	1.08

Table 4.1 shows the characteristic impedance and the effective permittivity of the parallel resonators for different values of the strips width at 10 GHz. The extracted data can be used to predict the physical length of parallel dipoles used for periodic structures.

The parallel dipole length for even and odd modes can be obtained as follows:

$$L_{Odd} = \lambda_{g\_Odd}/2 \tag{4.1}$$

Where $\lambda_{g\_Odd} = \lambda/\sqrt{\varepsilon_{eff\_Odd}}$

$$L_{Even} = \lambda_{g\_Even}/2 \tag{4.2}$$

Where $\lambda_{g\_Even} = \lambda/\sqrt{\varepsilon_{eff\_Even}}$

The parallel dipole length of a strip width of 0.2 mm was computed based on the extracted data shown in Table 4.1. For the odd mode, the computed length $L_{Odd} = 9.04$ mm, whereas the computed length for the even mode was $L_{Even} = 13.98$ mm. After computing the parallel dipole length for both modes, the simulation of the periodic structure was performed by using the periodic

boundaries conditions of the ANSYS HFSS. For the periodic structure, the gap between the elements was chosen to be 0.25 mm.

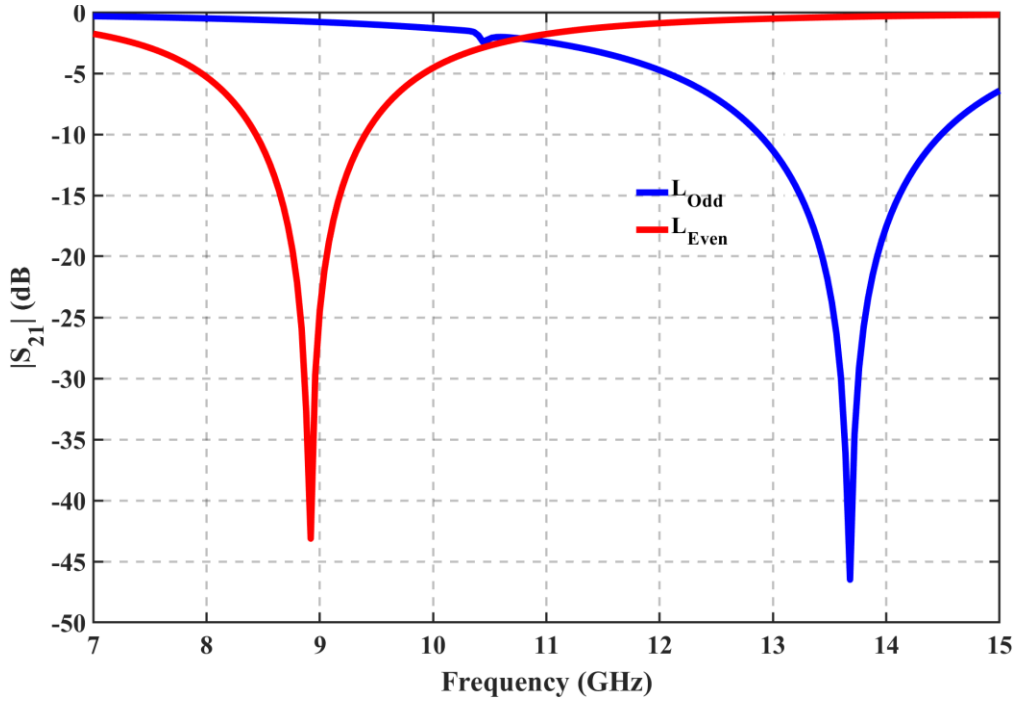

(a)

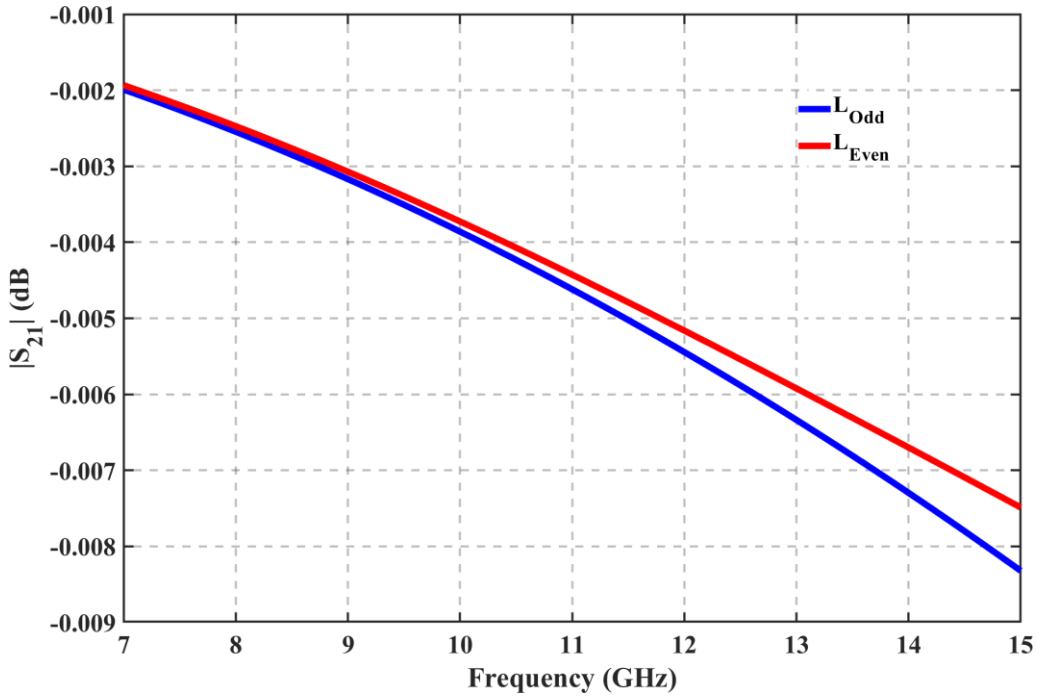

(b)

Figure 4.6 Simulated transmission coefficient at normal incidence. (a) E field parallel to strips. (b) E field orthogonal to strips.

The simulated result of the transmission coefficient for different modes of polarization for normal incidence is plotted in Figure 4.6. The simulated MS response when the electric field is parallel to the metal strips with different strips lengths is plotted in Figure 4.6(a), this response represents resonance behavior. It can be concluded that, the strips were driven by an equal current having the same polarity. From Figure 4.7(a), It can be seen that the electric field maintains odd symmetry with respect to the midline which is an indication of even mode excitation that can be modelled by the insertion of a perfect magnetic conductor in the middle as shown in Figure 4.7(b). Perfect reflection at the resonance frequency is generated by the even mode current. On the other hand, the odd mode renders the two coupled strips invisible to the incoming plane wave and supports perfect transmission. For this reason, even mode will be considered to predict dipole resonant length in the next step. Therefore, the uniform coupled strip can be represented by the characteristic impedance and propagation constant of the even mode.

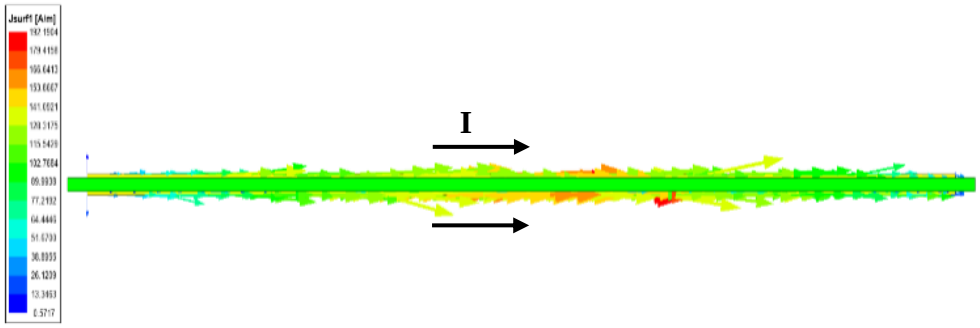

(a) Current distribution.

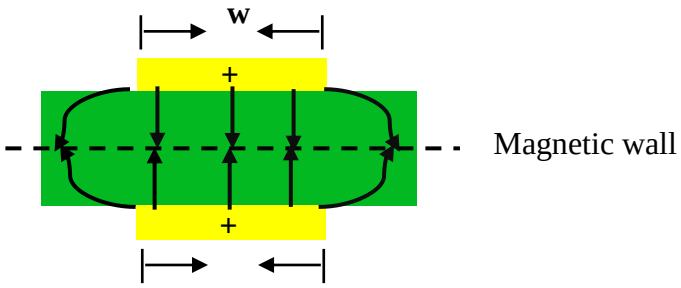

(b) Electric field.

Figure 4.7 Schematic of a broadside coupled resonator.

After the identification of the characteristic propagation mode, the uniform coupled strip was replaced by coupled stepped impedance strips to reduce the size of the unit cell. ANSYS HFSS was

used to predict the SIR length. The SIR used on the proposed unit cell is shown in Figure 4.8. This structure was used to design an analog filter in [104]. It consists of three coupled lines with different characteristic impedances, Z_1 (associated to W_1), and Z_2 (associated to W_2), and corresponding lengths L_1 (L_T /2), and L_2 (L_T /4), where L_T is the total length of the SIR. According to [105], the fundamental resonance condition can be expressed as

$$\theta_0 = tan^{-1}\sqrt{K} \tag{4.3}$$

where $K = Z_2/Z_1$ is the impedance ratio.

The relation between the total length of SIR θ_T and θ_0 is given as

$$\theta_T = 4\theta_0 \tag{4.4}$$

Finally, the SIR length was derived from (4.4) as follows

$$L_T = 4 * c * \varepsilon_{eff\_Even} * \tan^{-1}\sqrt{K}/2\pi f_0 \tag{4.5}$$

To compute the SIR length, terminal mode analysis in ANSYS HFSS was used to extract the strips' impedances and the effective permittivity. The SIR widths were chosen as follows: W_1 = 0.2 mm and W_2 = 3.2 mm. The high and low impedances associated with W_1 and W_2 are 215.06 Ω and 100.80 Ω, respectively. The extracted effective permittivity for the SIR is 1.04. Based on the values of the impedance ratio and the effective permittivity, the total length of SIR 'L_T' was derived using the equation (4.5) and given as: L_T = 8.3 mm.

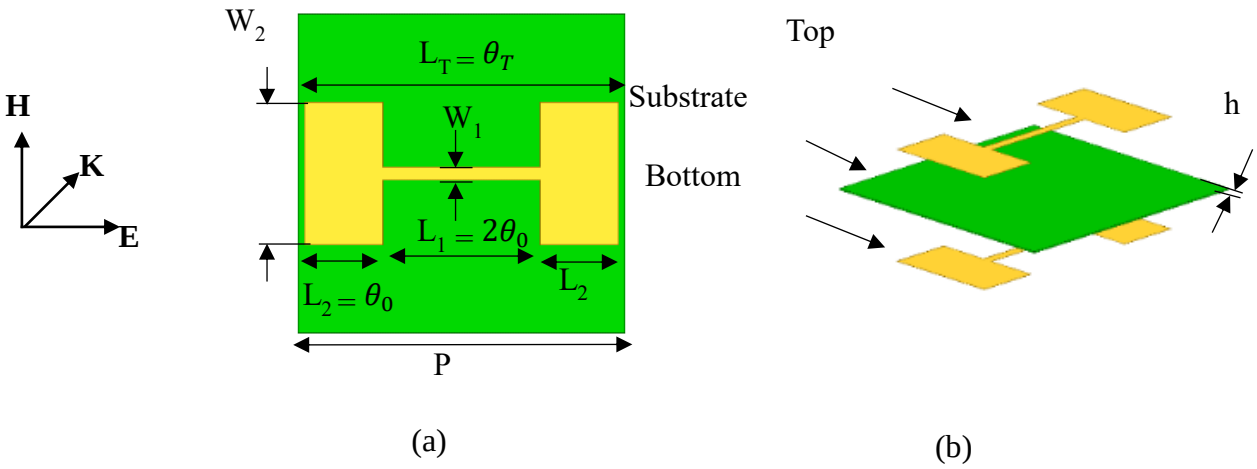

(a) (b)

Figure 4.8 MS model based on SIR, (a) Similar top & bottom unit cell formation, and (b) 3-D configuration.

Once the physical length of the SIR was obtained, the performance of the periodic structure was verified by ANSYS HFSS using the periodic boundary conditions. For the periodic structure, the inter-element spacing was defined as 0.25 mm. Figure 4.9 shows the comparison of the simulated transmission coefficient of MS considering the SIR length obtained from the circuit analysis and the optimized length which turned out to be 7.3 mm as compared to 8.3 mm obtained from the circuit analysis.

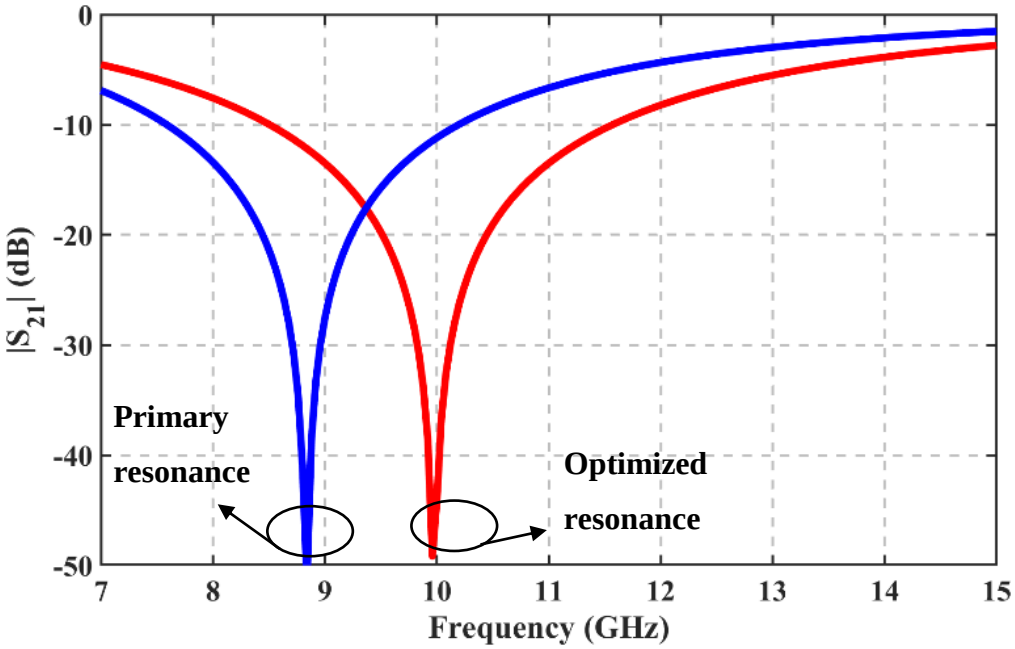

Figure 4.9 Transmission coefficient of the broadside coupled structure.

In summary, the design procedure of the unit cell based on SIR can be in general executed as follows:

1. With the given center frequency (f_0), dielectric proprieties and SIR widths, the characteristic impedances (Z_1 and Z_2) and effective permittivity can be extracted from commercial simulators.
2. According to the SIR equation (4.5), The SIR length 'L_T' can be computed.
3. Based on the computed length from the circuit analysis, the periodic structure can be simulated and the unit cell length can be slightly tuned to obtain the desired frequency response.

4.3 Simulation verification

The design approach described in the previous section was followed to design a miniaturized stop band MS having a resonant frequency at 10 GHz. The unit cell of the proposed MS consists of cross stepped impedance broadside coupled lines separated by a dielectric substrate as shown in Figure 4.10. The substrate material used for the MS is 0.13 mm thick RT/duroid 6002 substrate with a dielectric constant of 2.94 and a loss tangent of 0.001. The resonators are made of 17 μm thick copper. However, before the structure could be designed, a parametric study was carried out to understand the effect of the impedance ratio on the periodic structure frequency response. In the simulation analysis, the dimensions of the unit cell are kept constant, while the impedance ratio is

changed. It should be noted that for the uniform structure k = 1, W_1 and W_2 is equal to 0.2 mm and the operating frequency is 10 GHz.

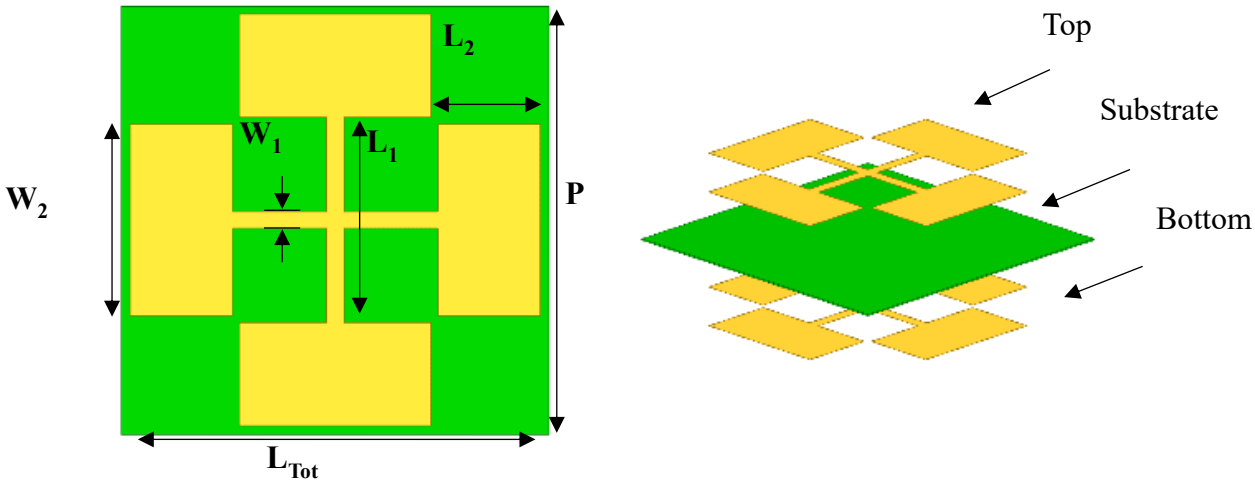

(a) (b)

Figure 4.10 Proposed MS model based on SI resonator, (a) Top & Bottom unit cell, and (b) 3-D configuration (P = 7.2, L_1 = 3.35, L_2 = 1.675, W_1 = 0.2, W_2 = 3.2, h = 0.76, all in mm).

The transmission coefficients of different impedance ratios in normal incidence for single polarization is given in Figure 4.11. The simulation was performed for three values of the impedance ratio (k = 0.8, k = 1 and k =1.2). In this parametric study, W_1 is kept constant, while W_2 is changed.

Table 4.2 Strip width and its characteristic impedance

Strip width (mm)	Characteristic impedance (Ω)
0.01	274
0.2	214
1	155

It can be observed from the simulation that the resonance frequency shifts to lower frequencies for k < 1 whereas for k > 1 it shifts to higher frequencies. Consequently, the SIR structure for k < 1 is considered to reduce in size. These observations are consistent with the trends observed in microwave filter theory. The resonance frequency shifted upward by reducing the geometric dimensions of the unit cell. In addition, it is evident from Figure 4.11 that the spurious resonance frequency of the MS can be controlled by the impedance ratio.

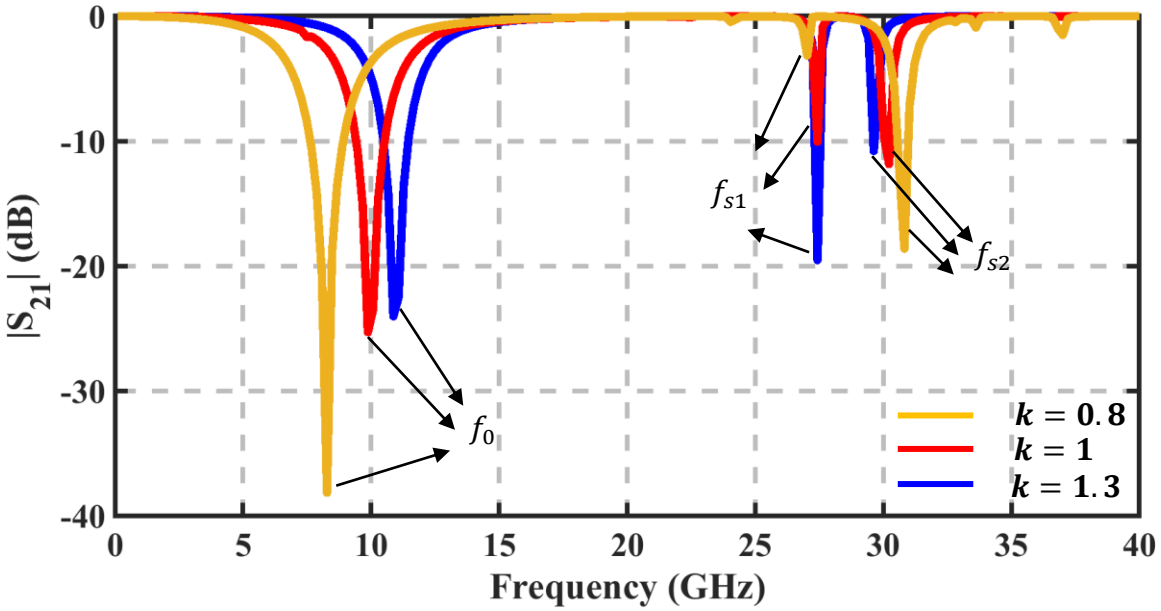

Figure 4.11 Transmission coefficient with different impedance ratio K.

The unit cell dimensions were chosen based on the analyzed example of the previous section which were: $W_1 = 0.2$mm, $W_2 = 3.2$ mm, $L_T = 7.3\,mm$ and $P = 7.8\,mm$. The simulated transmission coefficients under normal and oblique incidences for TE and TM polarizations are shown in Figure 4.12. It is seen that the new configuration exhibits the desired response under both polarizations. The simulated response of the structure has a bandstop response with a resonant frequency of 10 GHz. In addition, Figures 4.12(a) and (b) show the angular stability performance of the proposed structure for TE and TM polarizations, respectively. It is observed that the resonant behavior is stable up to 60° angle of incidence, while a maximum frequency shift occurs up to 0.9% only for TE.

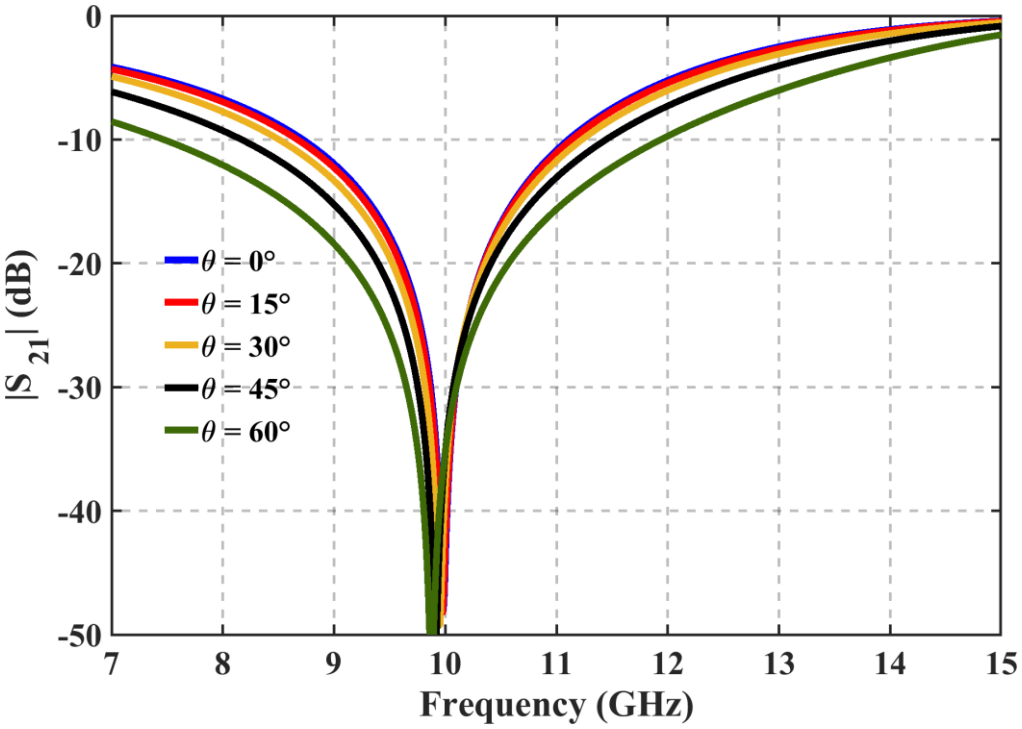

(a) TE mode

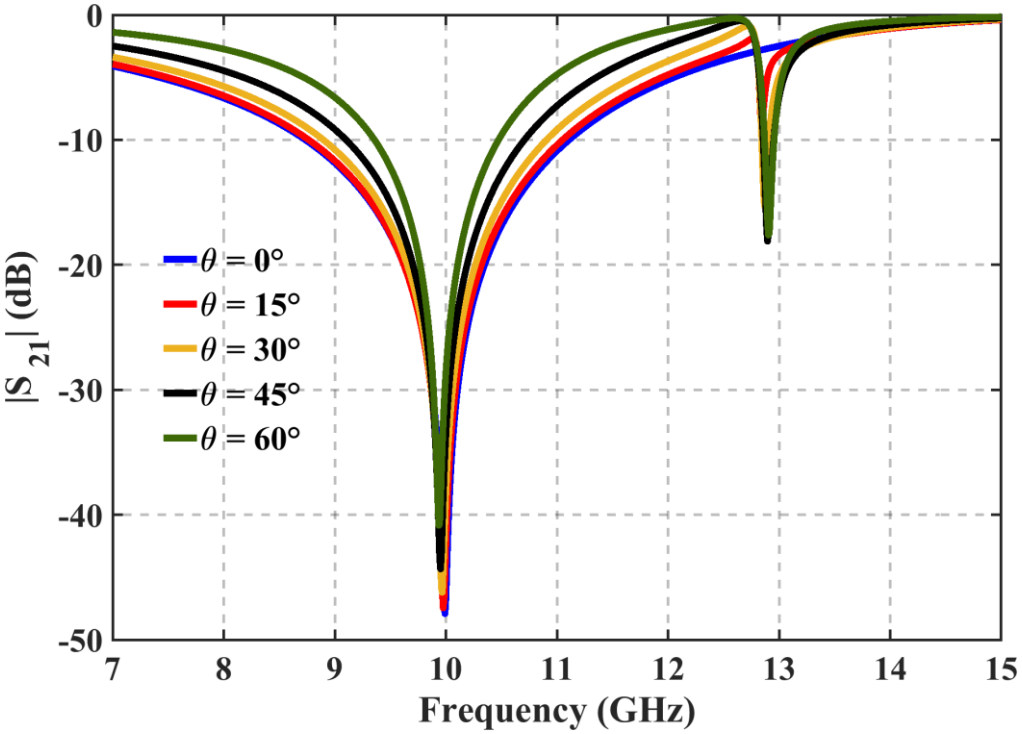

(b) TM mode

Figure 4.12 Simulated transmission coefficients under various angles of incidence for both polarizations.

4.4 Experimental results

To verify the validity of the proposed MS structure design, a prototype is fabricated on a 0.13 mm thick RT/duroid 6002. The fabricated MS is shown in Figure 4.13. The size of the MS prototype is 259.2 mm × 259.2 mm and it consists of 36 × 36 unit cells. It was measured by using the free-space method. A pair of horn antennas operating in the frequency band of X-band with 16 dBi gain and an Agilent vector network analyzer PNA-X N5242A were employed to perform the measurement. Figure 4.14 shows the experimental setup; the distance between the transmitting/receiving antennas and MS prototype is 0.5 m/0.5 m. The transmission coefficient without MS structure were measured in the beginning for obtaining the calibrated results. To measure the transmission coefficient for various angles of incidence and polarizations, a mechanical rotation system was used. Figure 4.15 shows the measured transmission coefficient of the proposed MS under various incident angles and for both polarizations (TE and TM). From the measured results, it was found that the proposed MS can produce a stable frequency response with respect to different polarizations and incidence angles.

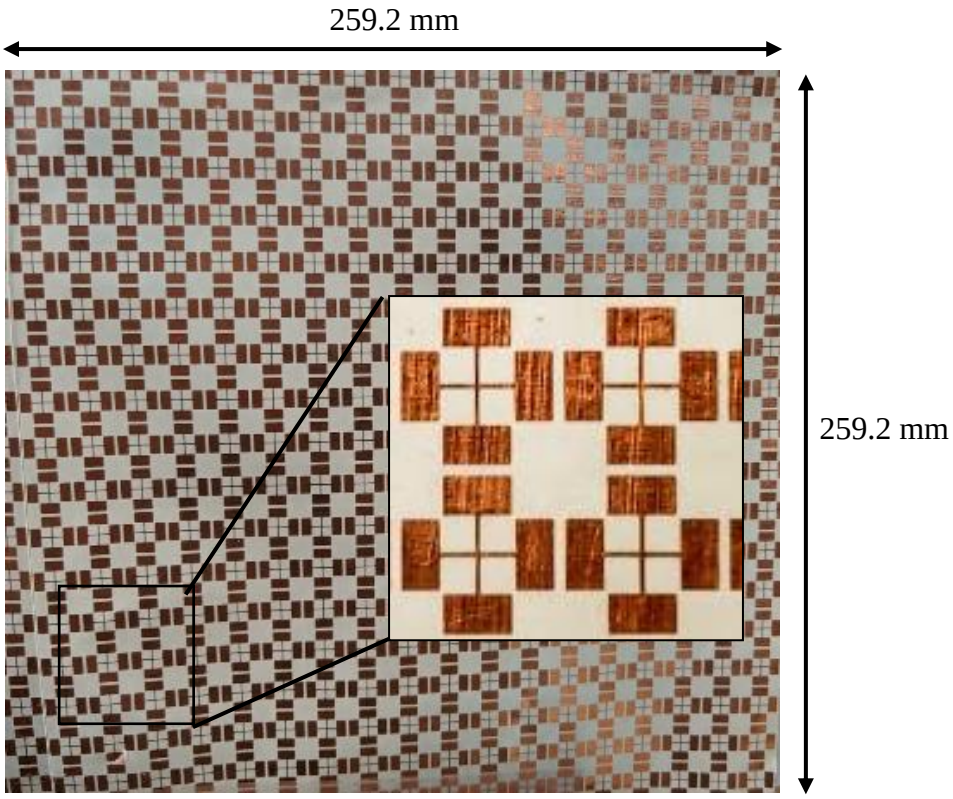

Figure 4.13 Photograph of the fabricated SIR MS prototype.

Figure 4.14 Measurement setup to measure the transmission coefficient of the MS.

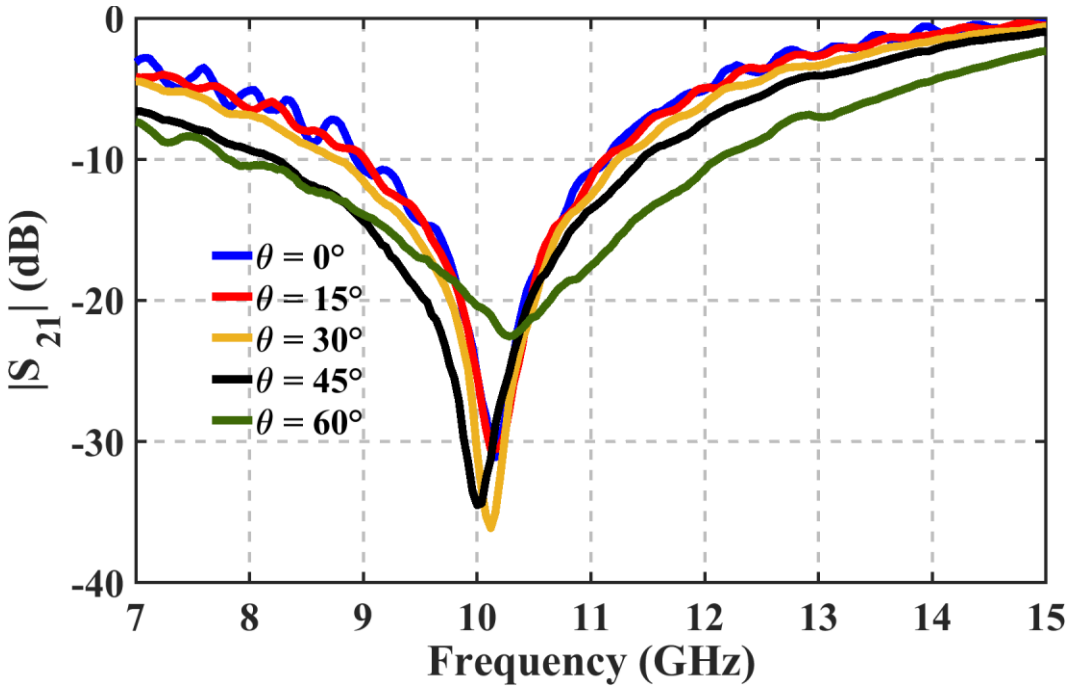

(a) TE mode

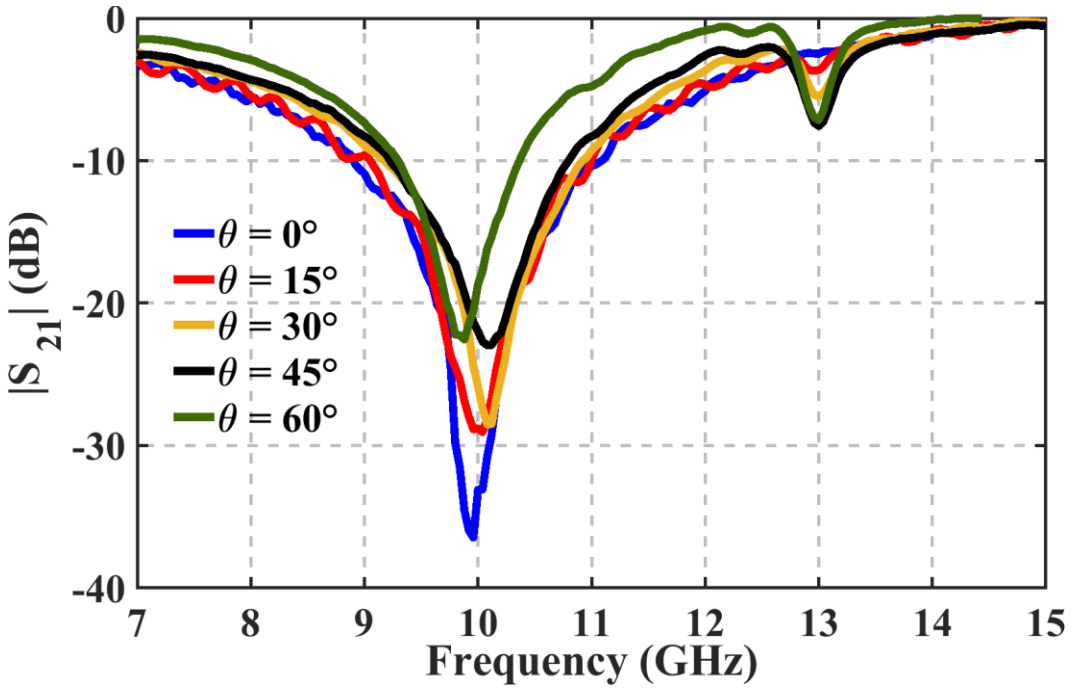

(b) TM mode

Figure 4.15 Measured Transmission coefficients under various angles of incidence for both polarizations.

Furthermore, the comparison of the proposed work with the related works is shown in Table 4.3. It evident from Table 4.3 that the proposed metasurface has the small unit cell compared with the listed reference. In addition, this structure exhibits very stable resonant frequency for different angles of incidence and for TE and TM modes. These features offer great flexibility for the proposed structure to be used for many applications.

Table 4.3 Comparison of the SIR element with related works

Ref	Substrate layers	Center frequency	Cell size	Polarization
[25]	Single	14 GHz	$0.22\lambda_0 \times 0.22\lambda_0$	Dual
[88]	Single	2.4 GHz	$0.104\lambda_0 \times 0.104\lambda_0$	Dual
[106]	Single	3.33 GHz	$0.086\lambda_0 \times 0.086\lambda_0$	Dual
Proposed work	Single	10 GHz	$0.25\lambda_0 \times 0.25\lambda_0$	Dual

4.5 Conclusion

In this chapter, a new method to design a miniaturized band-stop MS has been proposed. The miniaturized MS has been built by using stepped impedance resonators. The unit cell of the proposed MS consists of crossed stepped impedance resonators printed on both sides of a single dielectric substrate. A 65% reduction in the size of the unit cell of the MS has been achieved compared to the proposed structure of the previous chapter, by using stepped impedance resonators instead of uniform resonator in the unit cell. The proposed MS shows a stable frequency response for different angles of incidence and polarizations. In addition to the size reduction, a simple design procedure based on transmission line theory was developed to synthesize a step impedance unit cell. A prototype has been designed, fabricated, and measured to validate the simulated results. The measured data agrees well with the simulated results. The proposed design has been fabricated using printed circuit board technology, which highlights the simplicity of the fabrication for such structures.

CHAPTER 5 SYNTHESIS OF RIGOROUS HIGHER ORDER FREQUENCY SELECTIVE SURFACE DESIGN APPROACHES

5.1 Motivation and objective

As demand for spectrum continues to grow, propagation characteristics within buildings are becoming an increasingly important consideration. With companies installing new wireless systems operating at higher frequencies and a limitation in the number of available channels, the time has come to consider selecting different types of construction materials based on their RF characteristics. Reflecting material, for example, could he used to prevent signals from propagating into adjacent rooms; RF attenuating film could be added to double-glazed windows; and FSSs could be deployed to allow certain frequencies to propagate into a room, while reflecting other frequencies. One of the most difficult challenges is the prediction of frequencies to be used in the future, as new wireless technologies are planned. Buildings are constructed on a continuous basis and retrofits occur as the building ages. But with new wireless standards continuously being developed and re-developed, a detail understanding of the latest trends in wireless communications standards and products is required to make the indoor environment friendlier and more amenable to wireless communication.

Most of these applications require the frequency-selective surface to function as a close to ideal filter for a plane wave, whereby the in-band filtering response should be flat, and the out-of-band rejection skirt should be sharp roll-off. Furthermore, it is also desired that the frequency response become insensitive to the angle of incidence. The condition of angular stability basically requires that the unit cell size becomes much smaller than the operating wavelength.

However, the spectral and spatial responses of frequency selective surfaces (FSS) structures are affected by various physical and electrical parameters including the shape and type of their constituting elements, element configurations, element spacing, parameters of dielectric substrate, and superstrates. Similar to microwave filters, these spatial filters can be designed to demonstrate low-pass, high-pass, band-pass, or band-stop behaviour. Band-pass and band-stop (notch) FSSs are more widely used. However, unlike microwave filters, the frequency responses of these structures are not only functions of frequency, but also functions of the angle of incidence of the electromagnetic wave and its polarization.

Higher order filters have been used in the literature to realize rather complicated frequency responses. Different types of filters such as low-pass (LP), band-pass (BP), high-pass (HP), etc. have been realized using well-defined algorithmic approaches. Methodology for filter synthesis has been developed for microwave frequency band by considering the distributed nature of the elements. Lately, new advances have been made to apply the procedure of microwave filter design to the design of spatial filters, namely, frequency selective surface structures. The literature on band stop FSS filter is quite limited. General approach for the filter synthesis of a typical band reject filter will be outlined in the next section. The design of the filter using periodic structures along with a typical filter design in 10 GHz is presented in the subsequent section.

5.2 Design procedure

Several techniques and methodologies are available today for designing microwave filters. Review articles that survey the state of the art in this field may be found in the literature, enabling designers to select the most convenient approach for various filter topologies and applications. All these design approaches generally consist of two steps: first a synthesis problem is solved using techniques typically borrowed from lumped-element network synthesis, and then a suitable equivalence between the synthesized network and the actual distributed structure to be realized is established, enabling the physical dimensioning of the structure. In the past, the second step was generally carried out by means of simple (approximate) circuit modeling of the real filter structure, and often some experimental trial and error process was necessary to obtain the desired filter response. Today, the trend is to exploit optimization techniques and take advantage of the available full-wave electromagnetic (EM) simulators, which can now analyze the complete physical structure of many filters.

Optimization is a very powerful tool, but it must be applied judiciously. In fact, without a good starting point (i.e., the initially assigned dimensions of the physical structure to be optimized), the most elegant optimization procedure may not be able to find an acceptable solution. It is a significant computational burden to use optimization-only based procedures to design and realize higher order filters. The number of parameters is so vast that it is almost certain to miss the optimal design. On the other hand, the design is impervious to underlying physical principles of the operation of a given structure. Therefore, any minor modification of the specifications (e.g.

bandwidth, frequency band, roll-off, practical restrictions, etc.) would call for the repetition of the whole lengthy design and optimization process. The aim of this chapter is to demonstrate methods to combine approximate FSS dimensioning (based on network synthesis) and optimization (based on EM modeling), allowing a fast and accurate design that equip the designer with very effective and efficient technique to be exploited with a wide range of specifications whether theoretical or practical.

5.2.1 Multi-pole FSS design techniques

Traditional single layer resonant FSS exhibit first order bandpass or bandstop filter response, which are inherently narrow band. Thus, the frequency response of a single layer FSS is often too narrowband for practical applications. Moreover, their frequency responses are potentially susceptible to the angle of incoming EM wave. In order to address these drawbacks, multilayer FSSs have been employed to achieve higher order filter responses. Nonetheless, it is well known that stacking several metal layers opens up new design possibilities, such as the existence of transmission and rejection bands, an increase in operating bandwidth, and improved polarization converter performance. As stated in the preceding paragraph, higher order filter responses are traditionally realized by cascading single resonant FSS arrays with a quarter wavelength separation between adjacent arrays [107-110]. The frequency response of the constituent single layer FSSs has a significant impact on the parameters that measure the performance of the multilayer filter, such as ripple, centre frequency, bandwidth, roll-off, and so on. Due to exorbitant size, this approach is inefficient at low frequency (quarter wavelength dielectric layer spacers) but perfectly suitable for millimeter-wave frequencies. In light of this, the cross-coupling stubs filter class is the focus of this chapter's design technique for the aforementioned FSS structure. The dual pole FSS with cross-coupling stubs, in particular, was carefully considered in order to generate new ideas and develop synthesis technique with the goal of simplifying the design of multipole pole single layer FSS.

5.2.2 Band stop FSS Using Cross-Coupling Stubs

As previously stated, the design approach was inspired by traditional microwave theory. The new element was designed by combining various concepts from bandstop analogue filters. To design the multipole structure with specific properties, we borrowed a synthesis procedure from

cross-coupling stubs filter techniques [111]. The analog filter design shown in figure 5.1 consists of a pair of quarter wavelength open circuited stubs separated by quarter wavelength. Zs denotes the characteristic impedance of the shunt stubs, whereas Z_0 denotes the port impedance. C represents the capacity between the two stubs. The cross-coupling between the two stubs in this filter contributes to the band stop effect by introducing two transmission zeros within the stop band.

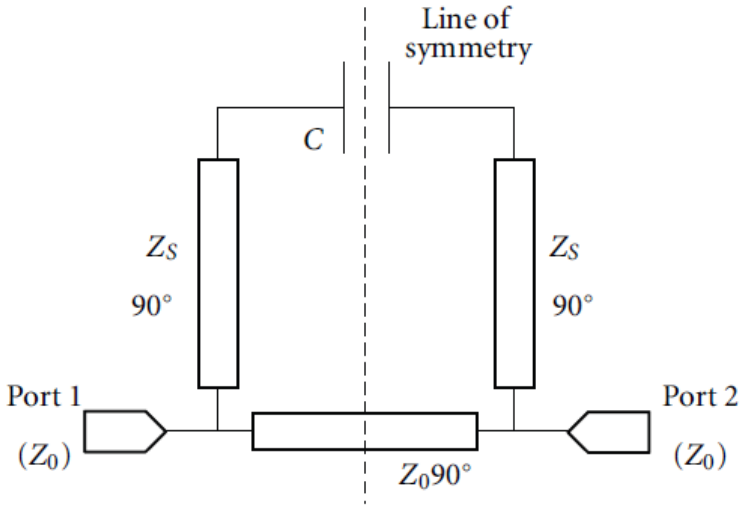

(a)

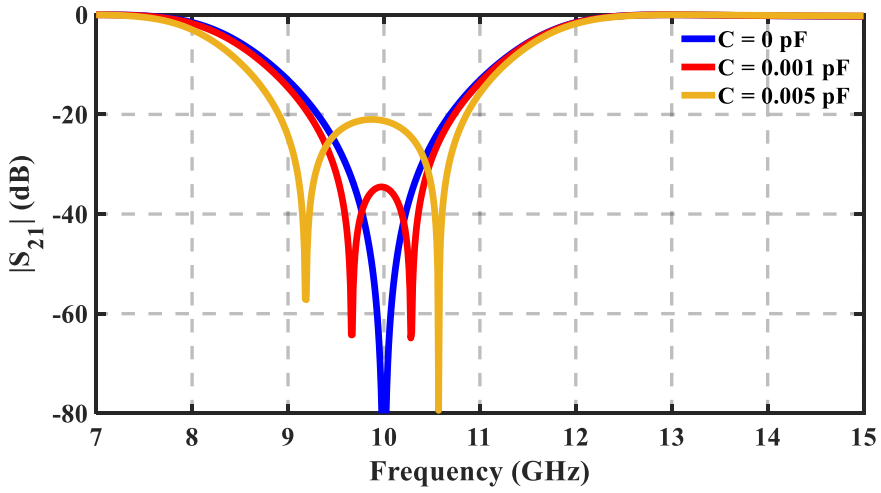

(b)

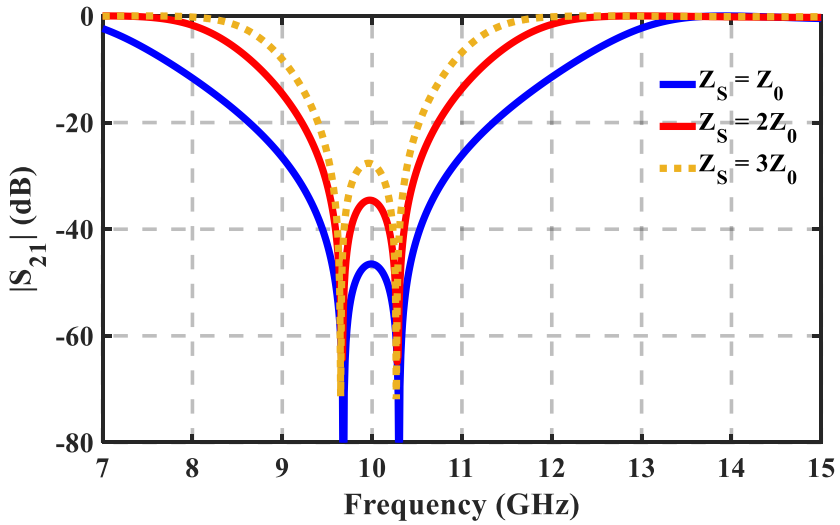

(c)

Figure 5.1 (a) Schematic diagram of the proposed bandstop filter. (b) Calculated frequency response of the |S21| with different C and fixed Z_S = 100Ω. (c) Calculated frequency response of the |S21| with different Z_S and fixed C = 0.001 pF.

The electrical lengths of all lines are 90°. The cross-coupling is represented by the capacitor C connected between the ends of the two stubs. The S parameters of the structure shown in Figure 1(a) are given by where $\theta = (\pi f/4f_0)$. f and f_0 are the center frequency and operating frequency, respectively.

Z_0 = 377 is chosen and corresponds to port impedance. Figures 1(b) and 1(c) depict parametric studies with different values of C and Z_S. At the stop band, the cross-coupling introduces two transmission zeros. The larger C, the stronger the cross-coupling between the two stubs. Cross-coupling can be used to improve the stop band bandwidth and roll-off. The characteristic impedance Z_S of the stubs is used to adjust the stop band bandwidth while keeping C constant. As Z_S increases, the bandwidth decreases.

5.2.3 Design Methodology

The following flowchart describes the methodology for designing a multipole FSS stopband in a single layer:

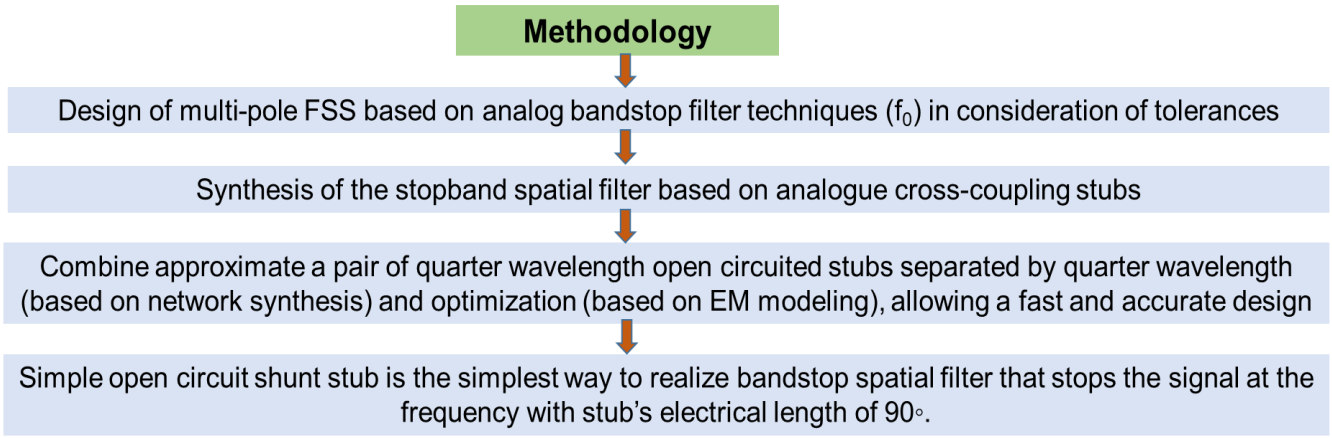

Figure 5.2 Flowchart of the design methodology.

5.3 Physical implementation of a single layer multipole stopband FSS

5.3.1 Single layer of polarization dependent dual pole stopband FSS

This section proposes the design of a dual pole FSS with single polarization. The design procedure described in section 5.2 was followed to design a stop-band FSS having a central resonance frequency at 10 GHz. Following the description presented in [111], the unit cell employs double folded stubs. The length of the open stubs and the separation between them are approximately equal to$(n + 1)\,\lambda/4$. The numerical analysis was performed by using ANSYS HFSS [75]. The unit cell boundary conditions were used to provide periodicity along the x and y axes. The structure was excited by an electromagnetic wave with the propagation vector (**k**) towards the z axis, an electric field vector (**E**) towards the x axis, and a magnetic field vector (**H**) towards the y axis. The proposed structure was designed on an RT/Duroid 6002 PCB. The dielectric substrate has a thickness of 0.25 and a relative dielectric constant of 2.94. Figure 5.3 shows the dimensions of the unit cell of the proposed FSS after tuning. The geometric parameters of the design are given in Table 5.1.

Table 5.1 Geometric parameters of the proposed unit cell

W	L_C	L_S	P
1.6 mm	17 mm	21 mm	17.6 mm

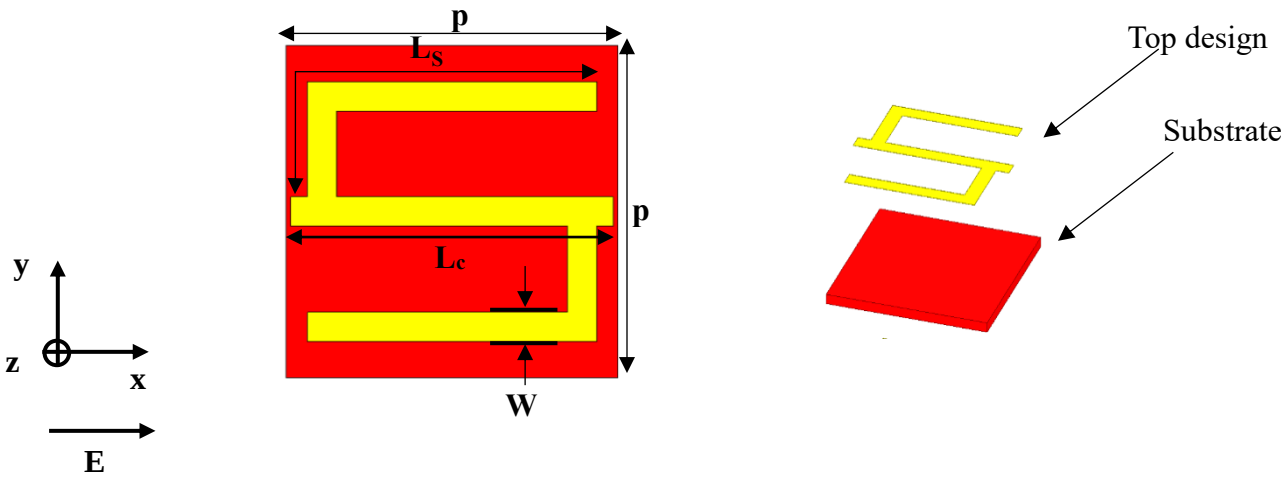

Figure 5.3 Unit cell topology of the proposed FSS.

5.3.2 Experimental results

The working prototype was generated using a standard printed circuit board fabrication technique. The dielectric substrate used is the same as described in the previous section. The realization shown in Figure 5.3 provides a clear guideline as to the implementation of spatial filter composed of a pair of quarter wavelength open circuited stubs separated by quarter wavelength in order to achieve a specified frequency response. By arranging two shunt open-circuited stubs in the antiparallel configuration as shown in Fig.5.3, a dual pole bandstop FSS is realized. I simply adjust the line width (W), line length (L_C), line separation (S), and overlapping line (L_O) for the optimization. The total size of the printed circuit board is 13.3cm by 13.3 cm.

The proposed prototype, as shown in Figure 5.4, has been fabricated and measured to validate the design. The dimensions of the prototype are 133 mm × 133 mm, containing 19 × 19 elements. The measurement is performed in an enclosed room. Two wideband horns (1 GHz to 18 GHz) and an Agilent (PNA-XN5242A) network analyzer were used in the experimental setup. The

measurement setup is shown in Figure 5.5. The prototype was placed between the two antennas. The measurement of the prototype was performed in two steps. Firstly, the transmission coefficient without structure was measured. The obtained measurement was used to calibrate the electromagnetic response of the structure. After that, the transmission coefficient with the presence of the structure was measured at the normal angle of incidence for TE polarization. Figure 5.6 shows the comparison of the simulated and the measured transmission coefficient of the proposed structure at the normal angle of incidence for single polarization. The measured result shows very good agreement with the simulated one. The discrepancy between the results from the measurement and the simulation are mainly due to the measurement process, which is performed in an enclosed room. As can be observed, the Metasurface exhibits a band-stop response. The centre frequency of the stop-band is around 10 GHz with a fractional bandwidth of 50% (8 GHz -13 GHz). The proposed structure can be qualified as a wideband structure. Its performance, however, is dependent on polarisation.

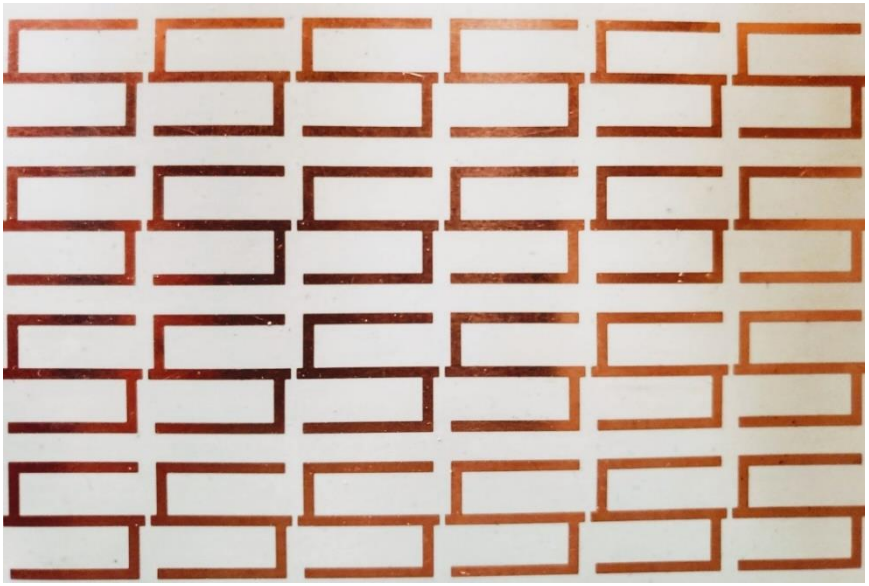

Figure 5.4 Photograph of the fabricated FSS prototype.

Figure 5.5 Measurement setup to measure the transmission coefficient of the FSS.

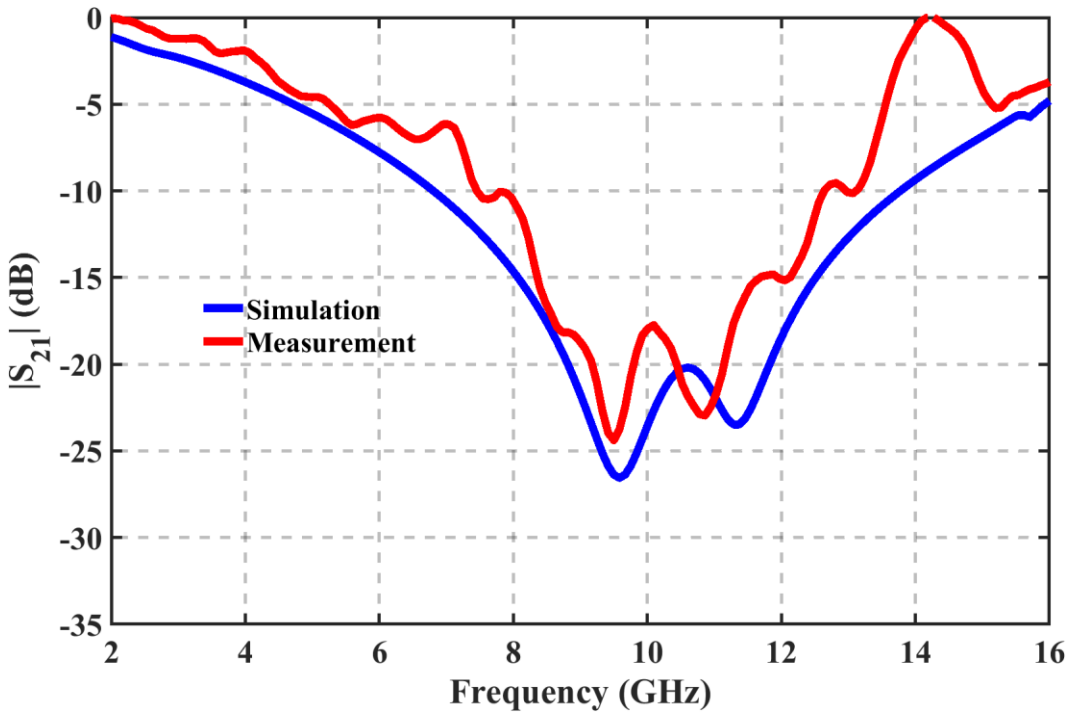

Figure 5.6 Simulated and measured transmission coefficient for the proposed FSS at normal incidence.

5.3.3 Single layer of polarization-insensitive dual pole stopband FSS

To mitigate the polarization dependence, a new FSS topology using double-sided based on back to back cross-coupling stubs was developed. The proposed unit cell in the last section is suitable for single polarized incident waves. The electromagnetic response of the structure is different when the E-field of the incident wave is along the y-axis. The previous unit cell is polarisation dependent, and the electromagnetic response of the structure differs when the incident wave's E-field is along the y-axis. The proposed unit cell can be modified to the one shown in Figure 5.7 to overcome the polarisation sensitivity. In this structure, the bottom element was rotated 90 degrees in the xy plane in relation to the top element, so that the electromagnetic response is the same whether the incident wave's E-field is in the direction of the x-axis or the y-axis. The resulting element is shown in Figure 5.7 and the corresponding geometry parameters are summarized in Table 5.2.

Table 5.2 Geometric parameters of the dual orthogonal polarized element

W	L_C	L_S	P
1.5 mm	17 mm	19.3 mm	16.125 mm

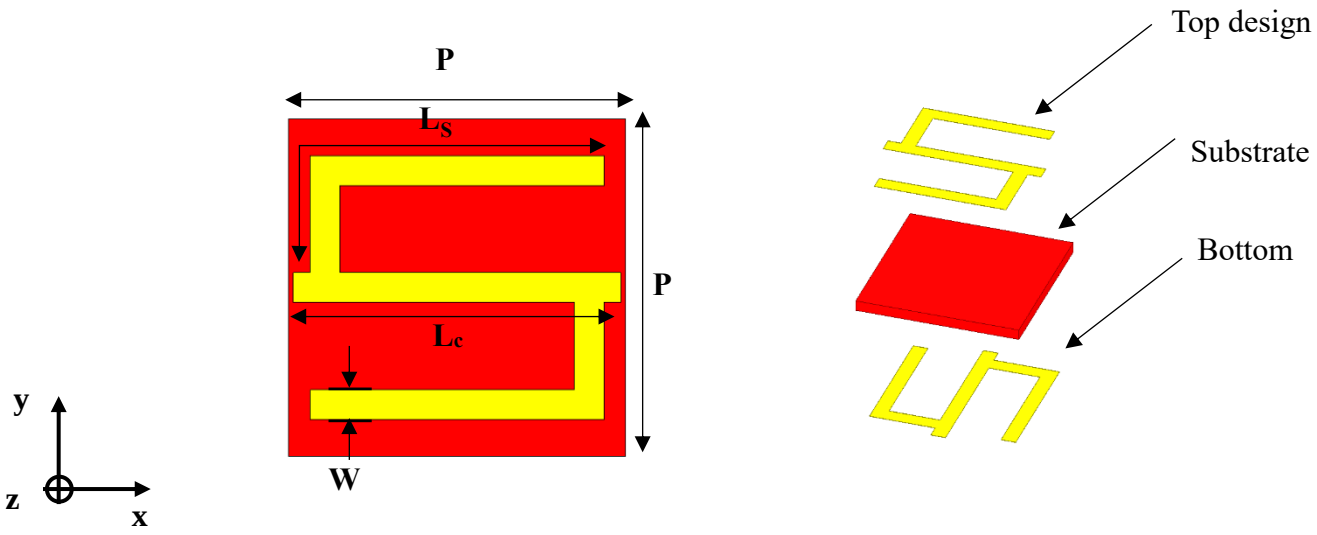

Figure 5.7 Unit cell of the proposed FSS.

5.3.4 Experimental results

To validate the design, a fabricated prototype of the proposed structure was built, measured, and tested. The dimensions of the new topology of the single layer of polarization-insensitive dual pole stopband FSS prototype are 140 mm × 140 mm, containing 9 × 9 elements. The same measurement setup from the previous section was used to validate the design. In addition, the structure was tested for different polarizations (TE and TM modes). It was shown that the frequency response is almost independent from polarization. This was achieved due to the symmetrical shape of the proposed unit cell.

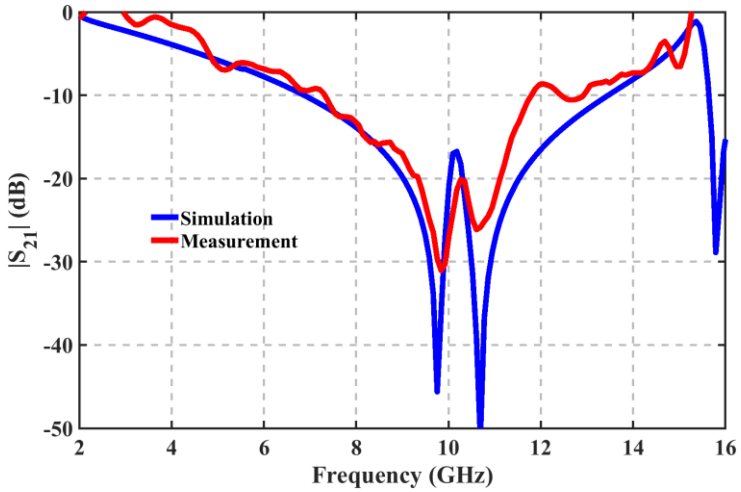

(a) TE mode

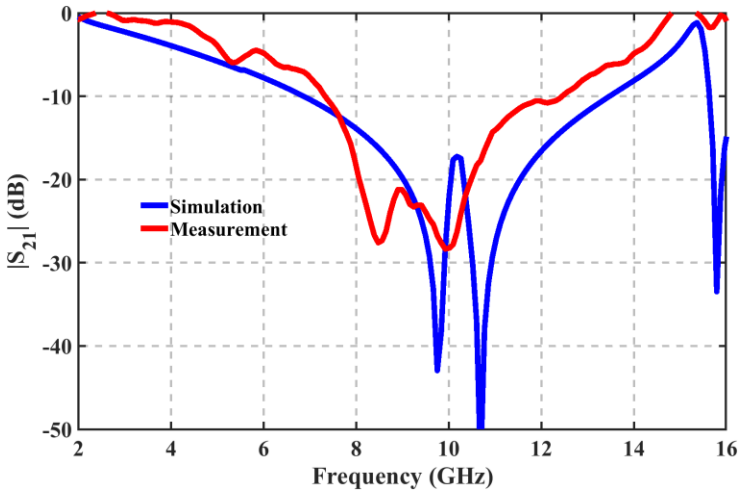

(b) TM mode

Figure 5.8 Simulated and measured transmission coefficient at normal incidence.

The transmission coefficient was measured for TE and TM modes at normal incidence. The measured results are shown in Figure 5.8 in comparison with the simulated ones. Figure 5.8 (a) shows the measured and simulated transmission coefficient for the TE mode. It is observed that the measured results are in close agreement with the simulated results. The center frequency of the stop-band is around 10 GHz with a fractional bandwidth of 53%. For the TM mode of polarization, it is observed that the measured result is in relatively good agreement with the simulated performance. The discrepancy between the measurement and simulation results is mainly due to inaccuracies involved in the measurement. The center frequency of the proposed structure for this polarization is around 9 GHz with a fractional bandwidth of 56%.

Table 5.3 illustrates a comparison of the proposed structures and other reported works. It can be observed that the proposed elements have a wide bandwidth compared with the listed references.

Table 5.3 Comparison with related works

Ref	Number of layers	Center frequency (GHz)	Cell size	FBW %
[112]	Multilayer	21	$0.15\lambda_0 \times 0.15\lambda_0$	5
[113]	Multilayer	10	$0.10\lambda_0 \times 0.10\lambda_0$	21
[114]	Multilayer	8.5	$0.20\lambda_0 \times 0.20\lambda_0$	15
Proposed work (Single polarized structure)	Single	10	$0.58\lambda_0 \times 0.58\lambda_0$	50
Proposed work (Double polarized structure)	Single	10	$0.53\lambda_0 \times 0.53\lambda_0$	56

5.4 Conclusion

In this chapter, a new approach to design a single layer dual pole band-stop polarization insensitive FSSs has been proposed. The proposed structures have been built by using shunt open-circuited stubs. Two prototypes have been designed, fabricated, and measured to validate the simulated results. The first structure is constructed by a single metal layer. The second is built by two metal layers to overcome the polarization sensitivity of the first design. The measured data agrees well with the simulated results. A comparison with similar work has been carried out to demonstrate that the proposed Frequency selective surface have a large bandwidth. Also in this chapter, the design methodology is discussed.

CHAPTER 6 CONCLUSION AND FUTURE RESEARCH WORK

6.1 Conclusion

The main interest of this thesis is the development of new techniques for the designing of FSSs for communications applications. The techniques used were inspired from microwave theory. These techniques allow us to solve some of the currently existing technical problems related to FSSs. The achieved work in this thesis can be summarized as follows:

In Chapter 3, a simple synthesis method for ultra-thin double-sided cross-dipole-based Metasurface (FSS) has been proposed. The presented technique was used to design a flexible band-stop FSS for Electromagnetic Interference (EMI) shielding applications operating at 10 GHz. An Equivalent Circuit (EC) model in combination with closed-form expression was used to synthesize and validate the response of the proposed element. In addition, a parametric study of the proposed FSS aiming to optimize its bandwidth has been presented. The proposed FSS holds similar responses for TE and TM mode of polarization at normal incidence. Further, the conformal behavior of the proposed FSS in comparison with a planar FSS was presented and evaluated. The proposed FSS was validated with the full-wave EM solver and a prototype was fabricated. The size of the proposed unit cell is $0.4\lambda_0 \times 0.4\lambda_0$, where λ_0 is the free space wavelength at the desired resonant frequency. In addition, the fractional bandwidth for TE and TM modes is 10.42% at normal incidence. The measured results of a proposed FSS are presented and validated in comparison with the simulations with good agreement.

In chapter 4, a new approach to miniaturise the size of MS's elements has been proposed by using stepped impedance resonators. The proposed approach was used to design a dual orthogonal polarization band-stop Metasurface with low sensitivity to the incident angles of plane wave excitation. The proposed structure consists of crossed stepped impedance resonators printed on the two interfaces of a single dielectric substrate. Borrowing the stepped impedance resonator concept from microwave filter theory, a significant size reduction of the cell element size can be achieved to the extent that $\boldsymbol{p = \lambda_0/16}$, where $\boldsymbol{\lambda_0}$ is the free-space wavelength of the resonant frequency and p is the periodicity of the element. In addition to the miniaturization of the cell element, harmonic frequencies can be controlled by simply changing SIR impedances. This will enable us to design a multiband MS which resembles a similar development for stepped impedance

resonators in microwave filter theory. A simple design procedure based on transmission line theory is developed to synthesize the step impedance unit cell. To demonstrate the validity of the proposed approach, the SIR MS was designed to operate at 10 GHz. The structure was fabricated and tested subsequently in a free space measurement facility which demonstrated a stable angular response up to 60^{o} of the incident angles for TE and TM plane wave excitations.

In chapter 5, a new class of wideband band-stop Frequency selective surface with dual pole transmission zeros has been proposed. The proposed structure was inspired from microwave filters. The proposed structure was designed by using folded stubs. The proposed element exhibits a wider bandwidth. The fractional bandwidth for TE and TM modes is 56 % and 50% at normal incidence respectively. The structure is also polarization independent at the stop-band.

6.2 Future work

The proposed structures presented in this work aims to resolve some of existing issues. Future work can be continuing in the following area:

As the wireless communication applications are moving in millimetre waves, it might be useful to investigate these structures in other frequencies to see if they provide similar results to the already proposed structures (the aforementioned structures currently only operating at 10 GHz).

In Chapter 4, a miniaturized MS with a stable angle of incidence has been introduced. Designing a similar structure with a wider bandwidth would be very promising in many applications.

In Chapter 5, the proposed structures have a broadband characteristic. The sensitivity of these structures under many angles of incidence was not evaluated. For this reason, it will be necessary to evaluate the angle sensitivity of these structure.

The designed and analyzed FSS could be used in other applications, such as devices for bio-electromagnetics and electromagnetic compatibility. The proposed FSS can be used to create a resonant medium for bio-electromagnetic sensing. Furthermore, the designed FSS may be used to reduce interference in satellite communications, thanks to the ability to shield 10 GHz signals.

REFERENCES

[1] Kammoun, Abla, Anas Chaaban, Mérouane Debbah, and Mohamed-Slim Alouini. "Asymptotic max-min SINR analysis of reconfigurable intelligent surface assisted MISO systems." IEEE Transactions on Wireless Communications 19, no. 12 (2020): 7748-7764, doi: 10.1109/TWC.2020.2986438.

[2] Di Renzo, Marco, Alessio Zappone, Merouane Debbah, Mohamed-Slim Alouini, Chau Yuen, Julien De Rosny, and Sergei Tretyakov. "Smart radio environments empowered by reconfigurable intelligent surfaces: How it works, state of research, and the road ahead." IEEE Journal on Selected Areas in Communications 38, no. 11 (2020): 2450-2525, doi: 10.1109/JSAC.2020.3007211.

[3] Liaskos, Christos, Shuai Nie, Ageliki Tsioliaridou, Andreas Pitsillides, Sotiris Ioannidis, and Ian Akyildiz. "A new wireless communication paradigm through software-controlled metasurfaces." IEEE Communications Magazine 56, no. 9 (2018): 162-169, doi: 10.1109/MCOM.2018.1700659.

[4] Petosa, Aldo, Nicolas Gagnon, César Amaya, Ming Li, Shailesh Raut, Jonathan Ethier, and Reza Chaharmir. "Characterization and enhancement of the environment for 5G millimetre-wave broadband mobile communications." In 12th European Conference on Antennas and Propagation (EuCAP 2018), pp. 1-5. IET, 2018, doi: 10.1049/cp.2018.0710.

[5] Q. Wu, S. Zhang, B. Zheng, C. You and R. Zhang, "Intelligent Reflecting Surface-Aided Wireless Communications: A Tutorial," in IEEE Transactions on Communications, vol. 69, no. 5, pp. 3313-3351, May 2021, doi: 10.1109/TCOMM.2021.3051897.

[6] M. Di Renzo et al., "Smart Radio Environments Empowered by Reconfigurable Intelligent Surfaces: How It Works, State of Research, and The Road Ahead," in IEEE Journal on Selected Areas in Communications, vol. 38, no. 11, pp. 2450-2525, Nov. 2020, doi: 10.1109/JSAC.2020.3007211.

[7] Q. Wu and R. Zhang, "Towards Smart and Reconfigurable Environment: Intelligent Reflecting Surface Aided Wireless Network," in IEEE Communications Magazine, vol. 58, no. 1, pp. 106-112, January 2020, doi: 10.1109/MCOM.001.1900107.

[8] C. Huang et al., "Holographic MIMO Surfaces for 6G Wireless Networks: Opportunities, Challenges, and Trends," in IEEE Wireless Communications, vol. 27, no. 5, pp. 118-125, October 2020, doi: 10.1109/MWC.001.1900534.

[9] Han, Sihui, and Kang G. Shin. "Enhancing wireless performance using reflectors." In IEEE INFOCOM 2017-IEEE Conference on Computer Communications, pp. 1-9. IEEE, 2017, doi: 10.1109/INFOCOM.2017.8056966.

[10] Akyildiz, Ian F., Shuai Nie, Shih-Chun Lin, and Manoj Chandrasekaran. "5G roadmap: 10 key enabling technologies." Computer Networks 106 (2016): 17-48, doi: 10.1016/j.comnet.2016.06.010.

[11] Landy, N. I, S. Sajuyigbe, Jack J. Mock, David R. Smith, and Willie J. Padilla. "Perfect metamaterial absorber." Physical review letters 100, no. 20 (2008): 207402, doi: 10.1103/PhysRevLett.100.207402.

[12] Liu, Xianliang, Tatiana Starr, Anthony F. Starr, and Willie J. Padilla. "Infrared spatial and frequency selective metamaterial with near-unity absorbance." Physical review letters 104, no. 20 (2010): 207403, doi: 10.1103/PhysRevLett.104.207403.

[13] Sievenpiper, Dan, Lijun Zhang, Romulo FJ Broas, Nicholas G. Alexopolous, and Eli Yablonovitch. "High-impedance electromagnetic surfaces with a forbidden frequency band." IEEE Transactions on Microwave Theory and techniques 47, no. 11 (1999): 2059-2074, doi: 10.1109/22.798001.

[14] Horie, Yu, Amir Arbabi, Ehsan Arbabi, Seyedeh Mahsa Kamali, and Andrei Faraon. "Dielectric metasurface narrowband filter array." In CLEO: Science and Innovations, pp. STh1E-7. Optical Society of America, 2016, doi: 10.1364/CLEO_SI.2016.STh1E.7.

[15] Mahdi Pakdin, Alireza Ghayekhloo, Pejman Rezaei, and Majid Afsahi. "Transparent dual band Wi-Fi filter for double glazed energy saving window as a smart network." Microwave and Optical Technology Letters, vol, 61, no. 11, pp. 2545-2550, 2019. doi: 10.1002/mop.31916

[16] Wood, Robert Williams. "XLII. On a remarkable case of uneven distribution of light in a diffraction grating spectrum." The London, Edinburgh, and Dublin Philosophical Magazine and Journal of Science 4, no. 21 (1902): 396-402, doi: 10.1080/14786440209462857.

[17] Kuester, Edward F., Mohamed A. Mohamed, Melinda Piket-May, and Christopher L. Holloway. "Averaged transition conditions for electromagnetic fields at a metafilm." IEEE Transactions on Antennas and Propagation 51, no. 10 (2003): 2641-2651, doi: 10.1109/TAP.2003.817560.

[18] Lapine, M., and S. Tretyakov. "Contemporary notes on metamaterials." IET microwaves, antennas & propagation 1, no. 1 (2007): 3-11, doi: 10.1049/iet-map:20050307.

[19] Achouri, Karim, Mohamed A. Salem, and Christophe Caloz. "General metasurface synthesis based on susceptibility tensors." IEEE Transactions on Antennas and Propagation 63, no. 7 (2015): 2977-2991, doi: 10.1109/TAP.2015.2423700.

[20] Holloway, Christopher L., Edward F. Kuester, Joshua A. Gordon, John O'Hara, Jim Booth, and David R. Smith. "An overview of the theory and applications of metasurfaces: The two-dimensional equivalents of metamaterials." IEEE antennas and propagation magazine 54, no. 2 (2012): 10-35, doi: 10.1109/MAP.2012.6230714.

[21] Holloway, Christopher L., and Edward F. Kuester. "Generalized sheet transition conditions for a metascreen—A fishnet metasurface." IEEE Transactions on Antennas and Propagation 66, no. 5 (2018): 2414-2427, doi: 10.1109/TAP.2018.2809620.

[22] C. L. Holloway, M. A. Mohamed, E. F. Kuester and A. Dienstfrey, "Reflection and transmission properties of a metafilm: with an application to a controllable surface composed of resonant particles," in IEEE Transactions on Electromagnetic Compatibility, vol. 47, no. 4, pp. 853-865, Nov. 2005, doi: 10.1109/TEMC.2005.853719.

[23] Albooyeh, Mohammad. "Electromagnetic characterization of metasurfaces." Aalto University publication series, doctoral dissertations, (2015).

[24] Yan, Mingbao, Shaobo Qu, Jiafu Wang, Jieqiu Zhang, Anxue Zhang, Song Xia, and Wenjie Wang. "A novel miniaturized frequency selective surface with stable resonance." IEEE antennas and wireless propagation letters 13 (2014): 639-641, doi: 10.1109/LAWP.2014.2313067.

[25] Glybovski, Stanislav B., Sergei A. Tretyakov, Pavel A. Belov, Yuri S. Kivshar, and Constantin R. Simovski. "Metasurfaces: From microwaves to visible." Physics reports 634 (2016): 1-72, doi: 10.1016/j.physrep.2016.04.004.

[26] Fallah, Mahmoud, Alireza Ghayekhloo, and Ali Abdolali. "Design of frequency selective band stop shield using analytical method." Journal of Microwaves, Optoelectronics and electromagnetic applications 14 (2015): 217-228, doi: 10.1590/2179-10742015v14i2536

[27] Ghayekhloo, Alireza, Majid Afsahi, and Ali A. Orouji. "Checkerboard plasma electromagnetic surface for wideband and wide-angle bistatic radar cross section reduction." IEEE transactions on plasma science 45, no. 4 (2017): 603-609, doi: 10.1109/TPS.2017.2675282.

[28] A. C. Strikwerda, K. Fan, H. Tao, D. V. Pilon, X. Zhang, R. D. Averitt, Comparison of birefringent electricsplit-ring resonator and meander line structures as quarter-wave plates at terahertz frequencies, Optics Express 17 (1) (2009) 136–149. doi:10.1364/OE.17.000136.

[29] A. Pors, M. G. Nielsen, R. L. Eriksen, S. I. Bozhevolnyi, Broadband focusing flat mirrors based on plasmonic gradient metasurfaces, Nano Letters 13 (2) (2013) 829–834. doi:10.1021/nl304761m.

[30] Munk, Ben A. Frequency selective surfaces: theory and design. John Wiley & Sons, 2005.

[31] A. O. Koca and T. Ege, "Effects of chiral loading on a frequency selective surface comprised of a two dimensional array of crossed dipoles," IEEE Antennas and Propagation Society International Symposium. 1996 Digest, 1996, pp. 1464-1467 vol.2, doi: 10.1109/APS.1996.549874.

[32] Hill, Roger A., and Benedikt A. Munk. "The effect of perturbating a frequency-selective surface and its relation to the design of a dual-band surface." IEEE Transactions on Antennas and Propagation 44, no. 3 (1996): 368-374, doi: 10.1109/8.486306.

[33] Savia, S. B., and E. A. Parker. "Equivalent circuit model for superdense linear dipole FSS." IEE Proceedings-Microwaves, Antennas and Propagation 150, no. 1 (2003): 37-42, doi: 10.1049/ip-map:20030107.

[34] D. Ferreira, R. F. S. Caldeirinha, I. Cuiñas and T. R. Fernandes, "Square Loop and Slot Frequency Selective Surfaces Study for Equivalent Circuit Model Optimization," in IEEE Transactions on Antennas and Propagation, vol. 63, no. 9, pp. 3947-3955, Sept. 2015, doi: 10.1109/TAP.2015.2444420.

[35] Hu, Xiao-Dong, Xi-Lang Zhou, Lin-Sheng Wu, Liang Zhou, and Wen-Yan Yin. "A miniaturized dual-band frequency selective surface (FSS) with closed loop and its complementary pattern." IEEE Antennas and Wireless Propagation Letters 8 (2009): 1374-1377, doi: 10.1109/LAWP.2009.2039110.

[36] J. Huang and S. W. Lee, "Tri-band frequency selective surface with circular ring elements," Antennas and Propagation Society Symposium 1991 Digest, 1991, pp. 204-207 vol.1, doi: 10.1109/APS.1991.174808.

[37] Lee, Shung-Wu, Gino Zarrillo, and Chak-Lam Law. "Simple formulas for transmission through periodic metal grids or plates." IEEE Transactions on antennas and propagation 30, no. 5 (1982): 904-909, doi: 10.1109/TAP.1982.1142923.

[38] Al-Joumayly, Mudar, and Nader Behdad. "A new technique for design of low-profile, second-order, bandpass frequency selective surfaces." IEEE transactions on antennas and propagation 57, no. 2 (2009): 452-459, doi: 10.1109/TAP.2008.2011382.

[39] Mittra, Raj, R. Hall, and Chich-Hsing Tsao. "Spectral-domain analysis of circular patch frequency selective surfaces." IEEE transactions on antennas and propagation 32, no. 5 (1984): 533-536, doi: 10.1109/TAP.1984.1143346.

[40] Callaghan, Peter, and Edward A. Parker. "Tuning interactions of cascaded-frequency selective-slot arrays." IEE Proceedings-Microwaves, Antennas and Propagation 141, no. 4 (1994): 290-294, doi: 10.1049/ip-map:19941169.

[41] Munk, B., R. Luebbers, and R. Fulton. "Transmission through a two-layer array of loaded slots." IEEE transactions on antennas and propagation 22, no. 6 (1974): 804-809, doi: 10.1109/TAP.1974.1140902.

[42] Chuprin, Andrei D., Edward A. Parker, and John C. Batchelor. "Convoluted double square: single layer FSS with close band spacings." Electronics Letters 36, no. 22 (2000): 1830-1831, doi: 10.1049/el:20001308.

[43] Sung, Grace Hui-hsia, Kevin W. Sowerby, Michael J. Neve, and Allan G. Williamson. "A frequency-selective wall for interference reduction in wireless indoor environments." IEEE Antennas and Propagation Magazine 48, no. 5 (2006): 29-37, doi: 10.1109/MAP.2006.277152.

[44] Chan, C. H. "Frequency Selective Surface and grid array (ed) TK Wu." (1995).

[45] Marcuvitz, Nathan. Waveguide handbook. No. 21. IET, 1951.

[46] Kanth, V. Krushna, and S. Raghavan. "EM design and analysis of frequency selective surface based on substrate-integrated waveguide technology for airborne radome application." IEEE Transactions on Microwave Theory and Techniques 67, no. 5 (2019): 1727-1739, doi: 10.1109/TMTT.2019.2905196.

[47] Park, Chan-Sun, Yi-Ru Jeong, Ic-Pyo Hong, Heoung-Jae Chun, Yong Bae Park, Yoon-Jae Kim, and Jong-Gwan Yook. "Analysis of Curved Frequency selective surface for radome using characteristic basis function method." In 2016 10th European Conference on Antennas and Propagation (EuCAP), pp. 1-4. IEEE, 2016, doi: 10.1109/EuCAP.2016.7481386.

[48] Savia, S. B., Edward A. Parker, and B. Philips. "Finite planar-and curved-ring-element frequency-selective surfaces." IEE Proceedings-Microwaves, Antennas and Propagation 146, no. 6 (1999): 401-406, doi: 10.1049/ip-map:19990733.

[49] Chen, Qiang, and Yunqi Fu. "A planar stealthy antenna radome using absorptive frequency selective surface." Microwave and Optical technology letters 56, no. 8 (2014): 1788-1792, doi: 10.1002/mop.28442.

[50] Costa, Filippo, and Agostino Monorchio. "A frequency selective radome with wideband absorbing properties." IEEE transactions on antennas and propagation 60, no. 6 (2012): 2740-2747, doi: 10.1109/TAP.2012.2194640.

[51] Genovesi, Simone, Filippo Costa, and Agostino Monorchio. "Low-profile array with reduced radar cross section by using hybrid frequency selective surfaces." IEEE Transactions on Antennas and Propagation 60, no. 5 (2012): 2327-2335, doi: 10.1109/TAP.2012.2189701.

[52] E. Marouby, J. R. Levrel, B. Bougerolles, J. Lenormand and C. Terret, "On the Use of Frequency Selective Surfaces in Stealth Techniques for Aerospace Applications," 1994 24th European Microwave Conference, 1994, pp. 585-589, doi: 10.1109/EUMA.1994.337273.

[53] Almoneef, Thamer S., and Omar M. Ramahi. "Metamaterial electromagnetic energy harvester with near unity efficiency." Applied Physics Letters 106, no. 15 (2015): 153902, doi: 10.1063/1.4916232.

[54] Ramahi, Omar M., Thamer S. Almoneef, Mohammed AlShareef, and Muhammed S. Boybay. "Metamaterial particles for electromagnetic energy harvesting." Applied Physics Letters 101, no. 17 (2012): 173903, doi: 10.1063/1.4764054.

[55] AlShareef, Mohammed R., and Omar M. Ramahi. "Electrically small resonators for energy harvesting in the infrared regime." Journal of Applied Physics 114, no. 22 (2013): 223101, doi: 10.1063/1.4846076.

[56] V. Agrawal and W. Imbriale, "Design of a dichroic Cassegrain subreflector," in IEEE Transactions on Antennas and Propagation, vol. 27, no. 4, pp. 466-473, July 1979, doi: 10.1109/TAP.1979.1142119.

[57] Unal, E., A. Gokcen, and Y. Kutlu. "Effective electromagnetic shielding." IEEE Microwave magazine 7, no. 4 (2006): 48-54, doi: 10.1109/MMW.2006.1663989.

[58] P. Gurrala, S. Oren, P. Liu, J. Song and L. Dong, "Fully Conformal Square-Patch Frequency-Selective Surface Toward Wearable Electromagnetic Shielding," in IEEE Antennas and Wireless Propagation Letters, vol. 16, pp. 2602-2605, 2017, doi: 10.1109/LAWP.2017.2735196.

[59] Kiani, Ghaffer I., Andrew R. Weily, and Karu P. Esselle. "A novel absorb/transmit FSS for secure indoor wireless networks with reduced multipath fading." IEEE Microwave and Wireless Components Letters 16, no. 6 (2006): 378-380, doi: 10.1109/LMWC.2006.875589.

[60] I. F. Akyildiz, A. Kak and S. Nie, "6G and Beyond: The Future of Wireless Communications Systems," in IEEE Access, vol. 8, pp. 133995-134030, 2020, doi: 10.1109/ACCESS.2020.3010896.

[61] https://en.wikipedia.org/wiki/Radome

[62] https://empossible.net/wp-content/uploads/2020/01/Lecture-Frequency-Selective-Surfaces-Metasurfaces.pdf

[63] Lin, Baoqin, Shaobin Liu, and Naichang Yuan. "Analysis of frequency selective surfaces on electrically and magnetically anisotropic substrates." IEEE transactions on antennas and propagation 54, no. 2 (2006): 674-680, doi: 10.1109/TAP.2005.863136.

[64] F. Mesa, R. Rodríguez-Berral, M. García-Vigueras and F. Medina, "Efficient Hybrid Full-Wave/Circuital Approach for Stacks of Frequency Selective Surfaces," in IEEE Antennas and Wireless Propagation Letters, vol. 17, no. 10, pp. 1925-1929, Oct. 2018, doi: 10.1109/LAWP.2018.2870567.

[65] Neto, Valdemir Praxedes Silva, Adaildo Gomes D'Assunção, and Henri Baudrand. "Analysis of finite size nonuniform stable and multiband FSS using a generalization of the WCIP method." IEEE Transactions on Electromagnetic Compatibility 60, no. 6 (2018): 1802-1810, doi: 10.1109/TEMC.2017.2785787.

[66] Ghayekhloo, Alireza, Majid Afsahi, and Ali A. Orouji. "An optimized checkerboard structure for cross-section reduction: Producing a coating surface for bistatic radar using the equivalent electric circuit model." IEEE Antennas and Propagation Magazine 60, no. 5 (2018): 78-85, doi: 10.1109/MAP.2018.2859165.

[67] Ghosh, Saptarshi, and Kumar Vaibhav Srivastava. "An equivalent circuit model of FSS-based metamaterial absorber using coupled line theory." IEEE Antennas and Wireless Propagation Letters 14 (2014): 511-514, doi: 10.1109/LAWP.2014.2369732.

[68] Li, Da, Tian-Wu Li, Ran Hao, Hong-Sheng Chen, Wen-Yan Yin, Hui-Chun Yu, and Er-Ping Li. "A low-profile broadband bandpass frequency selective surface with two rapid band edges for 5G near-field applications." IEEE Transactions on Electromagnetic Compatibility 59, no. 2 (2017): 670-676, doi: 10.1109/TEMC.2016.2634279.

[69] Zhao, Peng-Chao, Zhi-Yuan Zong, Wen Wu, Bo Li, and Da-Gang Fang. "Miniaturized-element bandpass FSS by loading capacitive structures." IEEE Transactions on Antennas and Propagation 67, no. 5 (2019): 3539-3544, doi: 10.1109/TAP.2019.2902633.

[70] Krushna Kanth, Varikuntla, and Singaravelu Raghavan. "Design and optimization of complementary frequency selective surface using equivalent circuit model for wideband EMI shielding." Journal of Electromagnetic Waves and Applications 34, no. 1 (2020): 51-69, doi: 10.1080/09205071.2019.1688691.

[71] Kaiser, Kenneth L. Electromagnetic compatibility handbook. CRC press, 2004.

[72] Zverev, Anatol I. Handbook of filter synthesis. John WILEY & sons, 2005.

[73] Langley, R. J., and A. J. Drinkwater. "Improved empirical model for the Jerusalem cross." In IEE Proceedings H (Microwaves, Optics and Antennas), vol. 129, no. 1, pp. 1-6. IET Digital Library, 1982, doi: 10.1049/ip-h-1.1982.0001.

[74] Costa, Filippo, Agostino Monorchio, and Giuliano Manara. "Efficient analysis of frequency-selective surfaces by a simple equivalent-circuit model." IEEE Antennas and Propagation Magazine 54, no. 4 (2012): 35-48, doi: 10.1109/MAP.2012.6309153.

[75] ANSYS HFSS Version 2018.0.0, [Online]. Available: https://www.ansys.com

[76] Nauman, Mudassar, Rashid Saleem, Amir Khurrum Rashid, and Muhammad Farhan Shafique. "A miniaturized flexible frequency selective surface for X-band applications." IEEE Transactions on Electromagnetic Compatibility 58, no. 2 (2016): 419-428, doi: 10.1109/TEMC.2015.2508503.

[77] Rumpf, Raymond C., Marvin Gates, Carrie L. Kozikowski, and William A. Davis. "Guided-mode resonance filter compensated to operate on a curved surface." Progress In Electromagnetics Research C 40 (2013): 93-103, doi: 10.2528/PIERC13041209.

[78] Syed, Irfan Sohail, Yogesh Ranga, Ladislau Matekovits, Karu P. Esselle, and Stuart G. Hay. "A single-layer frequency-selective surface for ultrawideband electromagnetic shielding." IEEE Transactions on Electromagnetic Compatibility 56, no. 6 (2014): 1404-1411, doi: 10.1109/TEMC.2014.2316288.

[79] Liu, Ning, Xianjun Sheng, Chunbo Zhang, Jingjing Fan, and Dongming Guo. "A design method for synthesizing wideband band-stop FSS via its equivalent circuit model." IEEE Antennas and wireless propagation letters 16 (2017): 2721-2725, doi: 10.1109/LAWP.2017.2743114.

[80] Cruz, Rossana MS, Paulo H. da F. Silva, and Adaildo G. D'Assuncao. "Synthesis of crossed dipole frequency selective surfaces using genetic algorithms and artificial neural networks." In 2009 International Joint Conference on Neural Networks, pp. 627-633. IEEE, 2009, doi: 10.1109/IJCNN.2009.5178927.

[81] Silva, Paulo Henrique da F., Rossana Moreno S. Cruz, and Adaildo Gomes d'Assuncao. "Blending PSO and ANN for optimal design of FSS filters with Koch island patch elements." IEEE Transactions on Magnetics 46, no. 8 (2010): 3010-3013, doi: 10.1109/TMAG.2010.2044147.

[82] T. Wu, "Improved Broadband Bandpass FSS Filters For 5G Applications," 2018 IEEE International Symposium on Antennas and Propagation & USNC/URSI National Radio Science Meeting, 2018, pp. 2033-2034, doi: 10.1109/APUSNCURSINRSM.2018.8609110.

[83] R. Natarajan, M. Kanagasabai, S. Baisakhiya, R. Sivasamy, S. Palaniswamy and J. K. Pakkathillam, "A Compact Frequency Selective Surface With Stable Response for WLAN Applications," in IEEE Antennas and Wireless Propagation Letters, vol. 12, pp. 718-720, 2013, doi: 10.1109/LAWP.2013.2264837.

[84] Denidni, Tayeb A., Yacouba Coulibaly, and Halim Boutayeb. "Hybrid dielectric resonator antenna with circular mushroom-like structure for gain improvement." IEEE Transactions on Antennas and Propagation 57, no. 4 (2009): 1043-1049, doi: 10.1109/TAP.2009.2015809.

[85] Akbari, M., M. M. Ali, M. Farahani, A. R. Sebak, and T. Denidni. "Spatially mutual coupling reduction between CP-MIMO antennas using FSS superstrate." Electronics Letters 53, no. 8 (2017): 516-518, doi: 10.1049/el.2017.0172.

[86] Ghayekhloo, Alireza, Mohammad Akbari, Majid Afsahi, Ali A. Orouji, Abdel R. Sebak, and Tayeb A. Denidni. "Multifunctional transparent electromagnetic surface based on solar cell for backscattering reduction." IEEE Transactions on Antennas and Propagation 67, no. 6 (2019): 4302-4306, doi: 10.1109/TAP.2019.2911196.

[87] Ghayekhloo, Alireza, Majid Afsahi, Ali A. Orouji, and Tayeb A. Denidni. "Triangle and aperiodic metasurfaces for bistatic backscattering engineering." physica status solidi (b) 256, no. 10 (2019): 1900059, doi: 10.1002/pssb.201900059.

[88] I. Lee, W. Oh, Y. J. Kim and I. Hong, "Design and Fabrication of Absorptive/Transmissive Radome Based on Lumped Elements Composed of Hybrid Composite Materials," in IEEE Access, vol. 8, pp. 129576-129585, 2020, doi: 10.1109/ACCESS.2020.3009486.

[89] Chiu, Cheng-Nan, and Keng-Ping Chang. "A novel miniaturized-element frequency selective surface having a stable resonance." IEEE Antennas and Wireless Propagation Letters 8 (2009): 1175-1177, doi: 10.1109/LAWP.2009.2034766.

[90] Liu, Hui Lai, Kenneth Lee Ford, and Richard J. Langley. "Design methodology for a miniaturized frequency selective surface using lumped reactive components." IEEE Transactions on Antennas and Propagation 57, no. 9 (2009): 2732-2738, doi: 10.1109/TAP.2009.2027174.

[91] Lin, Bao-qin, Shan-hong Zhou, Xing-yu Da, Ying-wu Fang, Yong-jun Li, and Wei Li. "Compact miniaturised-element frequency selective surface." Electronics Letters 51, no. 12 (2015): 883-884, doi: 10.1049/el.2015.0288.

[92] Bayatpur, Farhad, and Kamal Sarabandi. "Multipole spatial filters using metamaterial-based miniaturized-element frequency-selective surfaces." IEEE Transactions on Microwave Theory and Techniques 56, no. 12 (2008): 2742-2747, doi: 10.1109/TMTT.2008.2007332.

[93] Chiu, Cheng-Nan, and Keng-Ping Chang. "A novel miniaturized-element frequency selective surface having a stable resonance." IEEE Antennas and Wireless Propagation Letters 8 (2009): 1175-1177, doi: 10.1109/LAWP.2009.2034766.

[94] Sanz-Izquierdo, Benito, Edward A. Parker, Jean-Baptiste Robertson, and John C. Batchelor. "Singly and dual polarized convoluted frequency selective structures." IEEE transactions on Antennas and Propagation 58, no. 3 (2009): 690-696, doi: 10.1109/TAP.2009.2039321.

[95] Da Silva, Marcelo Ribeiro, Clarissa de Lucena Nóbrega, Paulo Henrique da Fonseca Silva, and Adaildo Gomes D'Assuncao. "Stable and compact multiband frequency selective surfaces with Peano pre-fractal configurations." IET Microwaves, Antennas & Propagation 7, no. 7 (2013): 543-551, doi: 10.1049/iet-map.2012.0673.

[96] Huang, Fan-Cheng, Cheng-Nan Chiu, Tzong-Lin Wu, and Yih-Peng Chiou. "A circular-ring miniaturized-element metasurface with many good features for frequency selective shielding applications." IEEE Transactions on Electromagnetic Compatibility 57, no. 3 (2015): 365-374, doi: 10.1109/TEMC.2015.2389855.

[97] Parker, Edward A., and A. N. A. El Sheikh. "Convoluted array elements and reduced size unit cells for frequency-selective surfaces." In IEE Proceedings H-Microwaves, Antennas and Propagation, vol. 138, no. 1, pp. 19-22. IET, 1991, doi: 10.1049/ip-h-2.1991.0004.

[98] B. Ashvanth, B. Partibane and M. G. N. Alsath, "An Ultraminiaturized Frequency Selective Surface With Angular and Polarization Stability," in IEEE Antennas and Wireless Propagation Letters, vol. 21, no. 1, pp. 114-118, Jan. 2022, doi: 10.1109/LAWP.2021.3119984.

[99] Campos, A. L. P. S., E. E. C. De Oliveira, and PH da F. Silva. "Miniaturization of frequency selective surfaces using fractal Koch curves." Microwave and Optical Technology Letters 51, no. 8 (2009): 1983-1986, doi: 10.1002/mop.24503.

[100] Wang, Wentao T., P. F. Zhang, S. X. Gong, B. Lu, J. Ling, and Tingting T. Wan. "Compact angularly stable frequency selective surface using hexagonal fractal configurations." Microwave and Optical Technology Letters 51, no. 11 (2009): 2541-2544, doi: 10.1002/mop.24676.

[101] Yu, Yi-Min, Cheng-Nan Chiu, Yih-Ping Chiou, and Tzong-Lin Wu. "A novel 2.5-dimensional ultraminiaturized-element frequency selective surface." IEEE Transactions on Antennas and Propagation 62, no. 7 (2014): 3657-3663, doi: 10.1109/TAP.2014.2321153.

[102] Shi, Yongrong, Wanchun Tang, Wei Zhuang, and Cheng Wang. "Miniaturised frequency selective surface based on 2.5-dimensional closed loop." Electronics letters 50, no. 23 (2014): 1656-1658, doi: 10.1049/el.2014.3113.

[103] Wei, Pei-Shen, Cheng-Nan Chiu, and Tzong-Lin Wu. "Design and analysis of an ultraminiaturized frequency selective surface with two arbitrary stopbands." IEEE Transactions on Electromagnetic Compatibility 61, no. 5 (2018): 1447-1456, doi: 10.1109/TEMC.2018.2864546.

[104] Rashid, Amir K., Bo Li, and Zhongxiang Shen. "An overview of three-dimensional frequency-selective structures." IEEE Antennas and Propagation Magazine 56, no. 3 (2014): 43-67, doi: 10.1109/MAP.2014.6867682.

[105] Makimoto, Mitsuo, and Sadahiko Yamashita. "Bandpass filters using parallel coupled stripline stepped impedance resonators." IEEE Transactions on microwave theory and techniques 28, no. 12 (1980): 1413-1417, doi: 10.1109/TMTT.1980.1130258.

[106] Bayatpur, Farhad, and Kamal Sarabandi. "Single-layer high-order miniaturized-element frequency-selective surfaces." IEEE Transactions on Microwave Theory and Techniques 56, no. 4 (2008): 774-781, doi: 10.1109/TMTT.2008.919654.

[107] Salehi, Mohsen, and Nader Behdad. "A second-order dual X-/Ka-band frequency selective surface." IEEE Microwave and Wireless Components Letters 18, no. 12 (2008): 785-787, doi: 10.1109/LMWC.2008.2007698.

[108] Gao, Meng, Seyed Mohamad Amin Momeni Hasan Abadi, and Nader Behdad. "A dual-band, inductively coupled miniaturized-element frequency selective surface with higher order bandpass response." IEEE Transactions on Antennas and Propagation 64, no. 8 (2016): 3729-3734, doi: 10.1109/TAP.2016.2580181.

[109] Sarabandi, Kamal, and Nader Behdad. "A frequency selective surface with miniaturized elements." IEEE Transactions on Antennas and propagation 55, no. 5 (2007): 1239-1245, doi: 10.1109/TAP.2007.895567.

[110] Yan, Mingbao, Jiafu Wang, Hua Ma, Mingde Feng, Yongqiang Pang, Shaobo Qu, Jieqiu Zhang, and Lin Zheng. "A tri-band, highly selective, bandpass FSS using cascaded multilayer loop arrays." IEEE Transactions on Antennas and Propagation 64, no. 5 (2016): 2046-2049, doi: 10.1109/TAP.2016.2536175.

[111] Hong, J-S., B-Z. Wang, and Y. Zhang. "Analysis of a double folded stub microstrip structure using generalized transmission line equations method." Journal of electromagnetic waves and applications 18, no. 9 (2004): 1235-1247, doi: 10.1163/1569393042955270.

[112] Abadi, Seyed Mohamad Amin Momeni Hasan, and Nader Behdad. "Inductively-coupled miniaturized-element frequency selective surfaces with narrowband, high-order bandpass responses." IEEE Transactions on Antennas and Propagation 63, no. 11 (2015): 4766-4774, doi: 10.1109/TAP.2015.2477850.

[113] Yan, Mingbao, Shaobo Qu, Jiafu Wang, Anxue Zhang, Lin Zheng, Yongqiang Pang, and Hang Zhou. "A miniaturized dual-band FSS with second-order response and large band separation." IEEE Antennas and Wireless Propagation Letters 14 (2015): 1602-1605, doi: 10.1109/LAWP.2015.2413942.

[114] Gao, Meng, Seyed Mohamad Amin Momeni Hasan Abadi, and Nader Behdad. "A hybrid miniaturized-element frequency selective surface with a third-order bandpass response." IEEE Antennas and Wireless Propagation Letters 16 (2016): 708-711, doi: 10.1109/LAWP.2016.2600524.